Studies on Catalysis of Metallic Species during CO2 Gasification of Lignite Char

ヌルルフダ, ハリム

Studies on Catalysis of Metallic Species during CO_2 Gasification of Lignite Char

by

Nurulhuda Halim

Department of Applied Sciences for Electronics and Materials

Interdisciplinary Graduate School of Engineering Sciences

Kyushu University

2020

ACKNOWLEDGEMENTS

In the name of Allah, the beneficent and the merciful.

This doctoral thesis would not be completed without the supports, contributions, and helps from many people who are gratefully acknowledged here.

First of all, I would like to express my sincere gratitude to my supervisor and my mentor, Prof. Jun-ichiro Hayashi, for his patience, motivation and also insightful discussion during my PhD journey. I am grateful for his guidance in helping me to develop my research skills.

I would also like to express my sincere appreciation and thank to the committee member, Prof. Hisahiro Einaga and Associate Prof. Shinji Kudo, for their valuable comments and suggestions, and also fruitful discussion during my study.

My sincere gratitude is also given to Prof. Koyo Norinaga, Associate Prof. Xianpeng Gao, Assistant Prof. Shusako Asano, and Dr. U.P.M., Ashik for their support on my research. They have provided a lot of technical suggestions, personal motivations, and emotional supports.

Special thanks for all of the member of Hayashi-Kudo laboratory, especially Mrs. Naoko Sudo, Ms. Yasuyo Hachiyama, Ms. Asuka Mori, Mr. Kentaro Shima, Mrs. Zayda F. Zahara, Mr. Huang Xin, Mrs. Ni'mah Ayu L., Mr. Aditya Wibawa, Ms. Phatchada Santawaja, Mr. Tianlong Liu and Mr. Akira Tajima for their kind help and smile in the laboratory.

I would like to thank to Ministry of Education, Culture, Sport, Science, and Technology (MEXT), Japan and General Foundation Seisankagaku Kenkyushoureikai for the financial support of my PhD study. I would also like to express my gratitude for Kyushu University for Intellectual Exchange and Innovation (IEI) Program.

I am also grateful to all my seniors and colleagues at the Department of Metallurgical Engineering, ITB, and also Dr. Miftahul Huda for supporting my PhD study.

Saving the best for last, I would like to appreciate my parents, Mr. Djaja Rahmat and Mrs. Diah Rodhiyati, and my brothers, Rais and Ilham, for their continuous support and prayer. I am also extremely grateful and appreciate all the sacrifices of my beloved wife, Nisa, and kids, Arisha and Ibrahim, for always supporting me in good and hard times, for always waiting for me in muggy or frosty night, and for always becoming energy for me to finish this intensive training.

CONTENTS

NOMENCLATURE

α_{cg} = Contribution rate of catalytic gasification to overall gasification [%]

β = Rate of volatilization of K species from gasifying char at t [-]

C_{cat} = Concentration of K catalyst in gasifying char at t [mol-K/kg-daf-char]

C_{Cn} = Concentration of catalyst Cn [–]

C_{C1prec} = Concentration of precursor of catalyst C1 [–]

ICA-1 = Initial catalytic activity at the beginning of gasification [min^{-1}]

ICA-2 = Potential catalytic activity at the beginning of gasification [min^{-1}]

ICD-1 = Initial rate of catalyst deactivation [min^{-1}]

ICD-2 = Overall rate of catalyst deactivation [min^{-1}]

k'_C = The rate of catalytic gasification per amount of catalyst [min^{-1}]

k'_{cat} = The rate of catalytic gasification per amount of K catalyst in gasifying char [kg-daf-char/(min·mol-K)]

k_{cat} = Rate constant for catalytic gasification [min^{-1}]

k_{Cn} = Rate of catalytic gasification defined by $k'_C.m_{Cn}$ [min^{-1}]

k_{C1prec} = Rate constant for transformation of C1 precursor to C1 [min^{-1}]

$k_{loss\text{-}n}$ = Rate constant for loss of Cn [min^{-1}]

k_{nc} = Rate constant for non-catalytic gasification [min^{-1}]

m_{cat} = Amount of K catalyst [mol-K]

m'_{cat} = Amount of K catalyst per initial mass of char at t [mol-K/kg-daf-char]

m_{Cn} = Amount of catalyst Cn [–]

m_{C1prec} = Amount of precursor of catalyst C1 [–]

m_{char} = The mass of char at t [kg-daf-basis]

t = Time from the initiation of gasification [min]

T = Gasification temperature [°C]

X = Mass-based conversion of char by gasification [–]

Chapter 1
General Introduction

1.1 Background

At present, more than 85% of the world's primary energy demand is provided by fossil fuels such as coal, oil, and natural gas. [1,2] This shows today's challenges regarding energy supply security and environmental conservation. In order to do transition to a long-term sustainable energy mix in the future, it is inevitable to implement more environmental-benign utilization methods of conventional fuels until renewable resources are capable of meeting our energy needs. Therefore, any improvement in the conversion efficiency of carbon resources, even if it is small, has a significant impact on resource reserve and CO_2 reduction.

Some studies reported that coal has the highest reserves-to-production ratio (R/P) among the conventional carbon resources, which means that coal reserves can contribute longer for supplying energy for us. [1,2] In 2018, more than 7.7 billion tons of coal had been produced to fulfill 22% of the world's energy consumption. [1,2] This was not only because of the competitive price of coal but also the availability of coal reserves/resources in almost every country worldwide, enabling energy access for the whole world. Despite those benefits, coal seems to have been marked out as an undesirable fuel in recent years. One of the reasons is that the major current consumption way for coal is combustion, by which power and steam are generated. The conventional combustion technology burns coal with air/oxygen by following Equation 1, at high operating temperatures (1300–1700°C) that causes a substantial loss of chemical energy and high CO_2 emission. [3,4] This situation is getting worse when inferior coal, *i.e.*, lignite, is used. In this context, it is therefore essential to develop a technology aiming to make coal conversion more efficient and less polluting.

$$C_{(s)} + O_{2(g)} = CO_{2(g)} \qquad \Delta H_{298} = -394 \text{ KJ/mol} \qquad (1)$$

Gasification has been studied for centuries yet has returned drawing attention in academic and industrial fields in recent decades due to its potential to reduce carbon emission. **Figure 1.1** shows the concept of a polygeneration gasification system with the flexibility of using multiple feedstocks and generating multiple products. [4,5] Steam/CO_2 gasification, which employs endothermic reactions (see Equations 2 and 3) and low-operating-temperatures (<

1000°C), is recognized as a promising conversion technology that can be used to minimize greenhouse gas (GHG) emissions from continued fossil fuel usage. [4,6,7] This technology, coupled with solid oxide fuel cell (SOFC) as a heat provider, becomes an excellent option for realizing carbon-neutral co-production process, in which CO_2 is recycled into the system. [4,8,9] Moreover, the use of CO_2 instead of steam as a gasifying agent reduces heat consumption (see Equation 4) and thus improves the overall thermal efficiency.

$$C_{(s)} + CO_{2(g)} = 2\,CO_{(g)} \qquad \Delta H_{298} = +172\ \text{KJ/mol} \qquad (2)$$

$$C_{(s)} + H_2O_{(g)} = CO_{(g)} + H_{2(g)} \qquad \Delta H_{298} = +131\ \text{KJ/mol} \qquad (3)$$

$$H_2O_{(l)} = H_2O_{(g)} \qquad \Delta H_{vap,373} = +41\ \text{KJ/mol} \qquad (4)$$

The usage of lignite as feedstock adds another advantage, an abundance of inherent catalyst species that bond to carboxyl groups. These species are capable to enhance the rate of char gasification, which commonly controls the overall rate of the lignite-to-syngas conversion. However, it is not an easy task to describe the kinetics and reveal the mechanism of CO_2 gasification of lignite char. Many factors influence the kinetics of char gasification such as char properties, metallic species content, and operating conditions *i.e.*, temperature and pressure. Therefore, it was thus necessary to comprehensively understand the complex properties of organic and inorganic matrices of lignite, and also the interaction between them in order to design and optimization of a gasifier. Here, some related aspects are discussed to understand the nature of CO_2 gasification of lignite char.

1.2 Thermochemical Conversion of Coal

There are several methods to convert coal into energy and chemicals by applying heat and controlling reactant gas. In this study, the main focus is given to pyrolysis and gasification.

1.2.1 Pyrolysis

Pyrolysis, also known as devolatilization, is the first stage (after drying) of thermochemical process for coal conversion, and it is performed by heating solid fuel at 300–600°C in the absence of oxygen. [10,11] During the heating, solid and gaseous products, *i.e.*, char and volatiles, respectively, are formed in proportions that largely depend on the nature of carbon material used and the operating parameters such as heating rate, holding temperature, and gas atmosphere. The volatiles consists mainly of low molecular weight gases (CO, CO_2, H_2), light hydrocarbon gases (C1–C5), and tar, which is organic compounds having > 6 carbon atoms per molecule. The char then can be directly used as fuels or further processed into syngas

via gasification, while the volatile is normally reformed to produce some functional chemicals. The presence of alkali and alkaline earth metallic (AAEM) species inhibits the release of the larger aromatic ring systems during the pyrolysis, and thus increases the yield of char. [11–13] However, a portion of these species underwent volatilization, leaving the char matrix and thus reducing the effective amount of catalyst for gasification. [13,14]

1.2.2 Gasification

Gasification is a process by which carbonaceous solid fuel such as lignite and biomass is heated with a limited amount of oxygen in the form of air, pure O_2, steam or CO_2 to form syngas (mainly H_2, CO, and CH_4) that can be used for co-production of power, fuels, and chemicals. [15–19]. The syngas, which its composition is mainly influenced by the temperature and gasifying agent, later undergoes further downstream processing, including gas cleaning before converted into a final product. [20] In the case that CO_2 is used as a gasifying agent, it can be more cost-effective than conventional carbon capture technologies. [7] Thus, the Boudouard reaction in Equation 2 might be an attractive option not only for CO_2 sequestration but also for its utilization.

The application of current gasification technology such as integrated coal gasification combined cycle (IGCC) or even Advanced-IGCC (A-IGCC) is generally considered as the most proper way to utilize low-rank coal for power production. [3] A-IGCC is promising a high net thermal efficiency by applying the recuperation of heat and reduction of oxygen production energy. [3] In A-IGCC, the required heat for the endothermic reactions, *i.e.*, those in Equations 2 and 3, in the coal gasifier are supplied from gas turbine exhaust. In other words, thermal energy in the exhaust is converted to chemical energy. This promotes autothermal gasification that is supported by additional steam instead of gasification by partial oxidation alone, enabling reduction in exergy loss. The presence of catalyst species can further reduce the activation energy of the process and thus improve the thermal efficiency.

1.3 Roles of Metallic Species during Char Gasification

It is well renowned that inherent as well as externally loaded alkali and alkaline earth metals (AAEM) and transition metals influence the reactivity of char, especially those produced from low-rank coal. The following sections describe the catalysis and behavior of those metallic species during char gasification.

1.3.1 Alkali metals

Kapteijn *et al*. [21] observed the catalytic activity of alkali metals during CO_2 gasification of carbon, and it increases with the atomic weight from lithium (Li) to cesium (Cs). Considers a trade-off between activity and relative abundance in coal (or cost for its addition), the compounds of sodium (Na) and potassium (K) have been regarded as promising catalysts for industrial application, and thus studied extensively. The water-soluble forms of Na such as NaCl, NaOH, and Na_2CO_3 are widely used as the catalyst for gasification, while K_2CO_3 and KOH are the most commonly-used K precursors. [22] **Figure 1.2** shows a typical example of the change in the rate of gasification, dX/dt, along char conversion, X, for Na and K-catalyzed gasification of carbon. [23] The dX/dt of these chars changed via a maximum in the course of gasification, suggesting either of the presence of optimum sizes of clusters/particles of alkali catalyst or the change in quality/activity of the catalyst. [24,25] Alkali metals have a propensity to be well dispersed in carbon matrix of char at an atomic scale at a lower concentration but to form more active nanoparticles/clusters as the concentration increases. [25] However, there have been no or, if any, very few trials to describe experimentally the catalytic mechanism of alkali metals and explain clearly the trend mentioned above.

One drawback of applying alkali metals-catalyzed gasification is the volatility of these species from pyrolyzing and gasifying char. [13,14,26,27] For example, the melting temperatures for Na_2CO_3 and K_2CO_3 are ~850 and ~890°C, respectively, which are in the range of typical temperature for gasification. These species also react with aluminosilicate minerals, losing its original activity during gasification. [28,29] It is thus important to remove mineral matters before analyzing the catalysis of alkali metal species during the gasification.

1.3.2 Alkaline earth metals

Although the activities of alkaline earth metallic species are not as high as those of alkali species, [30,31] its abundance in many coal samples [32,33] and its resistance to vaporization [13,34] sometimes made these species become the major catalyst for char gasification. As with alkali metals, the catalytic activity of alkaline-earth metals increases with increasing atomic weight. The carbonate of calcium (Ca) was found to be less active than those of barium (Ba) and strontium (Sr), while that of magnesium (Mg) had only slight effect on the kinetics. [35] Despite the higher activity of Sr and Ba, only a few studies using them as gasification catalysts, likely due to the higher natural abundance of Ca in coal. Many studies found that the catalytic activities of doped calcium species such as $CaCO_3$ and CaO depend on its dispersion in char matrix, [36,37], and therefore, an ion-exchange method is commonly applied to load these

types of catalysts. [5,38] As reported previously, the activity of Ca increased linearly with Ca content up to a loading saturation level (LSL). [36,39] Even though the rate of Ca-catalyzed gasification is initially high, but it slowly decreases with the progress of char conversion due to deactivation via sintering/agglomeration (see **Figure 1.2**). Recent studies also reported that the gasification of char from the coal that doped with a combination of alkali and alkaline earth metal catalyst species performs better than that from metal-loaded coal due to synergistic effects of these catalysts. [40–43]

1.3.3 Transition metals

Gasification is typically conducted under the catalysis of AAEM species, but some transition metals such as iron (Fe), cobalt (Co), and nickel (Ni) also showed promising performances. [44,45] These species are sometimes found naturally in coal or obtained inexpensively as a waste catalyst from a number of chemical processes such as Fischer-Tropsch synthesis. Figueiredo *et al*. [46] investigated the CO_2 reactivities of various activated carbons that were impregnated with Ni, Co, and Fe. They found that Ni and Co were better catalysts than iron, but in all cases, high conversions could not be achieved due to catalyst deactivation. The activities of Ni and Fe species are more sensitive to the initial surface area than those of alkali species, but these catalysts do not deactivate with aluminosilicates as alkali catalyst species do. However, previous studies showed that the activities of the heavy metal species during the steam gasification are lower than those of AAEM species. [47–49] This suggested that the heavy metals might be better to be used as catalyst in downstream processes such as tar reforming. [50]

1.4 Kinetic Analysis of Char Gasification

The development of kinetic models to describe the profiles of char conversion, which is the rate-determining step in coal gasification, is essentially important for enhancing the performance of a gasifier. However, proposing a universal model that can be applied for different coal types and various operation conditions remains a challenging subject due to the problematic complexity of char gasification reactions. Many previous researchers applied Langmuir-Hinshelwood (L-H) mechanism to explain the effects of temperature and total/partial pressure in reactor on the char reactivity, [51–53] while others made theoretical models based on the geometry of char particles and its change during the gasification such as random pore model (RPM), shrinking core model (SCM), and volumetric model (VM). On the

other hand, several authors proposed parallel reaction model (PRM) to describe the dynamic change in catalytic char gasification by considering not only the inherent char reactivity but also the composition of metallic species in coal/char.

1.4.1 Volumetric model

Volumetric model (VM) assumes that the reaction between the gasifying agents and the char particles takes place at all active sites, which uniformly distributed in the non-porous part and on the pore surface of char particles. The overall rate of gasification is assumed steady in the course of gasification. The rate follows first-order kinetics, and it is given by:

$$\frac{dX}{dt} = k_{\mathrm{VM}}(1 - X) \quad (5)$$

Different previous studies successfully applied this first-order kinetics to explain the gasification of chars from acid-washed biomass/lignites. [24,32,54] This model, however, has a difficulty to explain a maximum d*X*/d*t*, which usually occurs for the non-catalytic gasification of chars originated from coal ranked higher than or equivalent to sub-bituminous, [55–57] and that for the gasification of lignite char, in which contains an abundance of metallic species. [32,58,59]

1.4.2 Shrinking core model

In contrast to the VM, the shrinking core model (SCM) considers that the gasifying agents only react either on the surface of char particles or within the pores close to the outer particle surface. The SCM assumes that a char particle is an aggregation of smaller grains, each of which is in a uniform size. The reaction proceeds from the grain surface to the interface of the shrinking char, unreacted core through a layer of ash and/or catalyst, and moves toward the center of the char particle. The general equation of SCM is expressed as follows:

$$\frac{dX}{dt} = k_{\mathrm{SCM}}(1 - X)^n \quad (6)$$

k_{SCM} is the reaction rate constant, which related to the initial char properties (surface area and porosity), while *n* is the shape factor. By assuming the grain shape is a sphere, the exponent *n* in Equation 6 has the value of 2/3. The SCM enables to predict the rate of gasification of char from sub-bituminous coal that shown decreasing in the char reactivity with the progress of its conversion. [60] However, the main assumption of SCM, the dependency of the kinetics of char conversion on the surface area of char, is not valid for the non-catalytic gasification of chars from lignite/biomass. Kudo *et al*. [58] investigated the steam gasification of acid-washed chars from various types of biomass and lignite. They confirmed that the specific surface area

of chars increased with the conversion, while the specific rates of reaction were steady during the gasification.

1.4.3 Random pore model

Random pore model (RPM) is one of the most widely used structural models to fit the kinetic profiles of char gasification. [61,62] The model is developed for a gas-solid reaction by assuming that the internal surfaces of porous char particles serve as the reaction interfaces. [61] All pores are assumed in a cylindrical shape, and it grows and coalesces as the conversion proceeds. The rate of char conversion is expressed as:

$$\frac{dX}{dt} = k_{\mathrm{RPM}}(1-X)\sqrt{1-\psi\ln(1-X)} \quad (7)$$

$$\psi = \frac{4\pi L(1-\varepsilon)}{S^2} \quad (8)$$

where k_{RPM} is the reaction rate constant and ψ is the structural parameter, obtained from the morphology of coal particle (L; pore length, S; specific pore surface area, ε; solid porosity) or that from the reaction rate measurements. [63,64] The advantage of RPM over VM and SCM is the ability to predict the rate of char gasification with the maximal dX/dt in the range of char conversion, X, of 0–0.393. [23,62] However, the RPM failed to fit the reactivity profiles of lignite/biomass chars or alkali metals catalyzed chars, in which appears a maximum reactivity in high conversion range. [23,65–67] Zhang *et al*. [65] modified the RPM by introducing two empirical parameters to describe specific catalytic effects of K and Ca on the CO_2 gasification of coal char. The modified RPM was found to be capable of describing the measured kinetics well over the entire range of X. They also found that both empirical parameters have a good correlation with the contents of metallic species in char. This strongly suggested that the kinetics models should be developed not only by considering the geometry or property of char, but also by the catalysis of metallic species.

1.4.4 Parallel reaction model

The concept of simultaneous reactions of char with gasifying agents in the absence and presence of catalyst, which is hereafter termed non-catalytic gasification and catalytic gasification, respectively, has been known for long. [47,68] However, the first attempt to generalize the mathematical expression of the parallel reaction model (PRM) was conducted by Bayarsaikhan *et al*. [69] They investigated the steam gasification of nascent char from rapid or slow pyrolysis of a Victorian brown coal at 800–900°C in a fixed-bed reactor. They found that the rate of the gasification of char from the raw coal at $X > 0.8$ was similar to that from the

acid-washed coal, which follows first-order kinetics. The rate of non-catalytic gasification was defined as:

$$\frac{dX}{dt} = k_{\mathrm{nc}}(1 - X) \quad (9)$$

k_{nc} is the rate constant of the non-catalytic gasification and it was barely influenced by operating parameters such as total pressure in the reactor, heating rate for the pyrolysis, and even period of isothermal heating before the gasification. Recent studies confirmed the applicability of Equation 9 to describe the kinetics of gasification of chars from acid-washed lignite/biomass and also reported that k_{nc} is only slightly affected by the coal/biomass type. [32,58,70]

Bayarsaikhan *et al*. [69] also found that the difference in the kinetics of char from raw coal and that from acid-washed coal is mainly due to the catalysis of inherent AAEM species. They then proposed some equations to describe the kinetics of catalytic gasification. As confirmed in previous studies, AAEM species are highly dispersed in/on the carbonaceous matrix of the raw char. [71–73] It was thus reasonable to assume that the rate of the catalytic gasification is a function of the amount of the active AAEM species, while independent of the amount of char. In other words, the rate of the catalytic gasification obeys zeroth-order with respect to the unconverted fraction of char.

$$\frac{dX}{dt} = k_{\mathrm{cg}} \quad (10)$$

k_{cg}, which is the rate constant for catalytic gasification, is assumed to be proportional to the amount of active catalyst species, *i.e.*, AAEM species, remaining in/on the gasifying char.

$$k_{\mathrm{cg}} = k'_{\mathrm{cg}} C_{\mathrm{cat}} \quad (11)$$

where k'_{cg} and C_{cat} are the rate constant for catalytic gasification per unit amount of active catalyst species and the amount of active catalyst species, respectively. The amount of the active catalyst decreases during the gasification due to deactivation. Sams *et al*. [29] investigated the kinetics of catalyst loss during CO_2 gasification of carbon. Their result showed that the significant fraction of the potassium catalyst was lost by vaporization. They defined the rate of vaporization obeying first-order expression. Then, Equation 10 is modified to

$$k_{\mathrm{cg}} = k'_{\mathrm{cg}} C_{\mathrm{cat}} = k'_{\mathrm{cg}} C_{\mathrm{cat},0} \exp(-k_{loss} t) = k'_{\mathrm{cg},0} \exp(-k_{loss} t) \quad (12)$$

$C_{\mathrm{cat},0}$ and $k_{\mathrm{cg},0}$ are C_{cat} and k_{cg} at $t = 0$, respectively, while k_{loss} is overall rate constant for the loss of active catalyst species not only due to volatilization but also due to intraparticle deactivation. Equation 9 is combined with Equations 10–12 to give the total rate of the non-catalytic gasification and catalytic one.

$$\frac{dX}{dt} = k_{\mathrm{nc}}(1-X) + k_{\mathrm{cg}} = k_{\mathrm{nc}}(1-X) + k'_{\mathrm{cg},0}\exp(-k_{loss}t) \quad (13)$$

Equation 13 represents the progress of non-catalytic and catalytic gasification in parallel. This model successfully described the changes with time of char conversion during steam gasification of chars not only from Victorian brown coals but also that from Indonesian sub-bituminous coals, under various operating conditions. [69,74] Kajita, *et al*. [24] then studied the steam gasification of biochars and applied Equation 13 to analyze its kinetics. They confirmed that the non-catalytic and K-catalyzed gasification occurred in parallel, and the kinetics of each type of gasification was quantitatively described based on the L-H mechanism.

A further study, conducted by Kim *et al*. [5], revealed the dependency of the rate of Ca-catalyzed gasification on the concentration of Ca in lignite char (C_{Ca}). They investigated the kinetics of steam gasification of lignite char with different combinations of C_{Ca}, temperature, and partial pressures of H_2 and steam. They described successfully the kinetics of 41 sets of gasification experiments by employing two types of Ca-catalysts with different features, in other words, modifying Equation 13. They then found the optimum initial C_{Ca} in the char to minimize the time required for 99% char conversion.

Moreover, recent studies on the CO_2 gasification of lignite/biomass chars further enriching the application of the PRM. Byambajav *et al*. [32] and Zahara *et al*. [70] successfully describe the measured kinetics of gasification of chars from raw/acid-washed lignite and biomass, respectively, over a range of char conversion, 0−0.999, by employing the PRM, together with the presence of three to four types of catalysts having different activities and deactivation characteristics, and a type of precursor. They found that the catalysis of AAEM and Fe species is responsible for the overall catalytic activity. They also proposed the mechanism of catalyst deactivation by analyzing the metallic species composition in char.

1.5 Objective of This Study

The potential use of lignite to produce energy and chemicals is an important subject to explore. The conversion of lignite to syngas via gasification, in which steam/CO_2 is employed as a gasifying agent, offers some advantages such as high thermal efficiency and low carbon emission. To further promote the efficiency of a gasifier, the reaction mechanism during the gasification need to be understood well, generally by applying a kinetic model, so that the rate of char conversion can be maintained optimally. However, the development of the conventional kinetic models is mostly based on the assumption that the change in char reactivity is only caused by that in char structure. These models described well the kinetics of gasification of

highly ordered carbonaceous materials but failed to explain changes in the char reactivity of lignite and biomass, which contain inherent catalyst species. Recent studies also found the correlations of the rate of catalytic gasification with the metallic species composition. It was thus suggested that the kinetics model should take into account not only the char properties but also the catalysis of metallic species. Thus, the application of the parallel reaction model, which assumed the progress in parallel of catalytic and non-catalytic gasification, seems to be more reasonable to describe quantitatively the kinetics of gasification of lignite char. It is also noted from the review that there have been no trials to explain the differences in catalytic behavior between inherent and extraneous metallic species during CO_2 gasification of lignite char. Moreover, while the use of composite catalysts from AAEM species becomes a popular subject recently, very few studies made a focal point to understand the interaction mechanism of these species. Therefore, the focuses of this thesis is to understand the kinetics and mechanism of CO_2 gasification of lignite char under the catalysis of inherent metallic species (**Chapter 2**), and also that of extraneous (*i.e.*, intentionally added) metallic species (**Chapter 3**) using the parallel kinetic model, striving for a quantitative description of the overall rate of gasification, as a function of char conversion (X) over the entire range of X. The initial catalytic activity and the rate of catalyst deactivation of these types of metallic species are also compared and discussed (**Chapter 3**). This thesis also aimed to explain the kinetics of the K-catalyzed CO_2 gasification by proposing a new way to evaluate the catalytic activity of K and its change during the gasification (**Chapter 4)**.

1.6 Outline of This Study

This thesis contains 5 chapters. **Chapter 1** describes the current energy balance and relevant efforts to improve the conversion efficiency of fossil fuels. This chapter also comprehensively reviews the characteristics of alkali and alkaline earth metals (AAEM) and transitional metals that inherently abundance in lignite, making it a desirable feedstock for gasification. The features and basic assumptions of commonly used kinetic models are also discussed in order to find a proper model that able to describe the gasification of lignite char.

Chapter 2 discusses the results of the CO_2 gasification of lignite chars at 900°C. The twenty chars, which having different contents/chemical types of inherent metallic species, were prepared by multistage washing of two-parent lignites and subsequent pyrolysis. The time-dependent changes in char conversion up to 0.999 for all the chars are quantitatively described by a kinetic model that assumed the progress of non-catalytic and catalytic gasification in

parallel, and employed multicatalytic species with different initial activities and deactivation kinetics. A single piecewise linear function, which followed a nucleation-growth mechanism of catalysts, showed the relationship between the total concentration of Na, K, Ca, and Fe and the initial total catalytic activity (ICA-2) for the chars. The overall rate of catalyst deactivation (ICD-2) was given by a single linear function of ICA-2 and a factor for the composition of metallic species. This function was also applicable to previously reported ICA-2/ICD-2 relationships for chars from lignite and biomass, showing fast deactivation of Fe catalyst and an important role of Mg in the promotion of catalyst deactivation.

Chapter 3 discusses the results of the investigation on the interaction mechanisms of Ca with Mg or K during catalytic CO_2 gasification of lignite char. Two demineralized lignites, prepared by multi-stage removal of inherent inorganic species, were loaded with varying amounts of Ca, Mg, and K, separately or jointly, by ion exchange, then pyrolyzed and subsequently gasified at 900°C. The measured kinetics of the gasification of chars with different contents of metallic species was described quantitatively over a range of char conversion, 0−0.999, by the model that employed the progress of non-catalytic gasification and catalytic gasification in parallel, together with the presence of multicatalytic components with different characteristics. For Ca-catalyzed gasification, its initial rate was correlated well and linearly with the Ca concentration in char (0.14– 1.33 wt%-daf-char). When bi-metal catalysts were used, the kinetic analysis revealed that the Mg/MgO deactivated a portion of the most active Ca catalyst prior to and during the gasification. In contrast, the K showed synergistic performances with Ca. Its overall catalytic activity was similar to Ca on an equal mol basis, but its deactivation rate was much lower. It was also found that the catalytic performance of the extraneous metallic species was lower than that of inherent metallic species.

Chapter 4 discussed the results of the investigation of the change in catalytic activity of K with the char conversion during CO_2 gasification of lignite char at 800–900°C. Several physical and chemical properties of char that potentially influence the catalytic activity were examined. The char samples were prepared from an Indonesian lignite by a sequence of complete removal of inherent metallic species and mineral matter, K-loading by ion-exchange, and pyrolysis. The catalytic activity of K (k'_{cat}) was defined as the rate of catalytic gasification (after elimination of the rate of non-catalytic gasification and that of K volatilization from total mass release rate from char) per amount of K retained by the gasifying char. k'_{cat} increased by a factor of 5–20 with X over its range up to 0.98–0.99, depending on the initial K concentration in the char ($m_{cat,0}$) ranging 0.16–1.4 wt%-daf. Such significant increase in k'_{cat} was due to change in not the intrinsic reactivity of char but its porous nature, *i.e.*, the size and volume of

pores that retained the K catalyst. At $X < 0.4$, the entire portion of K catalyst was confined in micropores (width < 2.0 nm) having relatively small k'_{cat}, although it increased gradually. At $X > 0.4$, the gasification created greater mesopores (width > 2.0 nm), providing spaces for growth in the size of the K catalyst and allowing promotion of its activity. However, for low $m_{cat,0}$, its major portion continued to stay in micropores with a limited increase in k'_{cat}.

Chapter 5 provides a summary with general conclusions, perspectives, and recommendations based on the findings in preceding chapters.

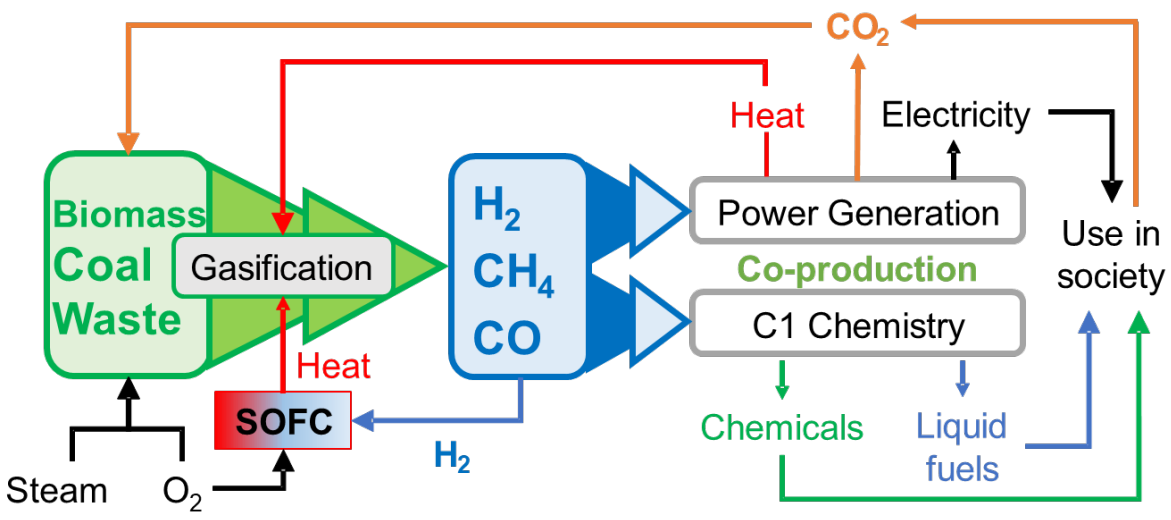

Figure 1.1. Scheme of polygeneration gasification system coupled with SOFC. [4,9]

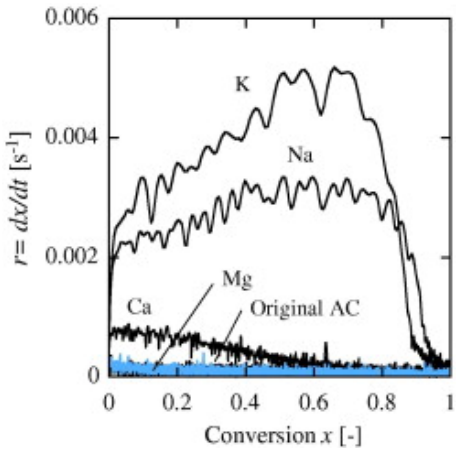

Figure 1.2. The rate of steam gasification of the original and AAEM-loaded activated carbon. [23]

1.7 References

1. BP Economics. *BP Statistical Review of World Energy*, **68** (2019) [Retrieved from https://www.bp.com].
2. IEA, *Key World Energy Statistics*, (2018). [Retrieved from https://www.iea.org/]
3. M. Kawabata, O. Kurata, N. Iki, H. Furutani, A. Tsutsumi, *Journal of Power Technologies*, **92** (2012), 90–100.
4. J. Hayashi, S. Kudo, H.S. Kim, K. Norinaga, K. Matsuoka, S. Hosokai, *Energy & Fuels*, **28** (2014), 4–21.
5. H. Kim, S. Kudo, K. Tahara, Y. Hachiyama, H. Yang, K. Norinaga, J. Hayashi, *Energy & Fuels*, **27** (2013), 6617–6631.
6. D. Fan, Z. Zhu, Y. Na, Q. Lu, *Journal of Thermal Analysis and Calorimetry*, **113** (2013), 599–607.
7. G. Skodras, G. Nenes, N. Zafeiriou, *Applied Thermal Engineering*, **74** (2015), 111–118.
8. J. Ahrenfeldt, T.P. Thomsen, U. Henriksen, L.R. Clausen, *Applied Thermal Engineering*. **50** (2013), 1407–1417.
9. V. Subotić, A. Baldinelli, L. Barelli, R. Scharler, G. Pongratz, C. Hochenauer, A. Anca-Couce, *Applied Energy*, **256** (2019).
10. R. Cypres, C. Soudan-moinet, *Fue*l, **59** (1988), 48–54.
11. C. Sathe, Y. Pang, C.Z. Li, *Energy & Fuels*, **13** (1999), 748–755.
12. J. Hayashi, H. Takahashi, S. Doi, H. Kumagai, T. Chiba, T. Yoshida, A. Tsutsumi, *Energy & Fuels*, **14** (2000), 400–408.
13. C.Z. Li, C. Sathe, J.R. Kershaw, Y. Pang, *Fue*l, **79** (2000), 427–438.
14. D.M. Quyn, H. Wu, S.P. Bhattacharya, C.Z. Li, *Fue*l, **81** (2002), 151–158.
15. R.M. Navarro, M.A. Peña, J.L.G. Fierro, *Chemical Reviews*, **107** (2007), 3952–3991.
16. G.W. Huber, S. Iborra, A. Corma, *Chemical Reviews*, **106** (2006), 4044–4098.
17. A. Corma, *Chemical Reviews*, **114** (2014), 1545–1546.
18. Q. Yi, W. Li, J. Feng, K. Xie, *Chemical Reviews*, **44** (2015), 5409–5445.
19. H.C. Butterman, M.J. Castaldi, *Environmental Science & Technology*, **43** (2009), 9030–9037.
20. C. Higman, S. Tam, *Chemical Reviews*, **114** (2014), 1673–1708.
21. F. Kapteijn, O. Peer, J. Moulijin, *Fue*l, **65** (1986), 1371–1376.
22. R.A. Arnold, J.M. Hill, *Sustainable Energy Fuels*, **3** (2019), 656–672.
23. Y. Zhang, M. Ashizawa, S. Kajitani, K. Miura, *Fue*l, **87** (2008), 475–481.

24. M. Kajita, T. Kimura, K. Norinaga, C.Z. Li, J. Hayashi, *Energy & Fuels*, **24** (2010), 108–116
25. H. Yang, S. Kudo, K. Norinaga, J. Hayashi, *Energy & Fuels*, **30** (2016), 1616–162.
26. D.M. Quyn, H. Wu, C.Z. Li, *Fuel*, **81** (2002), 143–149.
27. C. Sathe, J. Hayashi, C.Z. Li, T. Chiba, *Fuel*, **82** (2003), 1491–1497.
28. K. Formella, P. Leonhardt, A. Sulimma, K.H. van Heek, H. Jüntgen, *Fuel*, 6**5** (1986), 1470–1472.
29. D.A. Sams, T. Talverdian, F. Shadman, *Fuel*, **64** (1985), 1208–1214.
30. L.R. Radovic, P.L. Walker, R.G. Jenkins, *Fuel*, **63** (1984), 1028–1030.
31. R.P.W.J. Struis, C. Von Scala, S. Stucki, R. Prins, *Chemical Engineering Science*, **57** (2002), 3593–3602.
32. E. Byambajav, Y. Hachiyama, S. Kudo, K. Norinaga, J. Hayashi, *Energy & Fuels*, **30** (2016), 1636–1646.
33. M. Perander, N. DeMartini, A. Brink, J. Kramb, O. Karlström, J. Hemming, A. Moilanen, J. Konttinen, M. Hupa, *Fuel*, **150** (2015), 464–472.
34. D.M. Quyn, J. Hayashi, C.Z. Li, *Fuel Processing Technology*, **86** (2005), 1241–1251.
35. D.W. McKee, *Fuel*, **59** (1980), 308–314.
36. C.S.M. de Lecea, M. Almela-Alarcón, A. Linares-Solano, *Fuel*, **69** (1990), 21–27.
37. Y. Ohtsuka, K. Asami, *Energy & Fuels*, **9** (1995), 1038–1042
38. Y. Ohtsuka, K. Asami, *Energy & Fuels*, **10** (1996), 431–435.
39. T. late T.D. Hengel, P.L. Walker, Fuel. **63** (1984), 1214–1220.
40. J. Wang, Y. Yao, J. Cao, M. Jiang, *Fuel*, **89** (2010), 310–317.
41. M.-Q. Jiang, R. Zhou, J. Hu, F.-C. Wang, J. Wang, *Fuel*, **99** (2012), 64–71.
42. L.X. Zhang, S. Kudo, N. Tsubouchi, J. Hayashi, Y. Ohtsuka, K. Norinaga, *Fuel Processing Technology*, **113** (2013), 1–7.
43. Y. Bai, P. Lv, F. Li, X. Song, W. Su, G. Yu, *Energy Conversion Management*, **184** (2019), 172–179.
44. H.S. Kim, S. Kudo, K. Norinaga, J.I. Hayashi, *Energy & Fuels*, **28** (2014), 5623–5631.
45. J.T. Gallagher, H. Harker, *Carbon*, **2** (1964), 163–173.
46. J.L. Figueiredo, J. Rivera-Utrilla, M.A. Ferro-Garcia, *Carbon*, **25** (1987), 703–708.
47. W.J. Lee, S.D. Kim, *Fuel*, **74** (1995), 1387–1393.
48. E.J. Hippo, R.G. Jenkins, P.L. Walker, *Fuel*, **58** (1979), 338–344.
49. A. Tomita, T. Takarada, Y. Tamai, *Fuel*, **62** (1983), 62–68.
50. V. Claude, C. Courson, M. Köhler, S. D. Lambert, *Energy & Fuels*, **31** (2017), 1050–1050.

51. J. Tanner, K.B. Kabir, M. Müller, S. Bhattacharya, *Fue*l, **154** (2015) 107–113.
52. C. Heinze, J. May, J. Peters, J. Ströhle, B. Epple, *Fue*l, **250** (2019), 285–291.
53. L. Liu, Y. Cao, Q. Liu, J. Yang, *RSC Advances*, **7** (2017), 2193–2201.
54. X. Shenqi, Z. Zhijie, X. Jie, Y. Guangsuo, W. Fuchen, *Fue*l, **90** (2011), 1723–1730.
55. R.H. Hurt, A.F. Sarofim, J.P. Longwell, *Fue*l, **70** (1991), 1079–1082.
56. J. Kopyscinski, R. Habibi, C.A. Mims, J.M. Hill, *Energy & Fuels*, **27** (2013), 4875–4883.
57. J. Kopyscinski, M. Rahman, R. Gupta, C.A. Mims, J.M. Hill, *Fue*l, **117** (2014), 1181–1189.
58. S. Kudo, Y. Hachiyama, H.-S. Kim, K. Norinaga, J. Hayashi, *Energy & Fuels*, **28** (2014), 5902–5908.
59. J. Tang, X. Wu, J. Wang, *Fue*l, **141** (2015), 46–55.
60. F. Zhang, M. Fan, X. Huang, M.D. Argyle, B. Zhang, B. Towler, Y. Zhang, *Fuel Processing Technology*, **161** (2017), 145–154.
61. S.K. Bhatia, D.D. Perlmutter, *AIChE Journal*, **26** (1980), 379–386.
62. S. Kajitani, N. Suzuki, M. Ashizawa, S. Hara, *Fue*l, **85** (2006), 163–169.
63. A. Tremel, H. Spliethoff, *Fue*l, **107** (2013) 653–661.
64. K. Zubek, G. Czerski, S. Porada, *Energy & Fuels*, **32** (2018) 5684–5692.
65. Y. Zhang, S. Hara, S. Kajitani, M. Ashizawa, *Fue*l, **89** (2010), 152–157.
66. T. Liliedahl, K. Sjöström, *Fue*l, **76** (1997), 29–37.
67. K. Umeki, A. Moilanen, A. Gómez-Barea, J. Konttinen, *Chemical Engineering Journal*, **207–208** (2012), 616–624.
68. K. Miura, K. Hashimoto, P.L. Silveston, *Fue*l, **68** (1989), 1461–1475.
69. B. Bayarsaikhan, J. Hayashi, T. Shimada, C. Sathe, C.Z. Li, A. Tsutsumi, T. Chiba, *Fue*l, **84** (2005), 1612–1621.
70. Z.F. Zahara, S. Kudo, Daniyanto, U.P.M. Ashik, K. Norinaga, A. Budiman, J. Hayashi, *Energy & Fuels*, **32** (2018), 4255–4268.
71. D.P. Ye, J.B. Agnew, D.K. Zhang, *Fue*l, 77 (1998), 1209–1219.
72. B.B. Beamish, K.J. Shaw, K.A. Rodgers, J. Newman, *Fuel Processing Technology*, **53** (1998), 243–253.
73. J. Hayashi, H. Takahashi, M. Iwatsuki, K. Essaki, A. Tsutsumi, T. Chiba, *Fue*l, **79** (2000), 439–447.
74. T. Kitsuka, B. Bayarsaikhan, N. Sonoyama, S. Hosokai, C.Z. Li, K. Norinaga, J. Hayashi, *Energy & Fuels*, **21** (2007), 387–394.

Chapter 2
Quantitative Description of Catalysis of Inherent Metallic Species in Lignite Chars during CO_2 Gasification

2.1 Introduction

Gasification of lignite is a platform for the production of power, fuels, and chemicals, or their co-production. [1,2] Its efficiency, in terms of chemical energy recovery, is maximized by maximizing the utilization of endothermic gasifying agents such as steam and CO_2. [3–5] The advantage of CO_2 over steam is the omission of heat for vaporization, while the disadvantage is the lower reactivity. Inherent catalyst species with sufficient content neutralize the disadvantage. Many Indonesian lignites are rich in alkali and alkaline earth metallic species (Na and/or Ca) and also a transition metal (Fe), major portions of which are in the form of organically-bound cations. [6,7]

The quantitative description of the char gasification kinetics, which is the rate-determining step of the lignite-to-syngas conversion, is vital for the design and optimization of a gasifier. Previous studies have recently developed a kinetic model that assumes parallel progress of non-catalytic gasification and catalytic gasification of char, along with catalyst generation and deactivation. [8,9] This model has been applied successfully to describing the kinetics of steam and CO_2 gasification over entire ranges of char conversion up to 0.999 or even higher for chars from various types of lignites or biomass. [8–10] It has been demonstrated that inherent Na, K, Ca, and Fe species play important catalytic roles, and moreover, strongly suggested that different catalytic species undergo deactivation at different rates while interacting with one another. On the other hand, participation of Mg species in catalysis and catalyst activation/deactivation has been left unknown. [9,10]

To better understand the catalysis of metallic species, it is effective to prepare a sufficient number of char samples that contain metallic species at various concentrations. There are three different approaches to achieve this purpose. One is to remove metallic species from original lignite by leaching with aqueous solutions of strong acids such as HCl and HF, and then dope fresh metallic species as catalyst precursor. [11–15] However, this approach may not well represent the original mode of occurrence of the target metallic species present inherently in

the original lignite. Another approach is to employ a wide range of original lignites with or without acid washing. [9,16,17] The third approach is to sequentially remove metallic species by washing with increasingly aggressive acids or ion-exchanging reagents, *i.e.*, water, ammonium acetate (NH_4OAc), HCl, and then HF. This approach is useful in chemical fractionation analysis. [18,19] Preparation of a variety of samples from a parent lignite ensures the intrinsic reactivities of resulting chars are fixed. More importantly, such sequentially washed lignite samples contain inherent metallic species with different concentrations and/or chemical types such as water-soluble, ion-exchangeable, acid-soluble and acid-insoluble. [20–24]

The present authors investigated CO_2 gasification of chars from two series of original and sequentially washed Indonesian lignites that were prepared by removing the inherent metallic species sequentially with deionized water, NH_4OAc, HCl, and HF at various concentrations. This study reports that the catalytic/non-catalytic parallel reaction model successfully describes the kinetics of gasification of 20 lignite chars over a wide range of concentrations/forms of metallic catalyst species. It is also reported that the initial activity and subsequent deactivation of catalyst can be described by functions of the composition of metallic species.

2.2 Experimental

2.2.1 Lignite samples and sequential washing

Two Indonesian lignites, A and B, were used as the starting samples. These were dried partially at room temperature, pulverized to particle sizes smaller than 106 μm, and then dried at 60°C under vacuum until the moisture content decreased to *ca*. 5 wt%. The samples were further pulverized by ball milling for 10 h in a pot mill. Zirconia balls (diameter: 9.5–10 mm) were used for the milling. It was confirmed that the ball milling reduced the particle sizes to < 10 μm (see **Appendix 1**). The finely pulverized lignites A and B, which are hereafter referred to as A0 and B0, respectively, were subjected to the sequential washing. **Table 2.1** shows the properties of A and B.

A flow chart of the sequential washing is presented in **Figure 2.1**. Briefly, *ca*. 6 g of A0 or B0 was washed with 0.12 L of deionized water (resistivity ≥18.2 MΩ cm) in a plastic beaker. The lignite/water slurry was heated at 65°C for 24 h while stirred continuously. The washed lignite was separated from the water by vacuum filtration and then washed with other 1–3 L of deionized water repeatedly until no chlorine ion was detected in the filtrate. A portion (*ca*. 1 g)

of the water-washed lignite (A1 or B1) was vacuum-dried at 60°C, while the other (*ca*. 5 g) was washed with 0.1 L of 1 M NH_4OAc aq. A portion of the NH_4OAc aq.-washed lignite (A2 or B2) was washed sequentially with 3M HCl aq. for recovering A3 or B3, with 3 M HF aq. for A4 or B4, and then with 6 M HCl aq. for A5 or B5. A2 and B2 were also subjected to washing with 1 M NH_4OAc aq. once or twice for preparing A2-2/B2-2 or A2-3/B2-3, respectively. Such repeated washing was performed to remove ion-exchanged metallic species. A2 and B2 were also washed with 0.01 M HCl aq. or with 0.1 M HCl aq. for A2-H2/B2-H2 or A2-H1/B2-H1, respectively, to investigate the effect of pH of acidic solution on the removal of metallic species. For each washing, the ratios of solution volume to dry lignite mass were fixed at 20 ml/g, and the washing temperature and time were systematically at 65°C and 24 h, respectively. 10 samples were thus prepared from each lignite. **Table 2.2** shows the ash contents of the samples.

2.2.2 Quantification of metallic species

The contents of K, Na, Mg, Ca, and Fe in the individual samples were measured referring to previous reports. [25–27] In brief, each sample was ashed carefully and completely by heating in the air with a rate, holding temperature and holding time of 1 °C/min, 620°C, and 60 min, respectively. The lignite mass subjected to the ashing was 37±4 and 370±40 mg for A0–A2/B0–B2 and the others, respectively. The resulting ash was digested in an equivolume mixture of 1 M HF and 1 M HNO_3 at 60°C for 16 h. The acids and water were then evaporated at 120°C. The residue was dissolved in 4 mM aqueous solution of methanesulfonic acid, and analyzed by ion chromatography for K, Na, Mg, and Ca or by inductively coupled plasma-optical emission spectroscopy for Fe. Details of the analysis were reported elsewhere. [10]

2.2.3 Pyrolysis and gasification

Char samples were prepared from the individual lignite samples in a general way. [28,29] The fixed bed of lignite (0.5–1 g) was set in a horizontal quartz tube reactor, heated in an atmospheric flow of N_2 (purity; > 99.999 vol%, flow rate; 300 mL/min) at 30 °C/min to 600°C with a holding time of 15 min. The char from the pyrolysis was heated at a rate of 30 °C/min to 900°C and then gasified in a thermogravimetric analyzer (TGA; Hitachi Hi-Tech Science, model SII TGA/DTA 7200) with the total gas flow rate of 700 mL/min (50 vol% CO_2/N_2 flow). Details of the procedure for the gasification were reported previously. [9,10] The initial mass of char was a critical factor for eliminating the effects of heat and mass transfer, and its effect on the kinetics of gasification was examined preliminarily. Results are reported in **Appendix**

2. In summary, it was necessary to choose the initial mass as small as 1 mg for the chars from A0–A2 and B0–B2, which underwent fast gasification. Since the reactivities of the chars from A3–A5 and B3–B5 are much lower, the initial mass of these chars was 1–2 mg in order to obtain a reasonable DTG curve. Reproducibility of the above gasification conditions, which had been confirmed previously for steam and CO_2 gasification, [9,30] was successfully examined in the preliminary experiments.

2.2.4 X-ray diffractometry

Inorganic species in A0 and B0 chars with mass-based char conversions of 0%, 80%, and 100% were characterized by X-ray diffractometry (XRD). It was performed on a powder X-ray diffractometer (Rigaku, model TTRIII) applying Cu Kα radiation, a 50 kV tube voltage, a 300 mA tube current, and a scan rate of 0.5 °/min over a 2θ range of 15–65°. Specific compounds were identified by a general method, referring to International Centre for Diffraction Data. The char/ash samples were prepared by collecting the residue from several gasification experiments in TGA under the same condition.

2.2.5 Kinetic analysis

The kinetics of char gasification was analyzed by a model that has been developed by the present authors. [8-10] This model assumes progress of non-catalytic and catalytic gasification in parallel. The following equation describes the overall rate of gasification as a function of char conversion on the basis of the mass of carbonaceous portion, *X*.

$$\frac{dX}{dt} = k_{\mathrm{nc}}(1 - X) + k_{\mathrm{c}} \qquad (1)$$

k_{nc} and k_{c} are the rate constants for the non-catalytic and catalytic gasification, respectively, which obey first-order and zeroth-order kinetics with respect to the unconverted fraction of char. [8,26,27,31–33] The model also assumes the followings.

- The initial activity and rate of deactivation of the catalyst(s) distribute over wide ranges that are described quantitatively in a discrete manner by lumping various catalysts into four types (C*n*; *n* = 1 – 4). This number is necessary to describe the d*X*/d*t vs X* for all the chars and over the entire ranges of *X* as shown later. However, C*n* does not represent any specific elements (*i.e.*, K, Na, Ca, and Fe) individually.
- The presence of precursor ($C1_{\mathrm{prec}}$) that is transformed into C1.

The following equations, Equations 2–7, are details of Equation 1 and definitions of amounts (m_{Cn}) and concentrations of the catalysts (C_{Cn}) and C1 precursor (C_{C1prec}). More details of the model and kinetic equations were reported elsewhere. [9,10]

$$k_{\mathrm{c}} = \sum_n k_{\mathrm{Cn}} \quad (2)$$

$$k_{\mathrm{Cn}} = k'_{\mathrm{C}} m_{\mathrm{Cn}} \quad (3)$$

At $t = 0$, $k_{\mathrm{Cn}} = k_{\mathrm{Cn,0}} = k'_{\mathrm{C}} m_{\mathrm{Cn,0}}$, where k'_{C} is a rate of constant that defined to be common among C1–C4, and $\Sigma_n\, m_{\mathrm{Cn}} + m_{\mathrm{C1prec}} = \Sigma_n\, m_{\mathrm{Cn,0}} + m_{\mathrm{C1prec,0}} = 1$. The dynamic concentration of catalysts during char gasification is defined by:

$$\frac{dm_{\mathrm{C1,prec}}}{dt} = -k_{\mathrm{C1prec}} C_{\mathrm{C1prec}} \quad (4)$$

$$\frac{dm_{\mathrm{C1}}}{dt} = k_{\mathrm{C1prec}} C_{\mathrm{C1prec}} - k_{\text{loss-1}} C_{\mathrm{C1}} \quad (5)$$

$$\frac{dm_{\mathrm{Cn}}}{dt} = -k_{\text{loss-n}} C_{\mathrm{Cn}} \quad (n = 2\text{–}4) \quad (6)$$

$$C_{\mathrm{C1prec}} = \frac{m_{\mathrm{C1prec}}}{1 - X} \text{ and } C_{\mathrm{C1}} = \frac{m_{\mathrm{C1}}}{1 - X} \quad (7)$$

From the above equations, the following parameters for the overall initial catalytic activity and the overall initial rate of catalyst deactivation are derived.

$$\text{ICA-1} = \sum_n k_{\mathrm{Cn,0}} = \sum_n k'_{\mathrm{Cn}} m_{\mathrm{Cn,0}} \quad (8)$$

$$\text{ICA-2} = \sum_n k_{\mathrm{Cn,0}} + k'_{\mathrm{C}} m_{\mathrm{C1prec,0}} = k'_{\mathrm{C}} \quad (9)$$

$$\text{ICD-1} = \sum_n k_{\text{loss-n,0}}\, C_{\mathrm{Cn,0}} \quad (10)$$

$$\text{ICD-2} = k_{\text{loss-1,0}}\left(C_{\mathrm{C1,0}} + C_{\mathrm{C1prec,0}}\right) + \sum_n k_{\text{loss-n,0}}\, C_{\mathrm{Cn,0}} \quad (11)$$

ICA-1 represents the overall catalytic activity at $t = 0$, while ICA-2 involves the potential activity of C1. ICD-1 and ICD-2 are the overall rates of catalyst deactivation at $t = 0$, corresponding to ICA-1 and ICA-2, respectively. It is believed that the char contains various types of catalysts of that initial activity and deactivation kinetics distribute continuously over a wide range. The present kinetic model represents such continuous distribution by a discrete one. [9,10] Details of the method for optimizing the kinetic parameters were reported elsewhere. [9,10]

2.3 Results and Discussion

2.3.1 Occurrence of inherent metallic species

Table 2.2 presents the ash contents of the lignite samples. The ash contents of the lignites A and B decrease in manners similar to each other. Taking the A*n* series as an example, the difference between A0 and A1 and that between A1 and A2 were arisen from water-soluble salts and ion-exchangeable (organically bound) cations, respectively. It was suspected that the

organically-bound cations had not been exchanged by NH_4^+ ions completely. [34] A2 and B2 were then washed repeatedly with fresh 1 M NH_4OAc aq. according to a report by Matsuoka *et al*. [34] However, the ash content was decreased only slightly by the second and third washings. The A2–A3 difference is normally attributed to metallic species in forms of oxides, carbonates, sulfates, and/or sulfides. [35–37] However, as mentioned later, it was suspected that a limited portion of the organically-bound cations was removed with 1 M NH_4OAc aq. even by the repeated washing. It was believed that the A3 and A4 difference was due to silica, alumina, and aluminosilicates that were insoluble in HCl aq. but soluble in HF aq. The ash content of A5 was very low but not zero. The washing with 6 M HCl aq. left trace amount of ash-forming species, which were probably encapsulated in the organic matrix and therefore inaccessible to the aqueous media. [20,36]

Figure 2.2 displays the cumulative concentrations of five metallic species (Na, K, Mg, Ca, and Fe) in the original lignites that were leached at different stages. The cumulative concentrations of all the five metallic species agree well with those in the original lignites as determined by a sequence of ashing, its dissolution in HNO_3/HF aq. and ion-chromatography analysis. These data demonstrate that the sequential leaching and analysis were performed with sufficiently high accuracy.

Figure 2.2 also shows five important features that are reported below. *First*, both lignites contained very little amounts of Na and K. These consisted mainly of water- and NH_4OAc-solubles, in other words, salts (chlorides), and organically-bound cations. *Second*, Mg and Ca were much more abundant than Na and K and also mostly in the form of either water-soluble salts, organically-bound cations or 3 M HCl aq.-soluble. It was believed that water-soluble Mg and Ca species originated from those dissolved in the inherent pore water. [37–39] *Third*, major portions of Ca species were NH_4OAc aq.-insoluble but 3 M HCl aq.-soluble. Matsuoka *et al*. reported that even repeated leaching with NH_4OAc aq. could not remove Ca from lignite completely, while it removed a portion of Ca species in the form of minerals such as calcite. [34] It was thus suspected that more or less amount of organically-bound Ca remained in A2 and B2. As reported in the above, A2 and B2 were washed with 1 M NH_4OAc aq. repeatedly, but, additional leaching of Ca was insignificant (see **Appendix 3**). Then, A2 and B2 were washed with 0.01 M HCl aq. ($pH \approx 2$) and 0.1 M HCl aq. ($pH \approx 1$). The Ca-leaching ability of the 0.01 M HCl aq. was equivalent to that of the 1 M NH_4OAc aq. (see **Appendix 3**). On the other hand, the washing with the 0.1 M HCl aq. removed a major portion (*ca*. 80%) of NH_4OAc aq.-insoluble/3 M HCl aq.-soluble Ca (see **Appendix 3**). According to general knowledge, [35–37] these results are explained by that substantial portions of Ca in the lignites A and B were

in chemical forms of oxides, carbonates, sulfates, and/or sulfides. These minerals normally exist as particulate matter with insignificant catalytic activity. It was, therefore, suggested that a major portion of the 0.01 M HCl aq.-insoluble/0.1 M HCl aq.-soluble Ca was organically-bound. As reported later, this suggestion was consistent with the significant differences in the catalytic activity between A2-H2 and A2-H1 chars and also B2-H2 and B2-H1 chars. *Fourth*, the lignites A and B were much different from each other regarding Fe content. The lignite A contained Fe with a content of 1,150 ppm-wt on a dry lignite basis, a major portion of which was NH_4OAc aq.-insoluble but 3 M HCl aq.-soluble. On the other hand, the Fe content in the lignite B was negligibly small. *Fifth*, the sequential washing with 3 M HF aq. and 6 M HCl aq. removed almost entire portions of metallic species from the lignites A and B, leaving trace amounts of Na, K, Mg, Ca and Fe at total concentrations of 99 and 96 ppm-wt, respectively.

As reported above, the sequential washing enabled to prepare a range of samples with various compositions of 'remaining' inherent metallic species. For expedience, A0–A2 and B0–B2 samples were classified into H group while the others into L group according to the metallic species concentration and the char reactivity with CO_2, as shown later.

Figure 2.3 shows the char yields from the individual lignite samples on a dry-and-ash-free (daf) basis. The pyrolysis of the L-group lignites gave char yields systematically lower by 1–3 wt%-daf than those from the H-group lignites, which was more than the experimental error within ± 0.1 wt% daf that preliminary examined. [9] This trend was explained by the removal of organically-bound cations, which played a role of chemical cross-links and also a catalytic role of cross-linking during pyrolysis, causing the char yield increase. [8,40,41] It is also known that mineral particles have no significant catalytic effects on the char yield. This suggested that a substantial portion of the NH_4OAc aq.-insoluble/3 M HCl aq.-soluble metallic species were organically-bound cations, although a main reason for 'NH_4OAc aq.-insoluble' was unknown.

2.3.2 Overview of characteristics of char gasification

Figure 2.4 presents the relationship between the rate of gasification, dX/dt, and X. The initial dX/dt for the H-group chars and L-group chars are differing by 1–2 orders of magnitude reflecting that the chars from H-group lignites underwent faster gasification than that from L-group chars. It was thus clear that the inherent metallic species played catalytic roles in the gasification. In addition, the dX/dt for the A5 and B5 chars are lower than those for any other chars over the entire range of X. It was difficult to exactly determine the rate of non-catalytic gasification experimentally, because the removal of metallic species was nearly but not fully complete. It was, however, reasonable to approximate the rate by that for the gasification of

the A5 and B5 chars which had the lowest contents of metallic species. In fact, the initial dX/dt's for the A5 and B5 chars are as small as 1% of those for the A0 and B0 chars, respectively. Estimation of the rate of non-catalytic gasification will be discussed later.

It is seen in **Figures 2.4** that the dX/dt's for the L group chars are in the order of A5 < A4 < A3 and B5 < B4 < B3. Those chars had very low contents of metallic species, as shown in **Appendix 3**. However, such a trace amount of remaining metallic species had catalysis in the gasification. It is also noted that the dX/dt's for the A3–A4 and B3–B4 chars change via maxima. Increases in dX/dt are primarily due to the overall catalytic activity and also interpreted by the present kinetic model as a transformation of the C1 precursor to C1 catalyst. On the other hand, the dX/dt's for the A0–A2 and B0–B2 chars decrease monotonously with X. This trend is explained by the absence of the C1 precursor, or otherwise, the overall rate of catalyst deactivation was greater than that of the C1 catalyst generation.

2.3.3 Definition of rate of non-catalytic gasification

As shown in **Figure 2.2**, the sequential leaching finally reduced the total concentration of metallic species in A5 and B5 to < 100 ppm-wt-dry lignite. In consideration of difficulty in further removal of the metallic species, it was necessary to reasonably define the rate of non-catalytic gasification. Recent studies on steam gasification and CO_2 gasification of char strongly suggested that non-catalytic gasification of chars from lignite and biomass, *i.e.*, that in the absence of metallic species follows first-order kinetics with respect to unconverted fraction of char. [9,10,27]

Figure 2.5 exhibits profiles of dX/dt vs X and specific rate of char conversion vs X for the gasification of the A5 and B5 chars. The specific rate, r_{sp}, is defined by

$$r_{sp} = (\mathrm{d}X/\mathrm{d}t)/(1 - X) \qquad (12)$$

As seen in the graphs (a1) and (b1), neither of the gasification of A5 char nor that of B5 char followed first-order kinetics. It rather seemed that the dX/dt as a convex function of X, was contributed by the catalytic gasification. It is also seen in the graphs (a2) and (b2) that r_{sp} increases steeply at $X > 0.8$ and $X > 0.7$, respectively. These trends are attributed to the catalysis of metallic species that remained in A5 and B5 chars, and interpreted as follows.

- The residual metallic species were dispersed in the char matrix at an atomic or similar scale (as cations chemically and directly bonded to the carbonaceous structure of char), and therefore, had insignificant catalysis.

- The progress of gasification increased the concentration of those metallic species, and finally beyond a 'loading saturation level (LSL)' inducing the formation of clusters or nano-sized particles that had catalysis. [42]

Based on the above discussion, it was then assumed that the non-catalytic gasification occurred with k_{nc} = 0.0035 min^{-1} for both A5 and B5 chars, because it was certain that k_{nc} was equivalent to the initial dX/dt, or otherwise, smaller.

2.3.4 Results of kinetic analysis

Figure 2.6 shows measured and calculated (1–X) vs t profiles for the gasification of all the chars (except A5 and B5). The kinetic model describes the time-dependent changes in the char conversion quantitatively over its range up to 0.999 by optimization of the kinetic parameters. The optimized kinetic parameters and dX/dt vs X profiles (measured and calculated) are presented in **Table 2.3** and **Figure 2.7**, respectively. It is seen in **Figures 2.6** that the chars from H-group lignites underwent very fast gasification, and the char conversion was completed within 11 min and 6 min for the lignites A and B, respectively. On the other hand, the L-group chars were gasified very slowly. It took 200–500 min to complete the conversion. In addition, the gasification rate of A2 and B2 chars are considerably higher than those of A2-H1 and B2-H1 chars, respectively. The difference indicates that the 1 M NH_4OAc-insoluble and 1 M HCl-soluble metallic species shown catalytic activity and thus are categorized as the organically-bound catalyst.

Figure 2.8 shows the distribution of the initial catalytic activity (ICA-2), in other words, the initial-activity-based abundances of the catalytic components. The assumption of four catalytic components (*i.e.*, C1–C4) together with C1prec was necessary for drawing (1–X) vs t curves over the range of X up to 0.999 for the A0–A2 and B0–B2 chars. On the other hand, assuming only C1, C2, and C1prec were sufficient for the A3–A4 and B3–B4 chars. It is seen that C1 and C2 accounted for the major portion of the initial catalytic activity that is given by ICA-2. C3 and C4 were minor components, but necessary for describing the time-dependent change in the char conversion at X > 0.9.

Figure 2.9 presents the normalized initial composition of catalysts, showing two features of C1prec. First, C1prec accounts for only 0.5–10% of ICA-2 for the H-group A chars (A2-2, A2-3, A2-H2, and A2-H1), and also 0.6–14% for the H-group B chars. Second, on the other hand, C1prec accounts for 81–83% and 80–92% for the L-group A and B chars, respectively. The kinetic model recognizes that C1prec consists of metallic species that are dispersed in the carbon matrix of char at an atomic or similar scale, having insignificant catalytic activity. [43]

For a discussion of the variety of C_{C1prec}, its activity-based concentration ($k'_C C_{C1prec}$) is plotted against the total concentration of metallic species ($\Sigma C_{M,0}$) in **Figure 2.10(a)**. $k'_C C_{C1prec}$ increases through the maximum at $\Sigma C_{M,0}$ = 0.1–0.3 mol/kg-daf-char. This trend is explained by a concept shown in **Figure 2.10(b)**. The carbon matrix of char has an ability to 'dissolve' metallic species dispersing those at an atomic or similar scale. When $\Sigma C_{M,0}$ is sufficiently low (Region I), the entire portion of the metallic species is dissolved, and then its concentration (C) increases linearly with $\Sigma C_{M,0}$. In Region II, a further increase in $\Sigma C_{M,0}$ causes the metallic species undergo super-saturation and then precipitation, in other words, transformation into catalyst. This event is often called nucleation. The formed catalyst grows in size by incorporating the precursor as well as by agglomeration and coalescence. The progress of such catalyst growth may cause C decrease below the solubility (Region III). It is believed that the decrease in $k'_C C_{C1prec}$ at higher $\Sigma C_{M,0}$ is due to the incorporation of precursor into the performed catalyst during the pyrolysis. Although it is difficult to define the solubility of metallic species experimentally, it is estimated to be in the region indicated by the gray-colored belt in **Figure 2.10(a)**. Thus, the trends seen in **Figure 2.10(a)** are explained qualitatively by a generally known sequence of saturation (or super-saturation) of dissolved metallic species, nucleation (precipitation) and particles growth. An indication of the catalyst growth during gasification had been shown by Kim *et al*. [8] They performed steam gasification of Ca-loaded lignite char with the initial Ca concentration of 4.1 g-Ca/100 g-char at different conversion level and then characterized the resulting chars with energy dispersive X-ray spectrometry. They observed the increase in particle sizes of Ca-rich phase with the progress of gasification and corresponding deactivation of Type-1 catalyst (the one contributed to rapid char conversion in the early stage of gasification). It is believed that such a mechanism was followed by the present inherent catalyst, which mainly consisted of Ca species.

Figure 2.11 gives calculated contribution of catalytic gasification, α_{cg}, to the overall rate of char gasification, *i.e*., dX/dt. For the H-group chars, α_{cg} is 98–100% over the entire range of X. This demonstrates how the catalytic gasification was important in the gasification of the A and B chars of the H group. On the other hand, for the L-group chars, α_{cg}'s are quite small at the early stage (e.g., X < 21% for A3 char, and X < 11% for A4 char), but increase finally to 90% or even greater with the progress of gasification. Such a significant increase is explained by the transformation of C1prec into C1 catalyst.

2.3.5 Further analysis of ICA-2

Toward quantitative understanding of ICA-2, its relationship with the metallic species content is discussed. **Figure 2.12** plots ICA-2's for all the A and B chars (except A5 and B5) against the total concentration of Na, K, Ca, and Fe in the chars (see **Appendix 3**). Mg was not involved in the candidates of the inherent catalyst from the following three reasons. First, some previous studies investigated catalysis of organically bound Mg in steam gasification of char, but found no or insignificant activity. [44–46] Second, catalysis of Mg seemed to be implausible from a thermodynamic point of view. A table in **Appendix 4** lists chemical reactions involving carbon (C), CO_2, CO and metallic species (metal, oxides, and carbonates) together with Gibb's free energies (ΔG's) at 900°C. ΔG's of carbonation of MgO and further reduction by C are both greatly positive, indicating the difficulty of both carbonate-oxide and oxide-metal cycles. On the other hand, for Ca, carbonate-oxide cycles seem to be possible. It is also suggested for Na and K that the carbonates were the major species under the present experimental conditions. Third, the correlation factor (r^2) for **Figure 2.12(a)**, 0.95, was greatly reduced by involving the Mg concentration in $\Sigma C_{M,0}$.

As indicated by Line A, ICA-2 is a linear function of $\Sigma C_{M,0} = C_{Na,0} + C_{K,0} + C_{Ca,0} + C_{Fe,0}$ with a correlation factor (r^2) of 0.95, which is common between the A and B chars. This is consistent with catalysis of Na, K, Ca, and Fe. Trial-and-error was made for further improvement of r^2, and it was found that weighting the Fe concentration by a factor of 1.8 maximized r^2 at 0.965 as indicated by Line A', leaving the factors for Na, K, and Ca at 1.0. Varying the factor for either of these three species brought about negligible improvement of r^2. It was difficult to evidence the higher initial activity of Fe (per molar concentration) than the other three.

Haga *et al*. [47] investigated catalysis of single, binary and ternary metallic species (Na, Ca, and/or Fe) on steam-hydrogen and CO_2 gasification of activated carbon. They found positive synergistic effects of co-existence of two or three metallic species on the catalytic activity. For example, the activity of Ca/Fe catalysts was greater than that calculated by assuming additivity of the activities of Ca and Fe single catalysts by a factor of about two. Similar synergistic effects were found for Na/Fe and Na/Ca binary systems. Such synergistic effects were likely to occur under the present conditions. Although examination of such effects was difficult due to difficulty in controlling the composition of metallic species, it was reasonable that $\Sigma C_{M,0}$ and $\Sigma C'_{M,0}$ already involved positive synergistic effects among the four metallic species, as a result.

It is also noted in **Figure 2.12** that the catalyst activity on a molar basis, which is evaluated by $\Delta(\text{ICA-2})/\Delta(\Sigma C_{M,0})$, is much greater at lower $\Sigma C_{M,0}$ (up to 0.023 mol/kg-daf-char) than at higher $\Sigma C_{M,0}$. ICA-2 is thus presented by a piecewise linear function of $\Sigma C_{M,0}$, which is divided into three regimes; Regime I ($\Sigma C_{M,0}$ < 0.008 mol/kg-daf-char), Regime II (0.008–0.023) and Regime III (0.023–0.37). This particular type of function is explained reasonably by a nucleation-growth mechanism that is already mentioned. The piecewise linear function of $\Sigma C'_{M,0}$ is schematically shown in **Figure 2.13**.

Regime I

- The catalyst concentration is extremely low.
- The major portion of metallic species is present as C1prec with little or no catalytic activity.

Regime II

- C1prec has been transformed into C1 near completely.
- The catalyst consisted of highly active clusters (but, their sizes are unknown).

Regime III

- The catalyst has already undergone growth in size and to nano-sized particles consuming clusters by their coalescence.
- No significant change occurs in the size of catalytic particles.

Choi *et al*. [48] investigated the effect of SiO_2 on the catalytic activity of inherent metallic species in a lignite char. They claimed that the inherent metallic species (Na, Ca, and Fe) underwent deactivation during the pyrolysis by irreversible reactions with SiO_2, while such reactions were not important during the subsequent CO_2 gasification of the resulting char. [48] Byambajav *et al*. [9] and Zahara *et al*. [10] analyzed the kinetics of CO_2 gasification of chars from lignites and sugarcane bagasses, respectively, by the same kinetic model as employed in the present study. Their results strongly suggested partial deactivation of inherent metallic species during the pyrolysis but not during the subsequent gasification. It was thus likely under the present conditions that more or less portions of Na, K, Ca, and Fe species reacted with SiO_2 during the pyrolysis. To examine this suggestion, the relationship between ICA-2 and $\Sigma C_{M,0} = C_{Na,0} + C_{K,0} + C_{Ca,0} + C_{Fe,0}$ for the CO_2 gasification of chars from the Indonesian lignites (present work), Mongolian lignites, [9] and sugarcane bagasses [10] are compared in **Figure 2.14**. ICA-2 for the A and B chars is clearly greater than those for the chars from the Mongolian lignites (MLs) and sugarcane bagasses (SCBs). [9,10] The chars from MLs and SCBs contained SiO_2 and Al_2O_3 with total contents of 6–43 and 12–23 wt%-daf-char, respectively. These were

much more than those in the present chars ranging 1.0–3.5 wt%-daf-char. For the chars from MLs and SCBs, it was believed that SiO_2 and Al_2O_3 reacted with Na, K, Ca, and Fe to more or less extent during the pyrolysis and deactivated these metallic species. It was therefore necessary to consider the negative effects of the abundance of SiO_2 and Al_2O_3 in order to achieve a linear correlation between ICA-2 and $\Sigma C_{M,0}$. [9,10] On the other hand, in the present study, such consideration was not necessary, which is supported by the highly linear relationship between ICA-2 and $\Sigma C'_{M,0}$ in **Figure 2.12**.

2.3.6 Analysis of ICD-2

Figure 2.15 plots the overall rate constant for catalyst deactivation (ICD-2) with ICA-2 for the A and B chars. According to previous findings, a linear relationship was confirmed between these two kinetic parameters. [8–10,26,31] It is clear for each series of chars that more active catalyst underwent more rapid deactivation. This trend is in broad agreement with the previous studies. [8–10,26,31] It is, however, noted that ICD-2 increases with ICA-2 in non-linear manners, and also that ICD-2's for the A and B chars are clearly different functions of ICA-2.

Zahara *et al*. [10] investigated the relationship between ICD-2 and ICA-2 for 12 types of chars from 6 pairs of original and water-washed sugarcane bagasses, and proposed the following functions.

$$\text{ICD-2} = \frac{\text{ICA-2}}{k_{nc}} F \tag{13}$$

$$F = \frac{f_{Na}C_{Na} + f_K C_K + f_{Ca}C_{Ca} + f_{Fe}C_{Fe}}{C_{Na} + C_K + C_{Ca} + C_{Fe}} \tag{14}$$

They successfully found a single and linear relationship between ICD-2 and (ICA-2/k_{nc})·F by assuming $f_{Na} = f_K = f_{Ca} = 1$ and $f_{Fe} = 5.1$, for example. These combinations of f_M (M = Na, K, Ca or Fe) suggested a faster deactivation of Fe catalyst than the others, or otherwise, promotion of deactivation of K, Na, and Ca by their interaction with Fe catalyst. Following the report by Zahara *et al*. [10], the present authors introduced the following function of ICA-2.

$$\text{ICD-2} = \text{ICA-2} \cdot F \tag{15}$$

$$F = \frac{f_{Na}C_{Na} + f_K C_K + f_{Ca}C_{Ca} + f_{Fe}C_{Fe} + f_{Mg}C_{Mg}}{C_{Na} + C_K + C_{Ca} + C_{Fe} + C_{Mg}} \tag{16}$$

The right side of Equation 15 does not involve k_{nc}, because there was no necessity. That of Equation 16 involves the concentration of Mg and its coefficient, C_{Mg} and f_{Mg}, respectively, in the right side. In the preliminary examination, Equation 14 was applied to the correlation of ICD-2 with ICA-2, but it was not successful. This result is shown in **Figure 2.16(a)**. It was

then found that the introduction of C_{Mg} and f_{Mg} made dramatic improvement of the linearity of ICD-2 and (ICA-2·F) relationship, as shown in **Figure 2.16(b)**. The optimized f_{Fe} and f_{Mg} were 3.5 and 4.9, respectively. This suggested that Mg had no or insignificant catalytic activity, but played a role of promoting deactivation of Na, K, Ca, and/or Fe catalysts. The promotion of catalyst deactivation by Mg species is discussed later.

Equations 15 and 16 were also applied to the analysis of ICD-2 and ICA-2 reported by Byambajav *et al*. [9] and Zahara *et al*. [10] The contents of Na, K, Ca, Mg, and Fe in the initial chars were available. The results are shown in **Figure 2.17**. ICD-2 plots for Mongolian lignites [9] and those for Indonesian sugarcane bagasses [10] are on the same straight line in **Figure 2.16** or around it. Thus, within the range of the present study and the two previous studies, Equations 15 and 16 are applicable to the quantitative description of ICD-2 as a function of ICA-2 and composition of metallic species including not only Na, K, Ca, and Fe but also Mg.

2.3.7 Further discussion on the effect of composition of metallic species on catalyst deactivation

It is known that Fe catalyst undergoes more rapid deactivation during char gasification than Na, K, and Ca. [10,49] In this section, the main focus of the discussion is on the role of Mg species. From a thermodynamic point of view, both MgO and CaO can react with SiO_2 and be converted into silicates such as $CaSiO_3$ and $MgSiO_3$. These silicates can be further converted into composite oxides such as Ca_2SiO_4, Mg_2SiO_4, $CaMgSiO_4$, and $Ca_2MgSi_2O_7$. Then, in the presence of SiO_2, Mg oxides and silicates could provide more pathways to deactivate CaO. In fact, XRD of the ash from both A0 and B0 detected $CaMgSiO_4$ as well as $CaO/CaCO_3$ and MgO (see **Appendix 5**). However, as strongly suggested by recent studies by Byambajav *et al*. [9] and Zahara *et al*. [10], and then demonstrated by Choi *et al*. [48], such silicates formation was not important during the CO_2 gasification of char, probably due to sufficiently fast catalytic carbonate-oxide cycles of Ca.

Matsukata *et al*. [50] investigated catalytic and physical properties of Ca^{2+}-doped MgO. They prepared Ca^{2+}-doped MgO from calcium nitrate and basic magnesium carbonate as a catalyst for 1-C_4H_8 isomerization and also reverse water-gas shift reaction. They found that the doped Ca promoted the basicity of MgO while it was not transformed into $CaCO_3$. It was also found that Ca of another type of Ca^{2+}-doped MgO was in the form of CaO or $CaCO_3$ on the surface of MgO. Their results showed that the formation of $CaCO_3$, which is essential for the carbonate-oxide cycle, could be inhibited by chemical interaction with MgO. It was likely that nano-sized CaO had contact and interacted with MgO, losing its original catalytic activity.

The experimental demonstration of the inhibition of the carbonate-oxide cycles of Ca by Mg is discussed in **Chapter 3**.

Another possibility is that the promotion of growth in the size of $CaO/CaCO_3$ particles by their interaction with those of MgO. Alarcón *et al*. [51] investigated CaO/MgO composite catalysts for the steam reforming of naphthalene. They reported a slightly negative synergistic effect of CaO/MgO blending (when CaO was more abundant than MgO) on the surface of the composite particles. Such a negative effect could be promoted if MgO phase inhibited the contact between CaO phase and gasifying carbon matrix. It was, however, difficult to examine the formation of MgO/CaO composite particles as well as their sizes by transmission electron microscopy. Thus, the same as above, the examination of the effects of MgO/CaO interaction is discussed in **Chapter 3**.

2.4 Conclusion

The study investigated the kinetics of CO_2 gasification of the twenty chars with different composition of inherent metallic species which were prepared from two types of lignites. The following conclusions have been drawn from the kinetic analysis: (1) Time-dependent changes in the char conversion up to 0.999 were described quantitatively for all the 20 chars by the kinetic model that assumed the progress of non-catalytic and catalytic gasification in parallel and also multi-catalytic components. (2) The initial and overall catalytic activity, ICA-2, was a single piecewise linear function of the total concentration of Na, K, Ca, and Fe obeying a nucleation-growth mechanism that governed catalyst formation and deactivation. (3) The initial and overall rate of catalyst deactivation was described well by a single function of ICA-2 and the compositional factor;

$$F = (f_{Na}C_{Na} + f_{K}C_{K} + f_{Mg}C_{Mg} + f_{Ca}C_{Ca} + f_{Fe}C_{Fe})/(C_{Na} + C_{K} + C_{Mg} + C_{Ca} + C_{Fe}).$$

The optimized F showed fast deactivation of Fe catalyst and also a role of Mg species to promote the catalyst deactivation. This function, allowed to have some variety of f_M (M = Mg and/or Fe), successfully enabled to show the present ICD-2's and previously reported ICD-2's as the same function of (ICA-2)·F.

Table 2.1. Ultimate analysis of original lignites.

Lignite	Ultimate analysis (wt%, daf)				Ash content (wt%, db)
	C	H	N	O+S*	
A	70.3	5.0	0.8	24.0	2.6
B	67.5	4.5	1.1	26.9	5.0

*calculated by difference

Table 2.2. Ash contents of lignite samples.

Washing agent	Lignite A		Lignite B	
	ID	Ash content, wt% dry	ID	Ash content, wt% dry
none	A0	2.6	B0	5.0
deionized water	A1	2.6	B1	4.7
1 M NH_4OAc aq.	A2	2.1	B2	4.4
1 M NH_4OAc aq.	A2-2	1.9	B2-2	3.8
1 M NH_4OAc aq.	A2-3	1.8	B2-3	3.6
0.01 M HCl aq.	A2-H2	2.0	B2-H2	3.9
0.1 M HCl aq.	A2-H1	1.1	B2-H1	2.6
3 M HCl aq.	A3	0.8	B3	1.2
3 M HF aq.	A4	0.1	B4	0.1
6 M HCl aq.	A5	0.1	B5	0.1

Table 2.3. Lists of optimized kinetic parameters.

Sample ID	A0	A1	A2	A2-2	A2-3
$k_{ncg,}$ min^{-1}	3.5×10^{-3}	3.5×10^{-3}	3.5×10^{-3}	3.5×10^{-3}	3.5×10^{-3}
ICA-1, min^{-1}	3.6×10^{-1}	3.3×10^{-1}	3.0×10^{-1}	2.3×10^{-1}	2.3×10^{-1}
ICA-2, min^{-1}	3.6×10^{-1}	3.3×10^{-1}	3.1×10^{-1}	2.6×10^{-1}	2.5×10^{-1}
ICD-1, min^{-1}	2.5×10^{-2}	2.1×10^{-1}	2.0×10^{-1}	1.1×10^{-1}	1.1×10^{-1}
ICD-2, min^{-1}	2.5×10^{-1}	2.1×10^{-1}	2.1×10^{-1}	1.3×10^{-1}	1.3×10^{-1}
C_{C1prec} , -	4.5×10^{-3}	2.2×10^{-2}	5.0×10^{-2}	1.0×10^{-1}	9.0×10^{-2}
$C_{C1,0}$, -	5.4×10^{-1}	5.8×10^{-1}	6.7×10^{-1}	4.3×10^{-1}	4.3×10^{-1}
$C_{C2,0}$, -	3.1×10^{-1}	2.4×10^{-1}	1.7×10^{-1}	3.8×10^{-1}	3.9×10^{-1}
$C_{C3,0}$, -	1.3×10^{-1}	1.5×10^{-1}	8.9×10^{-2}	9.1×10^{-2}	9.4×10^{-2}
$C_{C4,0}$, -	2.1×10^{-2}	1.2×10^{-2}	2.0×10^{-2}	1.1×10^{-3}	7.0×10^{-4}
k_{C1prec} , min^{-1}	1.2×10^{-2}	6.0×10^{-1}	2.00	2.10	2.10
$k_{C1,0}$, min^{-1}	1.9×10^{-1}	1.9×10^{-1}	2.1×10^{-1}	1.1×10^{-1}	1.1×10^{-1}
$k_{C2,0}$, min^{-1}	1.1×10^{-1}	7.9×10^{-2}	5.3×10^{-2}	9.9×10^{-2}	9.9×10^{-2}
$k_{C3,0}$, min^{-1}	4.5×10^{-2}	5.1×10^{-2}	2.8×10^{-2}	2.4×10^{-2}	2.4×10^{-2}
$k_{C4,0}$, min^{-1}	7.5×10^{-3}	4.1×10^{-3}	6.3×10^{-3}	2.8×10^{-4}	1.8×10^{-4}
k_{loss-1} , min^{-1}	3.8×10^{-1}	3.2×10^{-1}	2.9×10^{-1}	2.1×10^{-1}	2.2×10^{-1}
k_{loss-2} , min^{-1}	1.3×10^{-1}	9.2×10^{-2}	3.7×10^{-2}	4.4×10^{-2}	4.7×10^{-2}
k_{loss-3} , min^{-1}	1.1×10^{-2}	1.2×10^{-2}	$1.2x\ 10^{-2}$	5.8×10^{-3}	5.8×10^{-3}
k_{loss-4} , min^{-1}	1.4×10^{-4}	2.0×10^{-3}	7.0×10^{-4}	1.0×10^{-4}	1.0×10^{-4}
Sample ID	A2-H2	A2-H1	A3	A4	A5
$k_{ncg,}$ min^{-1}	3.5×10^{-3}	3.5×10^{-3}	3.5×10^{-3}	3.5×10^{-3}	3.5×10^{-3}
ICA-1, min^{-1}	2.7×10^{-1}	1.1×10^{-1}	9.0×10^{-4}	4.3×10^{-4}	
ICA-2, min^{-1}	2.9×10^{-1}	1.2×10^{-1}	4.8×10^{-3}	2.5×10^{-3}	
ICD-1, min^{-1}	1.3×10^{-1}	4.0×10^{-2}	1.4×10^{-4}	2.4×10^{-5}	
ICD-2, min^{-1}	1.5×10^{-1}	4.4×10^{-2}	1.8×10^{-3}	7.5×10^{-4}	
C_{C1prec} , -	7.0×10^{-2}	7.5×10^{-2}	8.1×10^{-1}	8.3×10^{-1}	
$C_{C1,0}$, -	5.3×10^{-1}	6.3×10^{-1}	6.0×10^{-2}		
$C_{C2,0}$, -	2.9×10^{-1}	2.0×10^{-1}	1.3×10^{-1}	1.8×10^{-1}	
$C_{C3,0}$, -	1.1×10^{-1}	8.3×10^{-2}			
$C_{C4,0}$, -	1.2×10^{-3}	8.5×10^{-3}			
k_{C1prec} , min^{-1}	1.40	1.10	2.1×10^{-2}	2.4×10^{-2}	
$k_{C1,0}$, min^{-1}	1.6×10^{-1}	7.7×10^{-2}	2.9×10^{-4}		
$k_{C2,0}$, min^{-1}	8.5×10^{-2}	2.4×10^{-2}	6.2×10^{-4}	4.3×10^{-4}	
$k_{C3,0}$, min^{-1}	3.1×10^{-2}	1.0×10^{-2}			
$k_{C4,0}$, min^{-1}	3.5×10^{-4}	1.0×10^{-3}			
k_{loss-1} , min^{-1}	2.2×10^{-1}	5.8×10^{-2}	2.1×10^{-3}	8.8×10^{-4}	
k_{loss-2} , min^{-1}	4.9×10^{-2}	1.4×10^{-2}	1.5×10^{-4}	1.4×10^{-4}	
k_{loss-3} , min^{-1}	7.7×10^{-3}	3.8×10^{-3}			
k_{loss-4} , min^{-1}	1.0×10^{-4}	5.0×10^{-5}			

Table 2.3. Lists of optimized kinetic parameters. (cont.)

Sample ID	B0	B1	B2	B2-2	B2-3
$k_{ncg,}$ min^{-1}	3.5×10^{-3}	3.5×10^{-3}	3.5×10^{-3}	3.5×10^{-3}	3.5×10^{-3}
ICA-1, min^{-1}	4.8×10^{-1}	4.5×10^{-1}	3.8×10^{-1}	3.2×10^{-1}	3.1×10^{-1}
ICA-2, min^{-1}	4.8×10^{-1}	4.8×10^{-1}	4.2×10^{-1}	3.6×10^{-1}	3.4×10^{-1}
ICD-1, min^{-1}	2.3×10^{-2}	1.8×10^{-1}	1.4×10^{-1}	9.2×10^{-2}	9.8×10^{-2}
ICD-2, min^{-1}	2.3×10^{-1}	1.9×10^{-1}	1.5×10^{-1}	1.0×10^{-1}	1.1×10^{-1}
C_{C1prec} , -	6.0×10^{-3}	6.4×10^{-2}	8.0×10^{-2}	1.0×10^{-1}	9.2×10^{-2}
$C_{C1,0}$, -	6.6×10^{-1}	7.5×10^{-1}	6.9×10^{-1}	7.8×10^{-1}	7.5×10^{-1}
$C_{C2,0}$, -	2.9×10^{-1}	1.3×10^{-1}	1.4×10^{-1}	6.5×10^{-2}	8.5×10^{-2}
$C_{C3,0}$, -	3.7×10^{-2}	5.5×10^{-2}	8.3×10^{-2}	5.1×10^{-2}	6.7×10^{-2}
$C_{C4,0}$, -	9.1×10^{-3}	3.0×10^{-3}	1.0×10^{-2}	9.0×10^{-4}	5.8×10^{-3}
k_{C1prec} , min^{-1}	7.0×10^{-1}	2.00	1.90	8.0×10^{-1}	1.00
$k_{C1,0}$, min^{-1}	3.2×10^{-1}	3.6×10^{-1}	2.9×10^{-1}	2.8×10^{-1}	2.6×10^{-1}
$k_{C2,0}$, min^{-1}	1.4×10^{-1}	6.3×10^{-2}	5.8×10^{-2}	2.3×10^{-2}	2.9×10^{-2}
$k_{C3,0}$, min^{-1}	1.8×10^{-2}	2.6×10^{-2}	3.5×10^{-2}	1.8×10^{-2}	2.3×10^{-2}
$k_{C4,0}$, min^{-1}	4.4×10^{-3}	1.4×10^{-3}	4.2×10^{-4}	3.2×10^{-4}	2.0×10^{-3}
k_{loss-1} , min^{-1}	3.3×10^{-1}	2.3×10^{-1}	1.9×10^{-1}	1.2×10^{-1}	1.3×10^{-1}
k_{loss-2} , min^{-1}	5.3×10^{-2}	4.0×10^{-2}	5.9×10^{-2}	1.8×10^{-2}	2.9×10^{-2}
k_{loss-3} , min^{-1}	5.1×10^{-3}	8.0×10^{-3}	1.2×10^{-2}	6.4×10^{-3}	9.2×10^{-3}
k_{loss-4} , min^{-1}	5.6×10^{-3}	7.0×10^{-3}	2.0×10^{-3}	2.0×10^{-2}	1.0×10^{-5}
Sample ID	B2-H2	B2-H1	B3	B4	B5
$k_{ncg,}$ min^{-1}	3.5×10^{-3}	3.5×10^{-3}	3.5×10^{-3}	3.5×10^{-3}	3.5×10^{-3}
ICA-1, min^{-1}	3.6×10^{-1}	1.4×10^{-1}	9.1×10^{-4}	1.6×10^{-4}	
ICA-2, min^{-1}	3.9×10^{-1}	1.6×10^{-1}	4.6×10^{-3}	1.9×10^{-3}	
ICD-1, min^{-1}	1.2×10^{-1}	5.0×10^{-2}	2.4×10^{-4}	4.2×10^{-8}	
ICD-2, min^{-1}	1.3×10^{-1}	6.0×10^{-2}	1.7×10^{-3}	5.3×10^{-4}	
C_{C1prec} , -	8.0×10^{-2}	1.4×10^{-1}	8.0×10^{-1}	9.2×10^{-1}	
$C_{C1,0}$, -	6.8×10^{-1}	6.6×10^{-1}	1.2×10^{-1}		
$C_{C2,0}$, -	1.8×10^{-2}	1.2×10^{-1}	7.8×10^{-2}	8.4×10^{-2}	
$C_{C3,0}$, -	5.3×10^{-2}	7.4×10^{-2}			
$C_{C4,0}$, -	5.6×10^{-3}	9.7×10^{-3}			
k_{C1prec} , min^{-1}	2.00	1.00	1.3×10^{-2}	1.2×10^{-1}	
$k_{C1,0}$, min^{-1}	2.7×10^{-1}	1.1×10^{-1}	5.6×10^{-4}		
$k_{C2,0}$, min^{-1}	7.0×10^{-2}	1.9×10^{-2}	3.5×10^{-4}	1.6×10^{-4}	
$k_{C3,0}$, min^{-1}	2.1×10^{-2}	1.2×10^{-2}			
$k_{C4,0}$, min^{-1}	2.2×10^{-3}	1.5×10^{-3}			
k_{loss-1} , min^{-1}	1.6×10^{-1}	7.2×10^{-2}	1.9×10^{-3}	5.8×10^{-4}	
k_{loss-2} , min^{-1}	4.0×10^{-2}	2.4×10^{-2}	7.8×10^{-5}	5.0×10^{-7}	
k_{loss-3} , min^{-1}	1.1×10^{-2}	4.0×10^{-3}			
k_{loss-4} , min^{-1}	1.0×10^{-5}	6.0×10^{-4}			

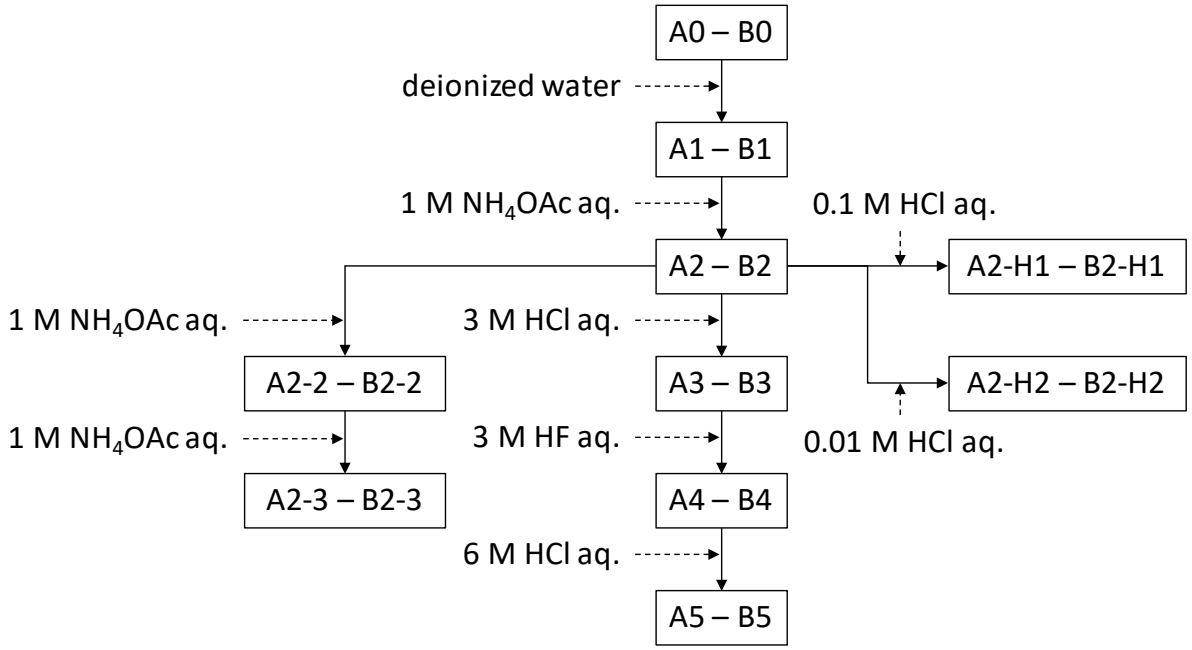

Figure 2.1. Flow diagram of sequential washing.

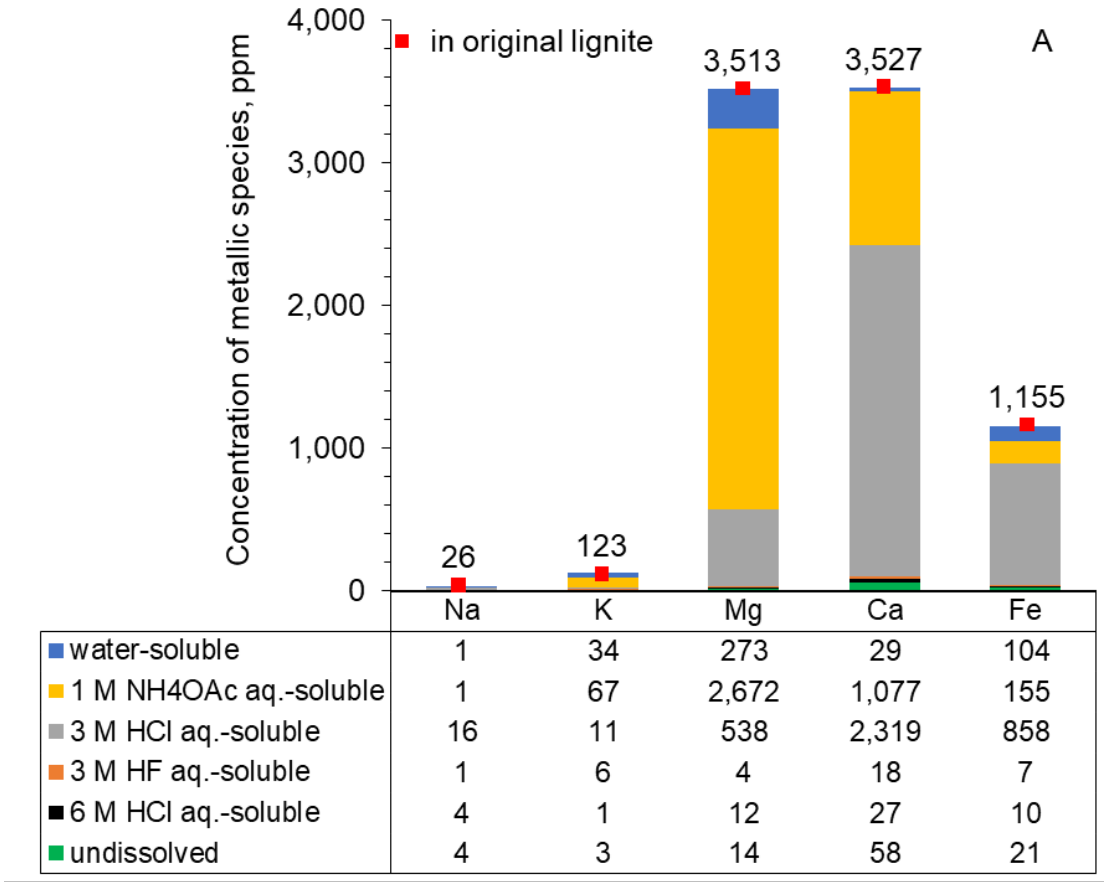

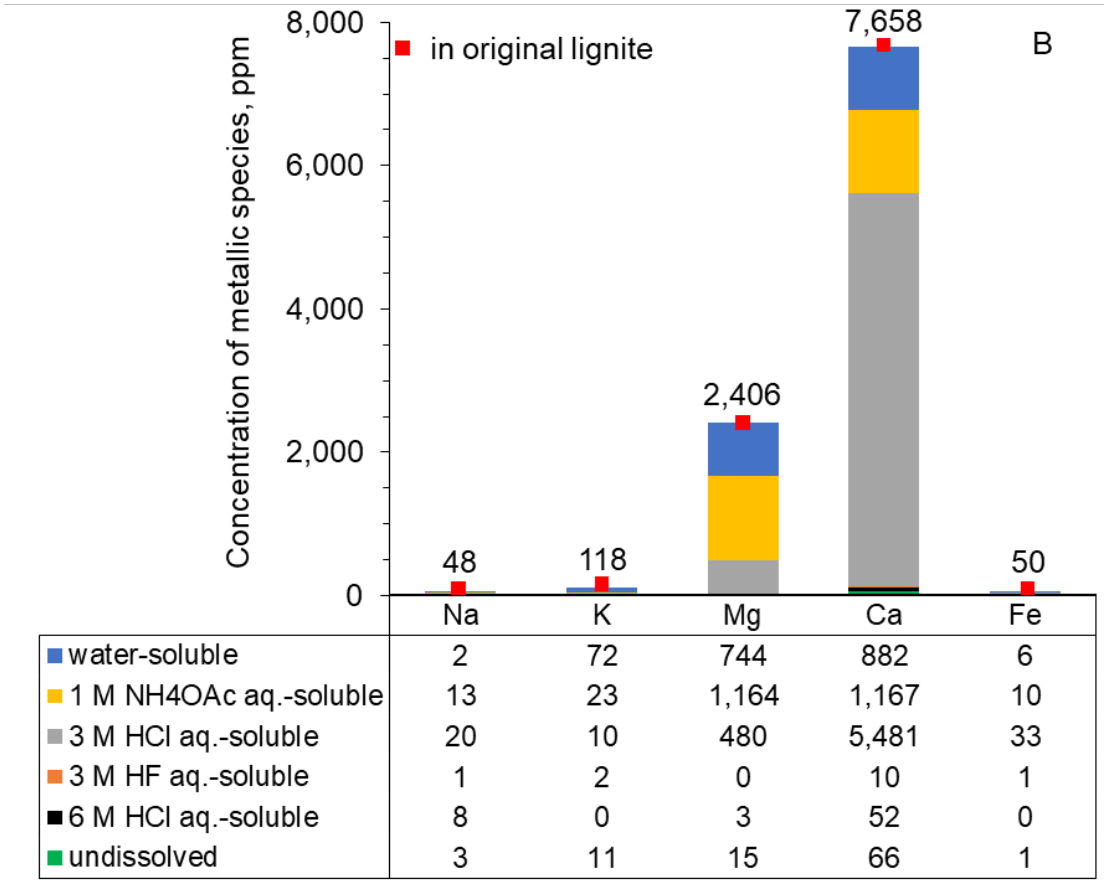

Figure 2.2. Cumulative concentration of metallic species in lignites.

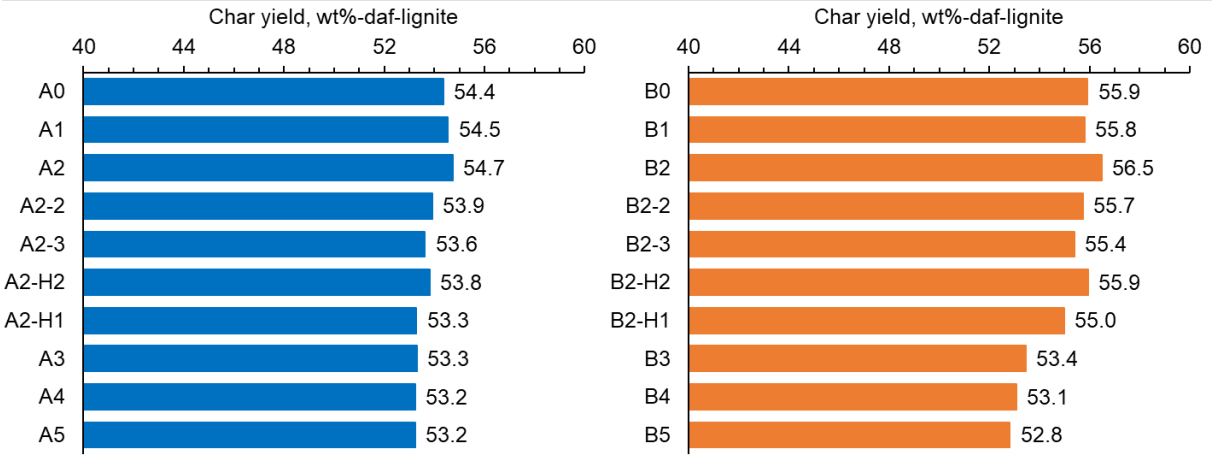

Figure 2.3. Char yields from the pyrolysis of lignites.

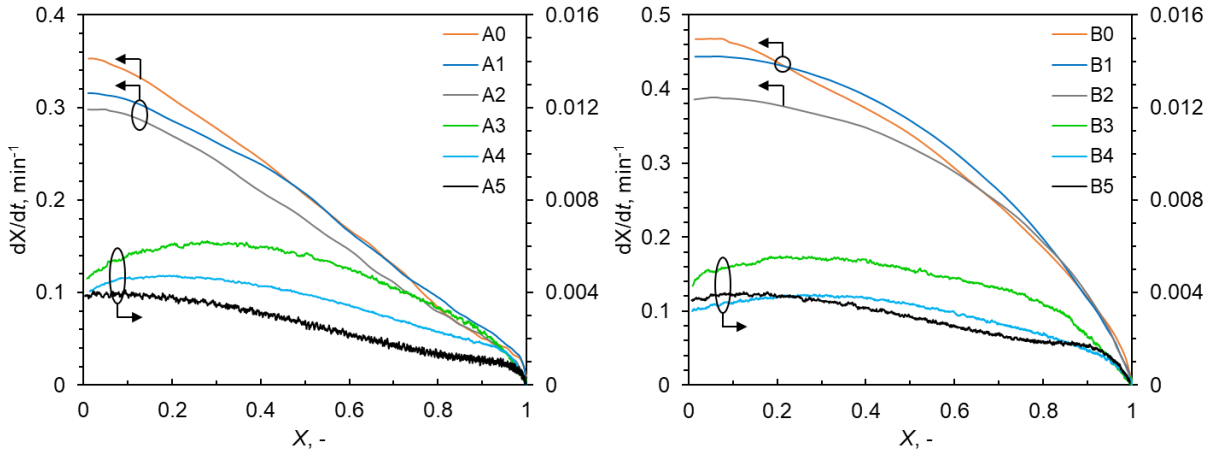

Figure 2.4. d*X*/d*t* profiles for the individual chars. d*X*/d*t* indicated at the left vertical axis for the gasification of chars from A0–A2 and B0–B2 (H group chars), while at the right for those from A3–A5 and B3–B5 (L group chars).

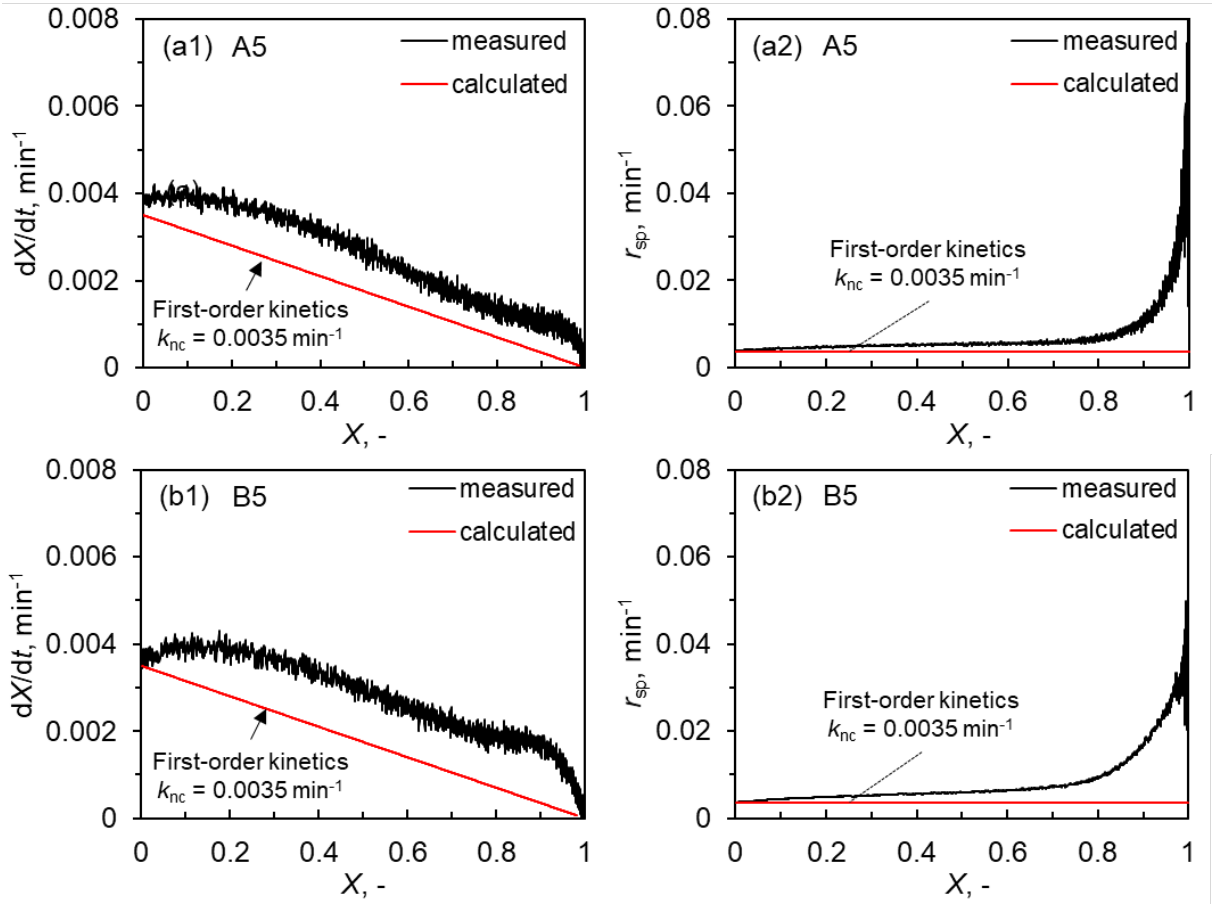

Figure 2.5. (a1) and (b1): dX/dt *vs* X profiles for A5 and B5 chars, respectively. (a2) and (b2): specific rates of gasification, r_{sp} = dX/dt/(1–X) as a function of X for A5 and B5 chars, respectively. The red-colored straight lines are drawn for indicating dX/dt or r_{sp} of first-order kinetics with k_{nc} = 0.0035 min^{-1}.

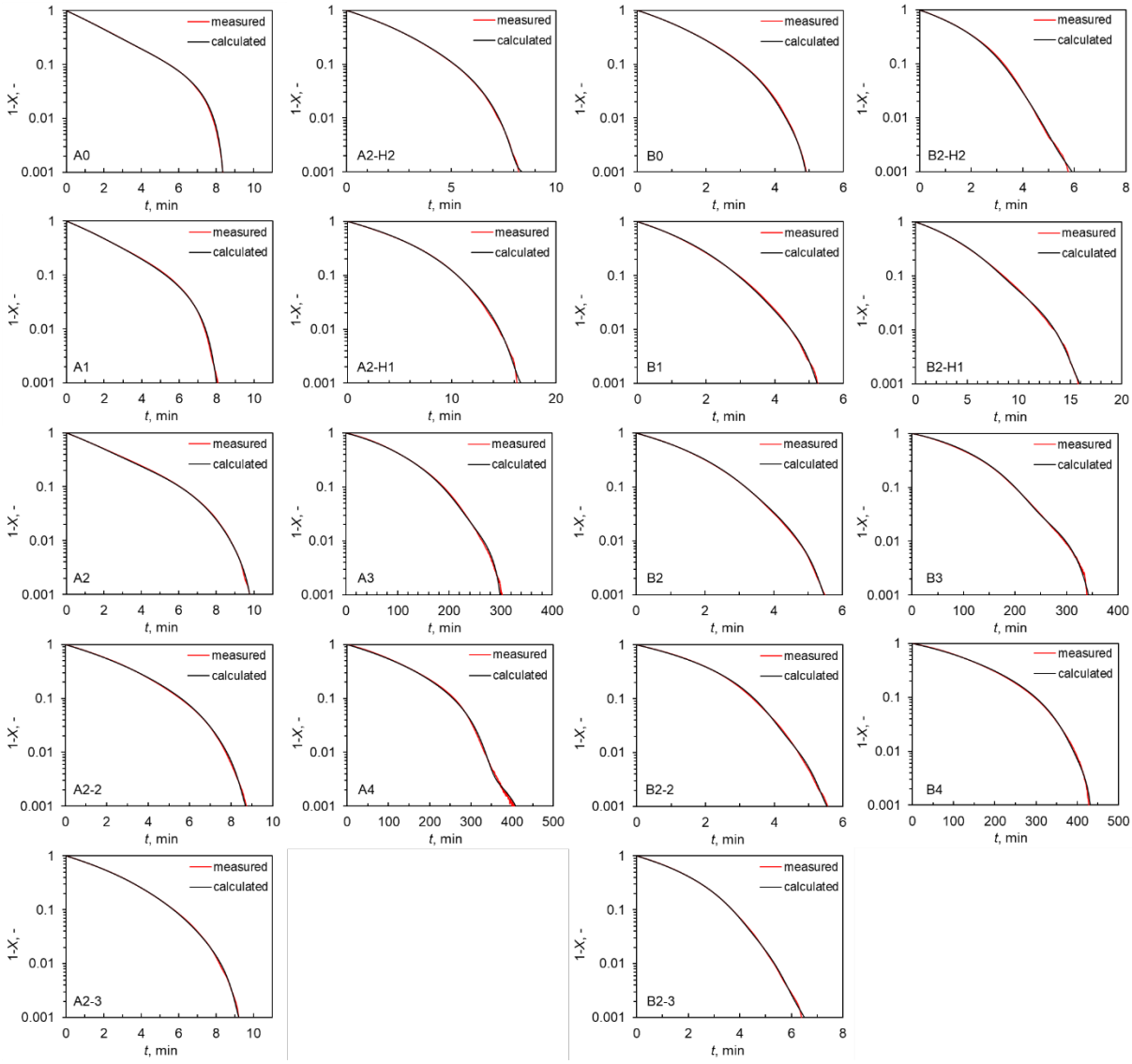

Figure 2.6. Measured and calculated 1–*X vs t* profiles for the gasification of A0–A4 chars (left side) and B0-B4 chars (right side). (1–*X*)'s are shown in logarithmic scales.

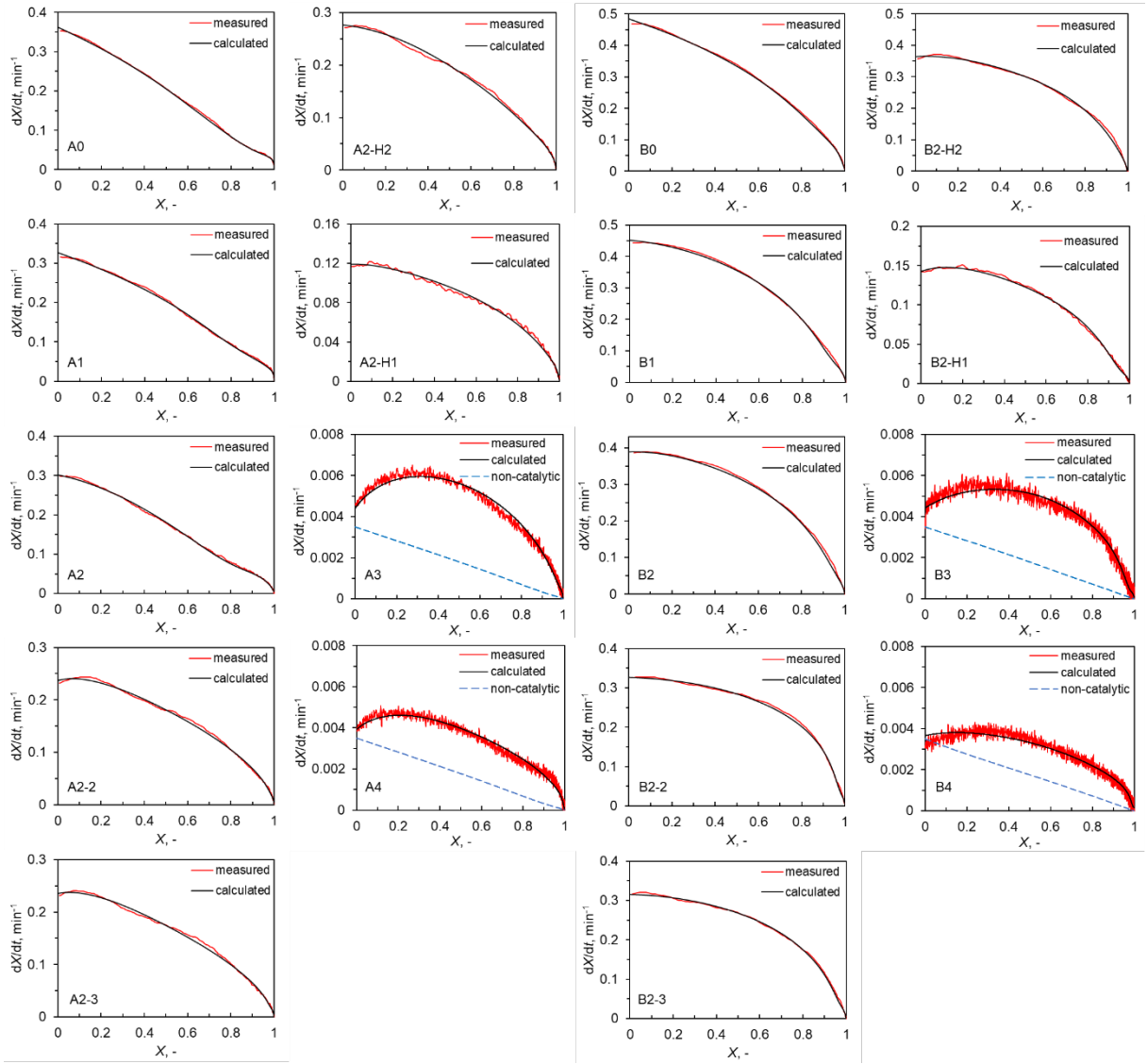

Figure 2.7. Measured and calculated changes in dX/dt with X for gasification of chars from original and washed lignites. The blue-colored broken lines were drawn for A3, A4, B3 and B4 to show dX/dt for the non-catalytic gasification with k_{nc} = 0.0035 min^{-1}.

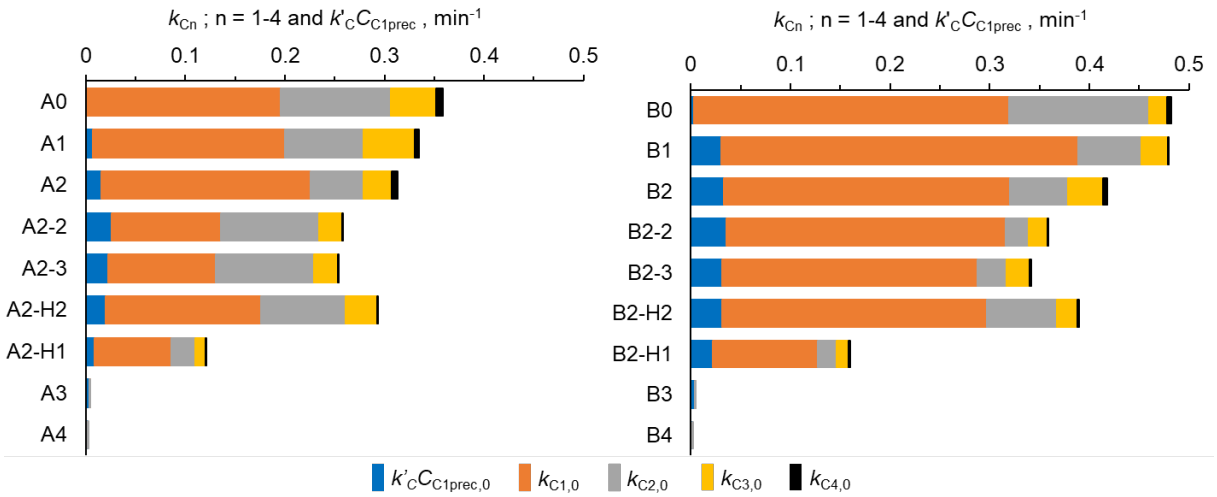

Figure 2.8. The initial activities ($k_{Cn,0}$; n = 1–4) and potential activity of C1 precursor ($k'_C C_{C1prec,0}$). The cumulative total of $k_{Cn,0}$ (*i.e.*, $\Sigma k_{Cn,0}$) and $k'_C C_{C1prec,0}$ equals to ICA-2.

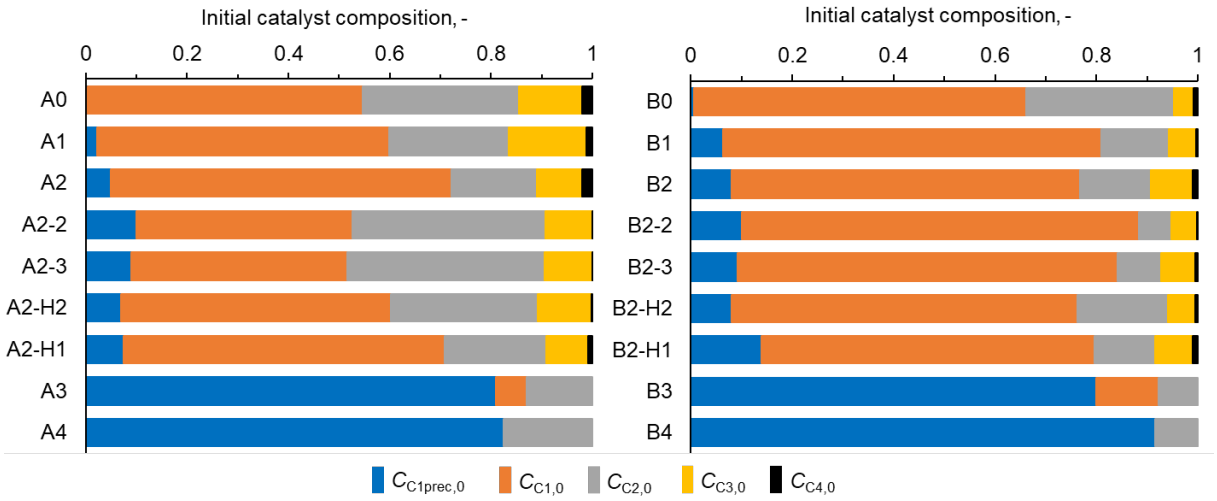

Figure 2.9. Normalized abundances of C1–C4 catalysts and C1prec at t = 0.

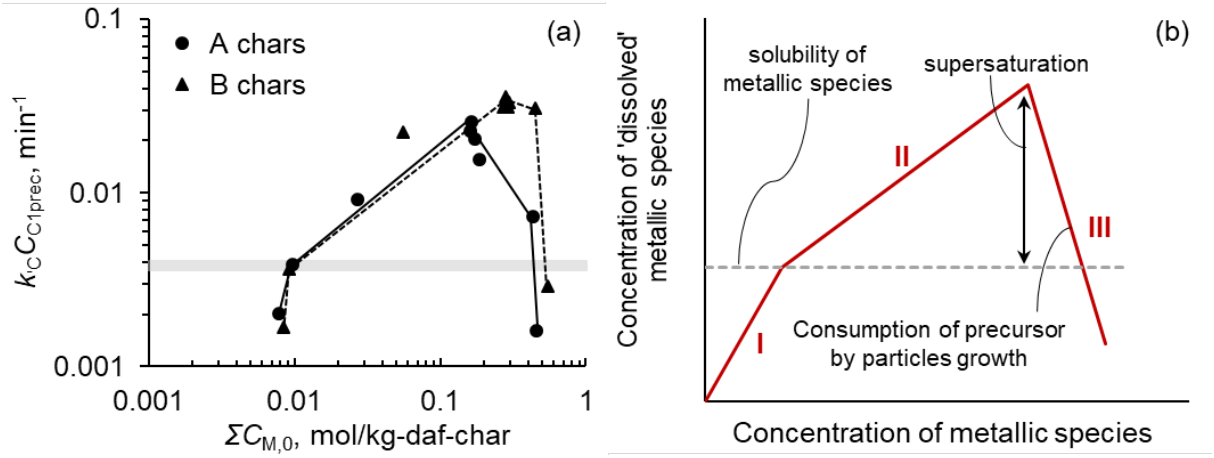

Figure 2.10. (a) Plot of $k'_{C}C_{C1prec}$ against total concentration of metallic species (Na, K, Mg, Ca, and Fe) at t = 0. (b) Schematic expression of the relationship between catalyst precursor concentration and the total concentration of metallic species.

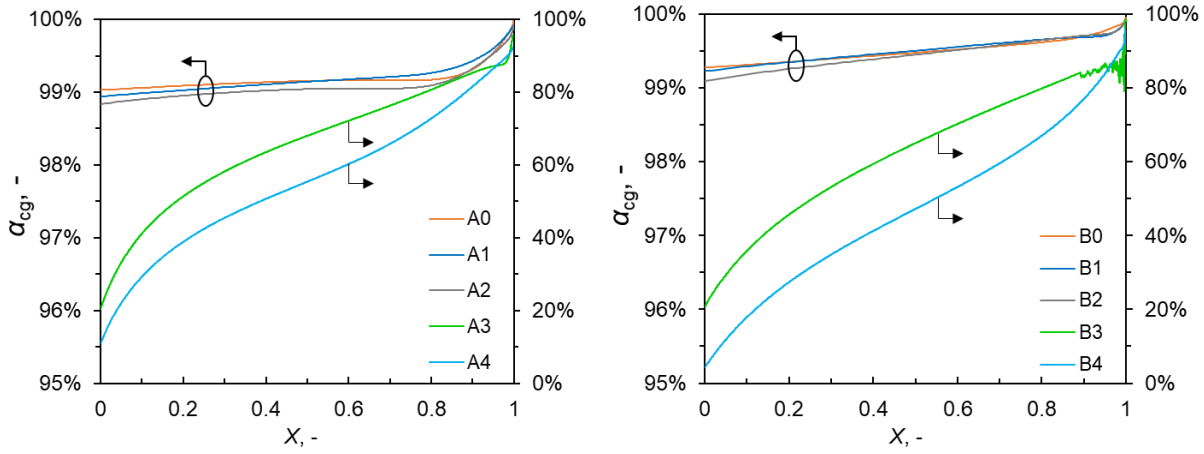

Figure 2.11. Contribution rate of catalytic gasification, α_{cg}, to overall rate of gasification, dX/dt as a function of X.

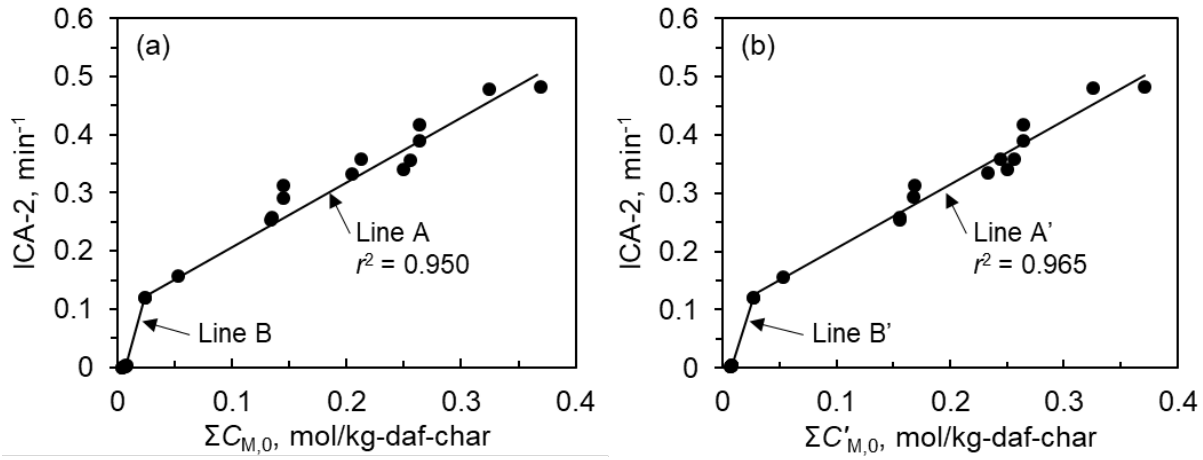

Figure 2.12. (a) ICA-2 as a function of $\Sigma C_{M,0} = C_{Na,0} + C_{K,0} + C_{Ca,0} + C_{Fe,0}$ (b) ICA-2 as a function of $\Sigma C'_{M,0} = C_{Na,0} + C_{K,0} + C_{Ca,0} + 1.8C_{Fe,0}$. $C_{M,0}$ means the concentration of M in the char at $t = 0$. Straight lines A and A' are derived from the method of least squares for the A and B chars except the L-group chars. Lines B and B' are drawn by connecting the plots for A2-H1 and A3 or B2-H1 and B3.

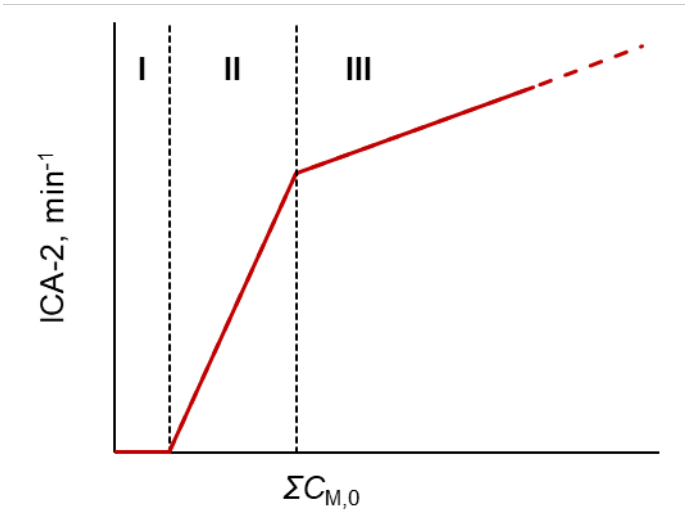

Figure 2.13. Schematic expression of relationship between ICA-2 and $\Sigma C_{M,0}$.

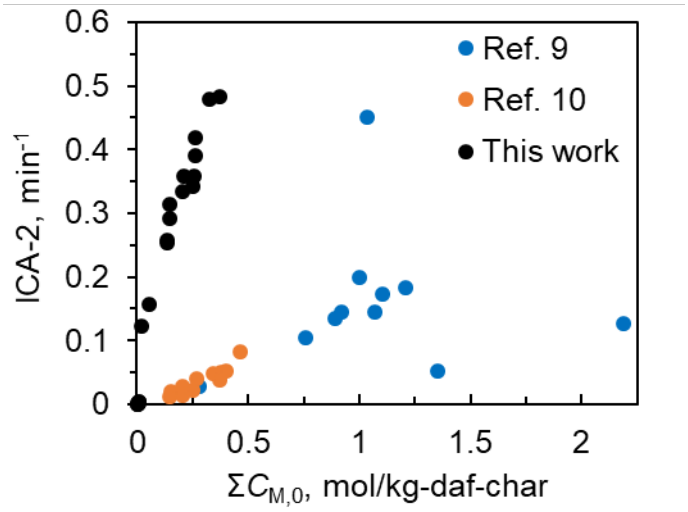

Figure 2.14. Relationships between ICA-2 and $\Sigma C_{M,0} = C_{Na,0} + C_{K,0} + C_{Ca,0} + C_{Fe,0}$ for present and previous works on CO_2 gasification of chars from Mongolian lignites (ref. 8) and sugarcane bagasses (ref. 9). $\Sigma C_{M,0}$ is defined as the total content of Na, K, Ca and Fe in the unit of mol/kg-daf-char.

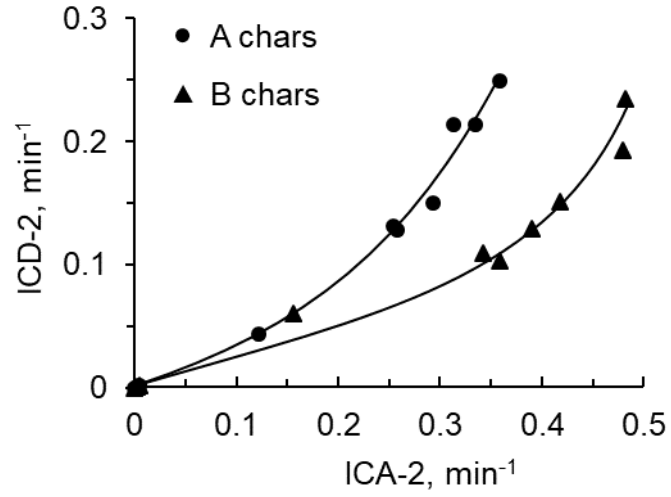

Figure 2.15. Relationship between ICD-2 and ICA-2.

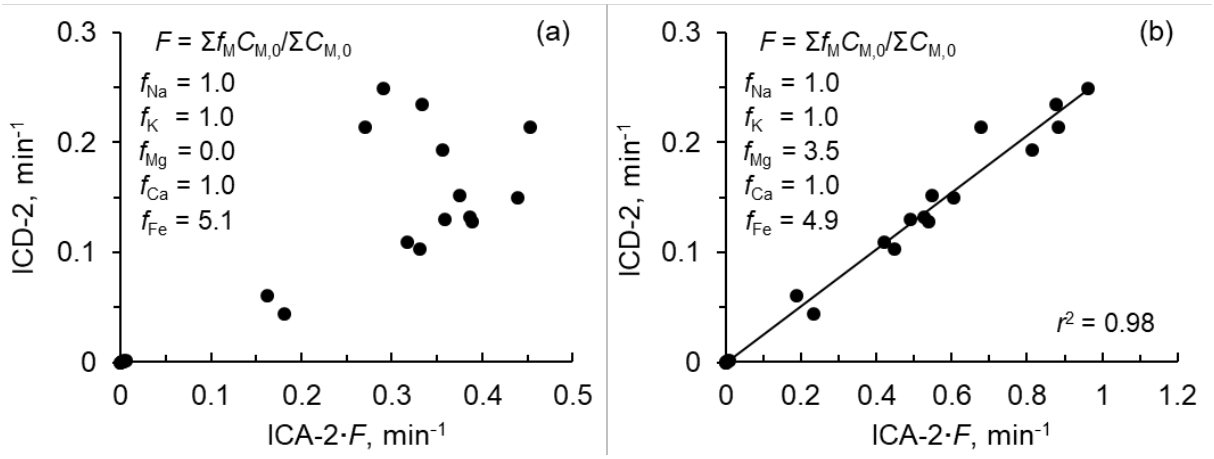

Figure 2.16. ICD-2 as a function of ICA-2. (a) Application of Eq.14 and optimization of f_{Fe} with f_{Na}, f_K and f_{Ca} fixed at 1. (b) Application of Eq.16 and optimization of f_{Fe} and f_{Mg} with f_{Na}, f_K and f_{Ca} fixed at 1.

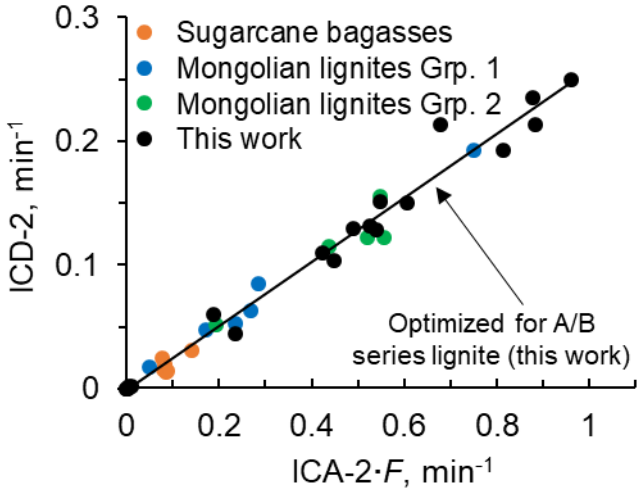

Figure 2.17. ICD-2 correlation with ICA-2 for present and previous studies. Parameters f_M's are as follows: Sugarcane bagasses (ref. 9; $f_{Na} = f_K = f_{Ca} = 1.0$, $f_{Mg} = 3.5$, $f_{Fe} = 4.9$), Lignites (Group 1) (ref. 8; $f_{Na} = f_K = f_{Ca} = 1.0$, $f_{Mg} = 3.2$, $f_{Fe} = 1.6$), Lignites (Group 2) (ref. 8; $f_{Na} = f_K = f_{Ca} = 1.0$, $f_{Mg} = 5.0$, $f_{Fe} = 7.4$). The solid line drawn in the figure represents the function, (ICD-2) = 0.258F (ICA-2) of that parameters were optimized for the A and B chars in the present study.

2.5 References

1. S. Bhattacharya, K.B. Kabir, K. Hein, *Progress in Energy and Combustion Science*, **39** (2013), 577–605.
2. C. Higman, S. Tam, *Chemicals Review*, **114** (2014), 1673–1708.
3. M. Kawabata, O. Kurata, N. Iki, H. Furutani, A. Tsutsumi, *Journal of Power Technology*, **92** (2012), 90–100.
4. J. Hayashi, S. Kudo, H.S. Kim, K. Norinaga, K. Matsuoka, S. Hosokai, *Energy & Fuels*, **28** (2014), 4–21.
5. Y. Shen, D. Ma, X. Ge, *Sustainable Energy Fuels*, **1** (2017), 1700–1729.
6. H.E. Belkin, S.J. Tewalt, J.C. Hower, J.D. Stucker, J.M.K. O'Keefe, *International Journal of Coal Geology*, **77** (2009), 260–268.
7. K. Murakami, M. Sato, N. Tsubouchi, Y. Ohtsuka, K. Sugawara, *Fuel Processing Technology*, **129** (2015), 91–97.
8. H. Kim, S. Kudo, K. Tahara, Y. Hachiyama, H. Yang, K. Norinaga, J. Hayashi, *Energy & Fuels*, **27** (2013), 6617–6631.
9. E. Byambajav, Y. Hachiyama, S. Kudo, K. Norinaga, J. Hayashi, *Energy & Fuels*, **30** (2016), 1636–1646.
10. Z.F. Zahara, S. Kudo, Daniyanto, U.P.M. Ashik, K. Norinaga, A. Budiman, J. Hayashi, *Energy & Fuels*, **32** (2018), 4255–4268.
11. E.J. Hippo, R.G. Jenkins, P.L. Walker, *Fuel*, **58** (1979), 338–344.
12. L.R. Radovic, K. Steczko, P.L. Walker, R.G. Jenkins, *Fuel Processing Technology*, **10** (1985), 311–326.
13. S. Tanaka, T. U-emura, K. Ishizaki, K. Nagayoshi, N. Ikenaga, H. Ohme, T. Suzuki, H. Yamashita, M. Ampo, *Energy & Fuels*, **9** (1995), 45–52.
14. H. Ohme, T. Suzuki, *Energy & Fuels*, **10** (1996), 980–987.
15. Y.L. Wang, S.H. Zhu, M.Q. Gao, Z.R. Yang, L.J. Yan, Y.H. Bai, F. Li, *Fuel Processing Technology*, **141** (2016), 9–15.
16. B.B. Beamish, K.J. Shaw, K.A. Rodgers, J. Newman, *Fuel Processing Technology*, **53** (1998), 243–253.
17. G.O. Çakal, H. Yücel, A.G. Gürüz, *Journal of Analytical and Applied Pyrolysis*, **80** (2007), 262–268.
18. S.A. Benson, P.L. Holm, *Industrial & Engineering Chemistry Product Research and Development*, **24** (1985), 145–149.

19. C. Andrea Jordan, G. Akay, *Fuel*, **91** (2012), 253–263.
20. A. Kolker, F.E. Huggins, C.A. Palmer, N. Shah, S.S. Crowley, G.P. Huffman, R.B. Finkelman, *Fuel Processing Technology*, **63** (2000), 167–178.
21. C.L. Senior, T. Zeng, J. Che, M.R. Ames, A.F. Sarofim, I. Olmez, F.E. Huggins, N. Shah, G.P. Huffman, A. Kolker, S. Mroczkowski, C. Palmer, R. Finkelman, *Fuel Processing Technology*, **63** (2000), 215–241.
22. Y. Yang, Y. Wu, H. Zhang, M. Zhang, Q. Liu, H. Yang, J. Lu, *Fuel*, **181** (2016), 951–957.
23. Z. Zhang, M. Zhu, Y. Zhang, H.Y. Setyawan, J. Li, D. Zhang, *Proceedings of the Combustion Institute*, **36** (2017), 2139–2146.
24. C. Zhu, S. Qu, J. Zhang, Y. Wang, Y. Zhang, *Fuel*, **190** (2017), 189–197.
25. C. Sathe, J. Hayashi, C.Z. Li, T. Chiba, *Fuel*, **82** (2003), 1491–1497.
26. B. Bayarsaikhan, J. Hayashi, T. Shimada, C. Sathe, C.Z. Li, A. Tsutsumi, T. Chiba, *Fuel*, **84** (2005), 1612–1621.
27. S. Kudo, Y. Hachiyama, H.-S. Kim, K. Norinaga, J. Hayashi, *Energy & Fuels*, **28** (2014), 5902–5908.
28. C. Sathe, Y. Pang, C.Z. Li, *Energy & Fuels*, **13** (1999), 748–755.
29. J. Hayashi, H. Takahashi, M. Iwatsuki, K. Essaki, A. Tsutsumi, T. Chiba, *Fuel*, **79** (2000), 439–447.
30. L. Bai, S. Kudo, K. Norinaga, Y. Wang, J. Hayashi, *Energy & Fuels*, **28** (2014), 7133–7139.
31. T. Kitsuka, B. Bayarsaikhan, N. Sonoyama, S. Hosokai, C.Z. Li, K. Norinaga, J. Hayashi, *Energy & Fuels*, **21** (2007), 387–394.
32. M. Kajita, T. Kimura, K. Norinaga, C.Z. Li, J. Hayashi, *Energy & Fuels*, **24** (2010), 108–116.
33. P.L. Walker, S. Matsumoto, T. Hanzawa, T. Muira, I.M.K. Ismail, *Fuel*, **62** (1983), 140–149.
34. K. Matsuoka, E. Rosyadi, A. Tomita, *Fuel*, **81** (2002), 1433–1438.
35. R.B. Finkelman, C.A. Palmer, P. Wang, *International Journal of Coal Geology*, **185** (2018), 138–160.
36. S. V. Vassilev, J.M.D. Tascón, *Energy & Fuels*, **17** (2003), 271–281.
37. R. Lin, M. Stuckman, B.H. Howard, T.L. Bank, E.A. Roth, M.K. Macala, C. Lopano, Y. Soong, E.J. Granite, *Fuel*, **232** (2018), 124–133.
38. N. Wijaya, L. Zhang, *Energy & Fuels*, **25** (2011), 1–16.
39. D. Feng, Y. Zhao, Y. Zhang, S. Sun, J. Gao, *Energies*, **11** (2018), 205.

40. J. Hayashi, H. Takahashi, S. Doi, H. Kumagai, T. Chiba, T. Yoshida, A. Tsutsumi, *Energy & Fuels*, **14** (2000), 400–408.
41. M.J. Wornat, P.F. Nelson, *Energy & Fuels*, **6** (1992), 136–142.
42. C.S.M. de Lecea, M. Almela-Alarcón, A. Linares-Solano, *Fuel*, **69** (1990), 21–27.
43. H. Wu, J. Hayashi, T. Chiba, T. Takarada, C.Z. Li, *Fuel*, **83** (2004), 23–30.
44. P. Lahijani, Z.A. Zainal, A.R. Mohamed, M. Mohammadi, *Bioresource Technology*, **144** (2013), 288–295.
45. Y. Huang, X. Yin, C. Wu, C. Wang, J. Xie, Z. Zhou, L. Ma, H. Li, *Biotechnology Advances*, **27** (2009), 568–572.
46. T. late T.D. Hengel, P.L. Walker, *Fuel*, **63** (1984), 1214–1220.
47. T. Haga, K. Nogi, M. Amaya, Y. Nishiyama, *Applied Catalysis*, **67** (1991), 189–202.
48. C. Choi, U.P.M. Ashik, S. Kudo, K. Uebo, K. Norinaga, J. Hayashi, *Carbon Resources Conversion*, **2** (2018), 13–22.
49. K. Asami, P. Sears, E. Furimsky, Y. Ohtsuka, *Fuel Processing Technology*, **47** (1996), 139–151.
50. M. Matsukata, E. Okanari, K. Kobayashi, E. Kikuchi, Y. Morita, *Sekiyu Gakkaishi*, **32** (1989), 97.
51. N. Alarcón, X. García, M. Centeno, P. Ruiz, A. Gordon, *Surface Interface Analysis*, **31** (2001), 1031–1041.

Chapter 3
Kinetics and Mechanism of the Interactions between Ca and Mg/K during CO_2 Gasification of Lignite Char

3.1 Introduction

Gasification is a promising method for converting carbonaceous solid feedstock such as lignite and biomass into syngas that is further processed into fuels or chemicals. [1,2] In the case that CO_2 is used as gasification medium, it can be more energy-efficient than conventional gasifying agents such O_2 and steam due to its endothermic reaction with the nascent char, produced by in situ pyrolysis of lignite, and its elimination of extra heat for producing water vapor. On the other hand, the CO_2-carbon reaction generally controls the overall rate of char conversion, and it is therefore conducted under the catalysis of metallic species to promote the gasification kinetics.

Alkali and alkaline earth metallic (AAEM) species are widely used as catalysts in gasification due to their catalytic activity, inherently abundance, and low cost. [3–5] In particular, Ca and K species have attracted considerable interest, not only as an individual catalyst, [6–8] but also as composite catalysts. [9–13] Ca is well known as a highly active catalyst, although its activity decreases with the progress of char conversion, mainly due to particle growth. [5,6,14] In contrast, the catalytic activity of K continuously increases as the gasification proceeds unless volatilization or deactivation by reacting with silica/alumina occurs. [15–18] It is expected that the presence of Ca and K catalysts in lignite char offers an excellent feedstock for gasification. On the other hand, the effects of co-existence of Mg and Ca species, which are commonly found in Indonesian lignites, on the catalyst activation/deactivation also need to be confirmed. [19,20]

A quantitative description of the overall rate of gasification as a function of char conversion is therefore important to examine the interactions of these species and determine the roles of each species during the gasification. Recent studies reported the synergistic effects between Ca and K catalysts by evaluating the time to achieve 50% char conversion, $t_{0.5}$, or the average rate of gasification. [9–11,13] However, such parameters do not consider changes in char reactivity along char conversion. Other previous studies also recognized that the

conventional kinetic models are not satisfactory for describing the rate of catalytic gasification, in which catalysts play significant roles in char gasification. [21,22] The catalytic activity of metallic species should be fairly compared by monitoring the measured rate of gasification over the entire range of its conversion and considering its abundance as a factor responsible for the kinetics of char gasification. A parallel reaction model (PRM), which is based on an assumption of parallel progress of non-catalytic gasification and catalytic gasification together with catalyst activation/deactivation, has been developed recently to overcome the limitations of the previous models and provide information on effects of metallic species composition on the rate of catalytic gasification. [6,23] Previous studies revealed that the PRM was able to describe the kinetics of CO_2 and steam gasification over the entire range of char conversion up to 0.999 for chars from various types of lignites or biomass with different concentrations of inherent metallic species. [6, 23–28] However, the applicability of the PRM to describe the interaction behavior of doped metallic species during CO_2 gasification has not been demonstrated. In order to improve the versatility of the PRM, it is necessary to examine the catalysis of a single and bi-metallic species that presence in char by employing the PRM.

The present authors have been studying the effects of Ca interactions with Mg or K on the kinetics of Ca-catalyzed gasification. First, the demineralized and metal(s)-loaded lignites were pyrolyzed and in-situ gasified with CO_2 at 900°C. Second, the measured rate of char conversion was quantitatively described by the model. Finally, based on the optimized kinetic parameters, the relationships between catalytic activity/deactivation rate and the concentration(s) of a single or bi-metallic species in char were scrutinized to reveal the interaction mechanism. This paper also compared the performance of extraneous catalyst species in this study and that of previously reported inherent catalyst species.

3.2 Experimental

3.2.1 Sample preparation

Two Indonesian lignites, A and B, were slowly air-dried at ambient temperature, pulverized and sieved to particle sizes smaller than 106 μm, then dried in a vacuum oven at 60°C for 24 h. The lignites were further pulverized in a pot mill for 10 h for reducing its particle sizes to < 10 μm (see **Appendix 1**). To eliminate the influence of inherent metallic species and mineral matter on catalytic gasification, the fine lignites were demineralized by washing with aqueous solutions of hydrogen chloride and hydrogen fluoride. Details of the procedure were displayed in **Appendix 6**. The demineralized A and B are hereafter referred to as DA and DB,

respectively. DA and DB are respectively identical to A5 and B5, which were mentioned in **Chapter 2**. **Table 3.1** shows the properties of the original and demineralized lignites. As shown in **Table 3.1**, the sequential acid washing successfully removed more than 99% (w/w) of the inherent metallic species from A and B. DA and DB were also mixed with 10 wt% SiO_2 nanoparticles in an agate mortar for approximately 30 min at room temperature and then vacuum-dried at 60°C for 24 h to produce SiO_2-mixed demineralized lignites, which are denoted by DAS and DBS, respectively. The SiO_2 nanoparticles were prepared by washing SiO_2 powder (Sigma-Aldrich, 99.5 wt%, 5–15 nm) in 3 M HCl aq. at 60°C for 24 h, exhaustively washing with deionized water, and then vacuum drying at 60°C.

DA or DB was then loaded with varying amounts of Ca, K, and Mg, separately or jointly, by an ion-exchange method. DA or DB was suspended in the aqueous solution of dissolved metallic species for 24 h, separated from the solution by filtration, rinsed with deionized water, and then dried *in vacuo* at 60°C. Taking Ca as an example, the resulting Ca-loaded DA and DB lignites with Ca concentration of α mol-Ca/kg-daf-char will be denoted by Ca-α-DA and Ca-α-DB, respectively (see **Table 3.2** and **3.3**). In the case of joint loading of Ca and Mg, or Ca and K into DA, the sample name was referred to Ca-α/Mg-β-DA or Ca-α/K-β-DA, respectively (see **Table 3.3**). The distribution of loaded metallic species in lignite is shown in **Appendix 7**.

3.2.2 Pyrolysis and CO_2 gasification in TGA

About 2 mg of the demineralized or metal(s)-loaded lignite was subjected to the pyrolysis and subsequent gasification in a thermodynamic analyzer (TGA, Hitachi Hi-Tech Science, model SII TGA/DTA 7200). This small initial mass of lignite was chosen to eliminate the effects of heat and mass transfer, as reported earlier. [23,28] The lignite was placed in a platinum pan and heated in a flow of atmospheric N_2 (purity; > 99.999 vol.%, flow rate; 700 mL/min) from room temperature to the holding temperature of 900°C at a rate of 30 °C/min. After confirming a steady mass of the sample, the CO_2 gasification was started by switching the flow of N_2 gas to that of N_2/CO_2 mixed gases (50:50 in volume) without changing the total flow rate. The reproducibility of the above gasification conditions was previously confirmed [23,28] and also successfully examined in the preliminary experiments (see **Appendix 8**).

3.2.3 Quantification of metallic species

The contents of metallic species in the individual samples were quantified by referring to previous reports. [24,28,29] In brief, a prescribed mass of A and B (40 mg), DA and DB (400 mg), and the chars from metal(s)-loaded lignites (10–20 mg) were ashed completely by

heating in air in a muffle furnace with a rate, holding temperature and holding time of 1 °C/min, 620°C, and 60 min, respectively. The resulting ash was dissolved in the mixture solution of HNO_3/HF at 60°C and suspended for 24 h. The solid residue after evaporation of liquid component at 120°C was dissolved into 4 mM CH_3SO_3H aq. Ion chromatography and inductively coupled plasma-optical emission spectroscopy were employed to analyze the contents of AAEM species (*i.e.*, Na, K, Mg, and Ca) and Fe in the solution, respectively.

.

3.2.4 Kinetic modeling

The kinetics of CO_2 gasification of lignite/biomass char was described by a Parallel Reaction Model that employs the following equations:

$$\frac{dX}{dt} = \left(\frac{dX}{dt}\right)_{\mathrm{nc}} + \left(\frac{dX}{dt}\right)_{\mathrm{C}} = k_{\mathrm{nc}}(1-X) + \sum_n k_{\mathrm{C}n} \quad (1)$$

The overall rate of char conversion, dX/dt, consists of the non-catalytic gasification, (dX/dt)$_{\mathrm{nc}}$, and catalytic gasification, (dX/dt)$_{\mathrm{C}}$, which follow first-order and zeroth-order kinetics with respect to the fraction of unconverted char (1–X), respectively. [6,23–25,28,30] k_{nc} and $k_{\mathrm{C}n}$ are the rate constants for the non-catalytic and catalytic gasification, respectively, where n is the catalytic component, Cn (n = 1–4). $k_{\mathrm{C}n}$, which represents the activity of Cn catalyst, is a function of the amount of retained catalysts in char ($m_{\mathrm{C}n}$) and rate constant (k'_{C}).

$$k_{\mathrm{C}n} = k'_{\mathrm{C}} m_{\mathrm{C}n} \quad (2)$$

k'_{C} is a rate constant that set to be common among the catalysts. $k'_{\mathrm{C}n,0}$ and $m_{\mathrm{C}n,0}$ are $k'_{\mathrm{C}n}$ and $m_{\mathrm{C}n}$ at t = 0, respectively. The activity of catalysts, $k_{\mathrm{C}n}$ changes with:

i. The change in $m_{\mathrm{C}n}$ due to the progress of char conversion. $C_{\mathrm{C}n}$ is introduced to express the dependency of the catalyst concentration in char on X.

$$C_{Cn} = \frac{m_{Cn}}{1-X} \quad (3)$$

ii. Deactivation of catalysts via agglomeration/growth mechanism, reactions with mineral matter (*i.e.*, silica, alumina, and aluminosilicate), and volatilization. The kinetics of catalyst deactivation is assumed following first-order kinetics with respect to the catalyst concentration and expressed by:

$$\frac{dm_{Cn}}{dt} = k_{loss-n} C_{Cn} = k_{loss-n} \frac{m_{Cn}}{1-X} \quad (4)$$

iii. Transformation of the catalyst precursor. The results from preliminary experiments and analysis showed that the necessity of assuming the presence of at least one type of catalyst precursor for gasification of lignite chars. Then Equation 4 is extended to:

$$\frac{dm_{\mathrm{C1}}}{dt} = k_{\mathrm{C1,prec}} C_{\mathrm{C1,prec}} - k_{\mathrm{loss-1}} C_{\mathrm{C1}} \quad n = 1 \quad (5)$$

$$\frac{dm_{Cn}}{dt} = -k_{\mathrm{loss-n}} C_{Cn} \quad n \geq 1 \tag{6}$$

the concentration and the rate of the transformation of $C_{Cn,prec}$ are defined the same way as C_{Cn} in Equations 3 and 4, respectively. The sum amount of the catalysts and the catalyst precursor is unity at $t = 0$.

$$\sum_n m_{Cn,0} + m_{Cn,\mathrm{prec},0} = 1 \tag{7}$$

The initial catalytic activity and the initial rate of catalyst deactivation are evaluated by these parameters:

$$\text{ICA-1} = \sum_n k_{Cn,0} = \sum_n k'_{Cn} m_{Cn,0} \tag{8}$$

$$\text{ICA-2} = k'_{C} m_{Cn,\mathrm{prec},0} + \sum_n k_{Cn,0} = k'_{C}\left(m_{Cn,\mathrm{prec},0} + \sum_n m_{Cn,0}\right) = k'_{C} \tag{9}$$

$$\text{ICD-1} = \sum_n k_{\mathrm{loss-n},0}\, C_{Cn,0} \tag{10}$$

$$\text{ICD-2} = k_{\mathrm{loss-1},0}\left(C_{C1,0} + C_{C1\mathrm{prec},0}\right) + \sum_n k_{\mathrm{loss-n},0}\, C_{Cn,0} \tag{11}$$

ICA-1 and ICA-2, which represents the overall rate of gasification, are the initial (at t = 0) and potential catalytic activity (by considering $C_{C1,prec}$). ICD-1 and ICD-2 are the overall rate of catalyst deactivation at t = 0, corresponding to ICA-1 and ICA-2, respectively. Both pairs are identical to each other when $m_{Cn,prec}$ = 0. More details of the model were reported elsewhere. [23,28]

3.3 Results and Discussion

3.3.1 Examination of kinetics of non-catalytic gasification

Figure 3.1 shows characteristics of the gasification of chars from the demineralized lignites with and without SiO_2-mixed. As seen in the graphs (a1) and (b1), the chars from DAS and DBS underwent very slow gasification, and it took more than 700 min to gasify char completely. On the other hand, the conversion of chars from DA and DB were completed within 530 and 430 min, respectively, which are more rapid than that from DAS and DBS, respectively. In addition to this, the rate of gasification, dX/dt, for chars from DA and DB are higher than those from DAS and DBS, respectively. It was thus clear that the differences in the kinetics of gasification of those chars were attributed to the catalysis of the metallic species that had remained in the demineralized lignites even after exhaustive acid washing. DA and DB contained 0.004 and 0.005 mol-metallic species/kg-daf-char, respectively. In the absence of SiO_2 particles, the residual metallic species are able to form clusters that had catalysis, even though very low, soon after the gasification started. On the other hand, the SiO_2 particles in DAS and DBS reacted with those metallic species and then suppressed their catalysis. A recent study on CO_2 gasification of cokes from the original and SiO_2-blend lignites suggested that

the metallic species in the lignite experienced deactivation during the pyrolysis by reacting with SiO_2 particles, while such reaction was not significant during the CO_2 gasification. [31] It was thus concluded that the sequential washing and SiO_2 mixing were required to remove and deactivate the residual catalyst species, respectively. These treatments were necessary or even mandatory to obtain the inherent reactivity of lignite char, k_{nc}, experimentally. Based on the above discussion, it is reasonable to define the rate of non-catalytic gasification as k_{nc} = 0.0035 min^{-1} for both DAS and DBS chars as k_{nc} was equivalent to the initial dX/dt.

3.3.2 Gasification of char from Ca-loaded lignite

Figure 3.2(a1) and **(b1)** present the measured and calculated time-dependent changes in (1–X) for the CO_2 gasification of chars from Ca-α-DA and Ca-α-DB, respectively. As expected, the gasification time for both groups of lignites becomes shorter as the Ca concentration in char, C_{Ca}, increases in the range of 0.035–0.332 mol-Ca/kg-daf-char. This trend is qualitatively in broad agreement with those in previous studies that reported the effects of C_{Ca} on the kinetics of char gasification. [6,23] **Figure 3.2(a2)** and **(b2)** depict profiles of dX/dt *vs* X for the gasification of Ca-α-DA and Ca-α-DB chars, respectively. Generally, dX/dt's for all char samples change via the maxima. In particular, the maxima seem to appear earlier as C_{Ca} increases. The kinetic model describes well such a variety of the shape of (1–X) *vs* t and dX/dt *vs* X curves in **Figure 3.2**. **Table 3.4** summarizes the optimized kinetic parameters for the Ca-catalyzed gasification. The model recognized those appeared trends as variations in ICA, ICD, and abundance of C1prec, $k'_C C_{C1prec}$ as discussed later.

3.3.3 Overall effects of Mg or K on the kinetics of Ca-catalyzed gasification

Panel (a1) and (b1) of **Figure 3.3** show the measured and calculated profiles of (1–X) *vs* t for the gasification of chars from Ca-0.06/Mg-0.17-DA and Ca-0.16/Mg-0.04-DB, respectively, and those from their counterparts with comparable Ca or Mg concentration in chars. The required time for completing the gasification of chars from Mg-0.16-DA and Mg-0.05-DB is nearly identical, 310 min, which is faster than those from DA/DB. This demonstrates that Mg has catalysis even though very low. The result is in good agreement with the previous studies that showed very little or insignificant catalytic activity of Mg. [4,33] On the other hand, the complete conversion of chars from Ca-0.06/Mg-0.17-DA and Ca-0.16/Mg-0.04-DB took 146 and 108 min, respectively, which is longer than those from Ca-0.06-DA and Ca-0.14-DB, respectively, with equal or even higher C_{Ca}. The presence of Mg appears to slow

down the kinetics of Ca-catalyzed gasification of lignite char. The discussion on the deactivation mechanism of Ca catalyst by Mg is mentioned later

Figure 4(a1) and **(b1)** show the measured and calculated profiles of (1–*X*) *vs t* for the gasification of chars from K-*α*, Ca-*α*, and Ca-*α*/K-*β*. In contrast with Mg, the presence of K enhances the overall rate of Ca-catalyzed gasification. The conversions of Ca-0.14/K-0.26-DA and Ca-0.14/K-0.13-DB chars were completed within 8 and 21 min, respectively, which are faster than their corresponding chars that were loaded only with Ca or K. The optimized kinetic parameters for describing the rate profiles for the gasification of Mg, Ca/Mg, K and Ca/K chars are shown in **Table 3.4**.

To further confirm the interactions between Ca and M (M = Mg or K) species during the gasification, the change in d*X*/d*t* with *X* for the conversion of Ca/M chars by the measurement was compared with that by the calculated one by assuming no interaction between those species, in other words, following the additive law. The $(dX/dt)_{\text{additive}}$ for Ca/Mg and Ca/K chars was represented by the blue-colored lines in **Figure 3.3** and **3.4**, respectively, and determined by the following equation:

$$\left(\frac{dX}{dt}\right)_{\text{additive}} = \left(\frac{dX}{dt}\right)_{\text{nc}} + \frac{C_{\text{Ca}}\text{in Ca/M}}{C_{\text{Ca}}}\left(\frac{dX}{dt}\right)_{\text{Ca}} + \frac{C_{\text{M}}\text{in Ca/M}}{C_{\text{M}}}\left(\frac{dX}{dt}\right)_{\text{M}} \qquad (12)$$

An inhibition effect is indicated if the measured d*X*/d*t* is lower than $(dX/dt)_{\text{additive}}$. The comparison between the measured and additive d*X*/d*t* profiles of Ca/Mg and Ca/K chars is shown in **Figure 3.3(a2)-(b2)** and **Figure 3.4(a2)-(b2)**, respectively. The measured d*X*/d*t*'s for Ca-0.06/Mg-0.17-DA and Ca-0.16/Mg-0.04-DB chars are lower than the additive d*X*/d*t*'s for the same samples over the entire range of *X*. It represents that the Ca-catalyzed gasification was inhibited by the presence of Mg. In contrast, as shown in **Figure 3.4(a2)** and **(b2)**, the cooperative effect between Ca and K is clearly indicated by the higher positions of the measured d*X*/d*t*'s of Ca/K chars compared to those of the additive d*X*/d*t*'s. Even though such effect depends on the amount and ratio of loaded metallic species.

Figure 3.4(a2) and **(b2)** also present other distinctive features. The d*X*/d*t*'s for chars from Ca-*α* and K-*α* show a maximum at $X \approx 0.15$ and 0.9, respectively, while those from Ca-*α*/K-*β* show maxima around $X = 0.15$ and 0.95. In general, increase in d*X*/d*t* can be attributed to that in the catalytic activity that interpreted by the present model as a transformation of catalyst precursor to be an active catalyst. These maxima seem to be contributed by two types of catalyst precursors from Ca and K species with different rates of transformation. To the authors' knowledge, this simultaneous maxima from Ca and K during the gasification has not been reported previously.

The calculated red-colored lines for Ca/K and K chars in **Figure 3.4** were drawn by modifying PRM. Two types of catalyst precursors, C1prec and C2prec, which exclusively convert to C1 and C2, respectively, were employed for describing two peaks in dX/dt's of Ca/K chars, while those for K chars employed only C2 and C2prec (see **Table 3.4**). The modified PRM estimated well the required conversion time. On the other hand, it was limited to describe the dX/dt *vs* X profiles for the gasification of Ca/K and K chars, particularly at the late-stage of its conversion, when the rapid increases in dX/dt occurred. The difficulty in describing the dX/dt *vs* X profiles might be caused either by the change in the transformation rate of catalyst precursor or the catalytic activity of K during the gasification. Further clarification on the kinetics of K-catalyzed gasification of char is discussed in **Chapter 4**.

3.3.4 Relationship between catalytic activity and composition of metallic species

As mentioned in **3.3.3**, the Ca interactions with Mg/K influenced the rate of Ca-catalyzed gasification. Further analysis was then conducted to understand the interaction mechanisms of those species. The optimized kinetic parameters in **Table 3.4** that represent the activity of a single or composite catalyst(s) were plotted against the concentration of metallic species.

$k'_C C_{C1prec}$ represents the potential activity of the C1 catalyst precursor (C1prec). As described in **2.3.4**, the kinetics of CO_2 gasification of chars from the original A and B lignites and also those from its derivatives with different compositions of inherent metallic species have been analyzed using an identical kinetic model as presently employed. A concept illustrated in **Figure 3.5(a)**, which was originally proposed in **Figure 2.10(b)**, was used to explain the correlation between the abundance of C1prec, $k'_C C_{C1prec}$, and the total concentration of inherent metallic species, ΣC_M (M = Na, K, Mg, Ca and Fe) that shown in **Figure 3.5(b)**. This concept follows a sequence of dissolution-saturation-nucleation-growth of metallic species in the carbon matrix of char. To examine this concept, the relationship between $k'_C C_{C1prec}$ and ΣC_M (M = K, Mg, and Ca) for all chars from metal(s)-loaded lignites were also plotted in **Figure 3.5(b)**. It is seen that $k'_C C_{C1prec}$ plots for Ca and Ca/Mg chars are on the same line in **Figure 3.5(b)** or around it. This indicates that the concept in **Figure 3.5(a)** is applicable to explain the variation in $k'_C C_{C1prec}$ as a function of C_{Ca} and $C_{Ca}+C_{Mg}$. However, those for the Mg chars are not able to be seen due to very small value of $k'_C C_{C1prec}$, while those for Ca/K chars are much higher than the others. The latter trend was not found in the previous study due to the low concentration of inherent K species in lignites. The examination of the potential catalytic activity of K species is conducted in **Chapter 4**.

Panels (a1)-(a2) and (b1)-(b2) of **Figure 3.6** plot initial (ICA-1) and potential (ICA-2) catalytic activity for all the char samples against C_{Ca} and $C_{Ca}+C_M$ (M = Mg or K), respectively. ICA-1's for chars from Ca-α-DA and Ca-α-DB are correlated linearly and well with C_{Ca} with a correlation factor (r^2) of 0.997 [see **Figure 3.6(a1)**]. **Figure 3.6(b1)** and **(b2)** present the correlation of ICA-2 value, which is the result of a sum of ICA-1 and $k'_C C_{Cn,prec}$ (see eqs. 8 and 9), with C_{Ca} that follows a plausible piecewise linear function. It is well known that the catalytic activity of Ca increases linearly with the Ca-loading level up to the loading saturation level (LSL) of about 2–4 wt%-char. [6,32,33] The present range of C_{Ca} is obviously far below such LSL. Thus, the linearity between ICA-1 and C_{Ca} relation is reasonable. **Figure 3.7** shows the relationship between $k_{Cn,0}$ (n = 1–3) and C_{Ca} for the Ca and Ca/Mg chars. It is seen that $k_{C1,0}$, $k_{C2,0}$, and $k_{C3,0}$ are correlated in linear manners with C_{Ca}. The linear relationship between the rate of catalytic activity and C_{Ca} was thus valid not only overall but also for the individual catalytic components. These relationships were then defined as a basis in determining the activities of Mg and K relative to Ca, by assuming that the all loaded metallic species behave in a similar way in both lignite matrices of DA and DB. The points of ICA-1 or ICA-2 *vs* C_{Ca} or $C_{Ca}+C_M$ for Mg, Ca/Mg, K and Ca/K chars were then compared with that for Ca chars. **Figure 3.6(a1)** and **(b1)** were displayed to show the changes in ICA-1 or ICA-2 due to the addition of Mg or K on Ca-loaded lignites. As shown in **Figure 3.6(a1)**, ICA-1 increases with increasing C_K, where the point of Ca-0.15/K-0.26-DA char, with the C_K/C_{Ca} ratio 1.7, is higher than that of Ca-0.14/K-0.13-DB char (C_K/C_{Ca} = 1.0). It demonstrates that not only Ca but also K contribute to ICA-1, even though the contribution of K (ICA-1/C_K) is lower than that of Ca in an equal mol basis [see **Figure 3.6(a2)**]. On the other hand, the contribution of K to ICA-2 is more or less in the same manner as that of Ca in Ca/K chars as seen in **Figure 3.6(b2)**. This shows the potential and overall catalytic activity per mol of Ca or K in char is similar to each other. The difference between ICA-1 and ICA-2 is due to the amount of the catalyst precursors (C1prec and C2prec), which is accounted for more than 50% of the total catalytic component of Ca/K chars.

In contrast with K, the point of Ca-0.06/Mg-0.17-DA char is slightly closer to the Ca-line than that of Ca-0.16/Mg-0.04-DB char although its C_{Mg}/C_{Ca} ratio is higher (2.8 *vs* 0.3). It shows that ICA-1 slightly decreases with the presence of Mg, in other words, a minor portion of active Ca catalyst was deactivated by Mg prior to the gasification. However, the degree of deactivation did not depend on the abundance of Mg, but on the amount of Ca itself. It should be noted that the catalysis of Mg, which is represented by the rate of gasification and as a result the gasification time, was similar for Mg-0.16-DA and Mg-0.05-DB chars, regardless of C_{Mg}

(see **Figure 3.3**). It was believed that the catalysis of Mg is contributed only via oxidation of Mg. It is known that ΔG's of carbonation of MgO and further reduction by C (see **Appendix 4**) are greatly positive. In other words, the carbonate-oxide and oxide-metal cycles of Mg seem to be impossible at 900°C, from the thermodynamic point of view. This behavior is clearly different from Ca that followed those cycles (see **Appendix 4**) and showed the catalysis along the char conversion (see **Figure 3.2**). [6,28] It was thus believed that a major portion of Mg in char after the pyrolysis has been in an oxide state, MgO, which has no catalysis. Matsukata *et al*. [34] investigated the effect of Ca^{2+} dopant on the catalysis of MgO for 1-butane isomerization. They found that the doped Ca enhanced the activity of MgO while it was not transformed into $CaCO_3$. It was also found that a type of Ca, which was in the form of CaO, is highly dispersed on the surface of MgO. [34] Their findings showed that the interaction between Ca/CaO and MgO inhibited the formation of $CaCO_3$, which is vital for the carbonate-oxide cycle of Ca as mentioned above. As shown in **Figure 3.7**, $k_{C1,0}$ of char from Ca-0.16/Mg-0.04-DB is lower than those of Ca-α samples in an equal C_{Ca}, in other words, $k_{C1,0}$ decreases with the presence of Mg. During the pyrolysis, the physical interaction between Ca and Mg particles becomes more intensive due to shrinkage in the volume of lignite char. It is well known that Ca is greatly more active catalyst than Mg. In particular, C1, which consists of nano-sized 'active' particles that had catalysis, is the most active component among C*n* catalysts. It was believed that a portion of active Ca/CaO in char matrix, mainly C1 catalyst, had interacted with MgO, losing its intrinsic catalytic activity. The kinetic analysis thus revealed that the Mg deactivated a portion of C1 before the gasification *i.e.*, during the pyrolysis. In addition, ICA-2's for Ca/Mg chars seem to be only contributed by Ca, which is indicated by ICA-2 plots for those chars that are on the same line in **Figure 3.6(b1)**.

3.3.5 Discussion on catalysis of inherent and extraneous metallic species in lignite char

This section discussed the differences in activity and deactivation of catalyst species that inherently present or intentionally added into lignite. As mentioned in **2.3.5**, the overall rate of catalytic activity and that of catalyst deactivation of CO_2 gasification of chars from twenty lignites, derived from identical A and B, with different compositions of inherent catalyst species, have been described successfully by using PRM. **Figure 3.8** plots ICA-2's for all the lignite char samples with inherent and extraneous catalysts against the total concentration of Na, K, Ca, and Fe in the chars. Mg was not involved due to its insignificant catalytic activity as discussed previously. The major portion, ranging 66–98% in mol basis, of catalytic species in those twenty chars is Ca (see **Appendix 3**), which is similar to the present conditions (see

Table 3.2 and **3.3**). ICA-2 for the chars from the lignites that contained inherent metallic species is clearly greater than those from the metal(s)-loaded lignites on an equal mol basis. It should be noted that the present metal(s)-loaded lignite samples have been nearly free from SiO_2/Al_2O_3. This was much different from the twenty lignites used in **Chapter 2** that contain 0.1–3.5 wt%-daf-char of SiO_2 and Al_2O_3. It demonstrates the outstanding catalytic activity of inherent metallic species in lignite that cannot be replicated by that of doped metallic species.

Figure 3.9(a) plots the overall rate constant for catalyst deactivation (ICD-2) with ICA-2 for the chars from the metal(s)-loaded lignites and the previous twenty lignites (Group A and B chars). ICD-2 increases with ICA-2, even though its relation not in linear manners. It demonstrates for each series of lignite chars that more active catalyst underwent more rapid deactivation. The deactivation rates of the chars from Ca and Ca/Mg-loaded lignites are higher than those from K and Ca/K-loaded lignites and those from the Group A and B lignites on an equal ICA-2 basis. This shows the advantage of employing K over Ca as catalyst is the much lower rate of deactivation. **Figure 3.9(b)** plots ICD-2 against modified ICA-2 (ICA-2·F). As mentioned in **2.3.6**, Equations 13 and 14 were employed to estimate the mechanism of catalyst deactivation. It was found that a single and linear relationship between ICD-2 and (ICA-2·F) for chars from both groups can be obtained by assuming $f_{Na} = f_K = f_{Ca} = 1.0$, $f_{Mg} = 3.5$ and $f_{Fe} = 4.9$. This suggested a faster deactivation of Ca catalyst by their interactions with Mg and Fe.

$$\text{ICD-2} = \text{ICA-2}\cdot F \tag{13}$$

$$F = \frac{f_{Na}C_{Na} + f_K C_K + f_{Ca}C_{Ca} + f_{Fe}C_{Fe} + f_{Mg}C_{Mg}}{C_{Na} + C_K + C_{Ca} + C_{Fe} + C_{Mg}} \tag{14}$$

These functions were then applied for the data in **Table 3.2–3.4**. By trial and error, it was found that $f_K = 1.1$, $f_{Ca} = 3.2$ and $f_{Mg} = 3.5$ were necessary so that the resulted plots fit with the linear line that that represents (ICD-2) = 0.258F (ICA-2) in **Figure 3.9(b)**. The coefficient f_{Ca} increased triple, while f_{Mg} unchanged in the present study. The result suggests a faster deactivation of doped Ca catalyst compare to that of the inherent Ca catalyst. Moreover, char from Ca-0.33-DB underwent very fast deactivation, even though the reason was not fully understood for now. It also suggests that Mg played a consistent role in promoting the deactivation of Ca catalyst, probably C1, which is the most active Ca species, during the gasification. On the other hand, the gasification of chars from K-loaded lignites experienced very little deactivation. It is believed that the volatilization of a portion of K species from char is responsible for the deactivation since the content of SiO_2 in chars has been minimized. The examination of potassium volatilization was left for **Chapter 4**. Overall, within the range of the present experimental conditions, Equations 13 and 14 are applicable to the quantitative

description of ICD-2 as a function of ICA-2 and composition of metallic species in char, regardless of its origin. The activity of catalysts during the gasification depends mainly on its nature, its concentration in char, and its dispersion in the carbon matrix of char. [35,36] It was believed that the nature of the inherent metallic species in carbon matrix of lignite/char somewhat differences with that of loaded metallic species via an ion-exchange process.

Solano *et al*. [35] investigated the CO_2 chemisorption of CaO particles in bulk CaO and CaO-carbon system by using TG-DTA, MS, and XRD techniques to determine dispersion, average particle size, and specific CaO surface area. They also measured the rate of CO_2 gasification of carbon char, prepared by the pyrolysis of Ca-loaded phenol-formaldehyde resin. They found that CaO particles on the carbon matrix are smaller than those in the CaO sample. It was also found that the available surface area of the Ca catalyst, which decreased with the progress of CO_2 gasification, is an important factor controlling its catalytic activity. Their results suggested that the chemical bonding between Ca and carbon matrix in char plays important roles to stabilize Ca particles and to inhibit growth of the nanosized CaO particles. [37] It was likely that Ca species in chars from the twenty lignites have stronger bonding with carboxylic groups and thus have a lower deactivation rate than that from the Ca-loaded lignites. The examination of the properties of formed bonding in lignite will be left for a future study.

3.4 Conclusion

This study investigated the effects of Ca interactions with Mg or K species on the kinetics of CO_2 gasification of lignite char. The following conclusions have been drawn from the kinetic analysis. (1) The parallel reaction model that employed multi-catalytic species described the time-dependent changes in the char conversion up to 0.999 for the gasification of chars from Ca, Mg, K, Ca/Mg, and Ca/K-loaded lignites. (2) The initial catalyst activity, *i.e*., the rate of catalytic gasification, was correlated well and linearly with the Ca concentration in char (0.035–0.332 mol-Ca/kg-daf-char). (3) The Mg/MgO deactivated a portion of the most active component of Ca catalyst, prior to and during the gasification of Ca/Mg chars. (4) The overall catalytic activity per mol of K was similar to that of Ca, but its deactivation rate was much lower. (5) The inherent catalyst species in lignite performed better in terms of activity and deactivation kinetics than doped catalyst species during CO_2 gasification of lignite char.

Table 3.1. Ultimate and proximate analysis, and metallic species contents of original and demineralized lignites.

	Ultimate analysis (wt%, daf)				Proximate analysis (wt%, db)			Metallic species (wt%, db)				
Lignite	C	H	N	O[a]	ash	VM[b]	FC[c]	Na	K	Mg	Ca	Fe
A	70.3	5.0	0.8	24.0	2.6	52.1	45.3	0.003	0.012	0.351	0.353	0.115
DA	68.9	5.0	0.8	25.3	< 0.1	53.1	46.9	0.000	0.000	0.001	0.006	0.002
B	67.5	4.5	1.1	26.9	5.0	48.7	46.3	0.005	0.012	0.241	0.766	0.005
DB	64.6	4.6	1.0	29.8	< 0.1	53.1	46.9	0.000	0.001	0.001	0.007	0.000

[a] by difference. [b] volatile matter. [c] fixed carbon.

Table 3.2. Ca concentration and yield of char from original, demineralized, and Ca-loaded lignites.

Original Sample	Ca concentration		Char yield
	in suspension, g-Ca/100-g-lignite	in char, mol-Ca/kg-daf-char	wt% daf lignite
DA	-	0.003	42.3
Ca-0.04-DA	0.05	0.036	43.6
Ca-0.06-DA	0.10	0.060	43.6
Ca-0.15-DA	0.25	0.150	43.2
Ca-0.32-DA	0.50	0.318	43.5
A	-	0.166	44.3
DB	-	0.003	42.9
Ca-0.04-DB	0.05	0.038	43.3
Ca-0.06-DB	0.10	0.056	43.7
Ca-0.14-DB	0.25	0.141	43.9
Ca-0.33-DB	0.50	0.332	43.6
B	-	0.359	45.7

Table 3.3. Ca, Mg and/or K concentrations and yield of char from M-loaded lignites.

Sample	Metallic concentration in char		Char yield,
	Ca, mol/kg daf-char	*M* (Mg or K), mol/kg daf-char	wt% daf lignite
Mg-0.16-DA	-	0.156	42.7
Ca-0.06/Mg-0.17-DA	0.060	0.167	43.8
Mg-0.05-DB	-	0.052	43.5
Ca-0.16/Mg-0.04-DB	0.160	0.043	43.4
K-0.28-DA	-	0.282	46.1
Ca-0.15/K-0.26-DA	0.151	0.257	45.9
K-0.18-DB	-	0.182	45.5
Ca-0.14/K-0.13-DB	0.136	0.133	45.7

Table 3.4. Optimized kinetic parameters.

Sample ID	Ca-0.04-DA	Ca-0.06-DA	Ca-0.15-DA	Ca-0.32-DA
$k_{ncg,}$ min^{-1}	3.5×10^{-3}	3.5×10^{-3}	3.5×10^{-3}	3.5×10^{-3}
ICA-1, min^{-1}	4.7×10^{-3}	1.2×10^{-2}	8.2×10^{-2}	1.8×10^{-1}
ICA-2, min^{-1}	1.9×10^{-2}	3.0×10^{-2}	1.2×10^{-1}	2.0×10^{-1}
ICD-1, min^{-1}	1.8×10^{-3}	5.1×10^{-3}	6.1×10^{-2}	1.4×10^{-1}
ICD-2, min^{-1}	1.1×10^{-2}	2.0×10^{-2}	9.6×10^{-2}	1.7×10^{-1}
C_{C1prec} , -	7.5×10^{-1}	6.0×10^{-1}	2.9×10^{-1}	1.1×10^{-1}
$C_{C1,0}$, -	1.4×10^{-1}	1.8×10^{-1}	4.7×10^{-1}	6.1×10^{-1}
$C_{C2,0}$, -	7.5×10^{-2}	1.3×10^{-1}	1.8×10^{-1}	2.5×10^{-1}
$C_{C3,0}$, -	3.7×10^{-2}	7.0×10^{-2}	5.0×10^{-2}	2.2×10^{-2}
$C_{C4,0}$, -		2.0×10^{-2}	9.0×10^{-3}	6.2×10^{-3}
k_{C1prec} , min^{-1}	7.6×10^{-2}	1.5×10^{-1}	1.3	3.0
$k_{C1,0}$, min^{-1}	2.6×10^{-3}	5.3×10^{-3}	5.5×10^{-2}	1.2×10^{-1}
$k_{C2,0}$, min^{-1}	1.4×10^{-3}	3.8×10^{-3}	2.1×10^{-2}	5.1×10^{-2}
$k_{C3,0}$, min^{-1}	6.9×10^{-4}	2.1×10^{-3}	5.8×10^{-3}	4.6×10^{-3}
$k_{C4,0}$, min^{-1}		5.9×10^{-4}	1.0×10^{-3}	1.3×10^{-3}
k_{loss-1} , min^{-1}	1.2×10^{-2}	2.5×10^{-2}	1.2×10^{-1}	2.2×10^{-1}
k_{loss-2} , min^{-1}	1.4×10^{-3}	3.1×10^{-3}	2.4×10^{-2}	3.1×10^{-2}
k_{loss-3} , min^{-1}	1.0×10^{-4}	1.3×10^{-3}	5.3×10^{-3}	3.6×10^{-3}
k_{loss-4} , min^{-1}		1.5×10^{-5}	1.1×10^{-4}	9.1×10^{-5}

Sample ID	Ca-0.04-DB	Ca-0.06-DB	Ca-0.14-DB	Ca-0.33-DB
$k_{ncg,}$ min^{-1}	3.5×10^{-3}	3.5×10^{-3}	3.5×10^{-3}	3.5×10^{-3}
ICA-1, min^{-1}	4.0×10^{-3}	1.2×10^{-2}	7.1×10^{-2}	2.0×10^{-1}
ICA-2, min^{-1}	1.8×10^{-2}	2.9×10^{-2}	1.2×10^{-1}	2.1×10^{-1}
ICD-1, min^{-1}	1.2×10^{-3}	5.1×10^{-3}	4.4×10^{-2}	2.8×10^{-2}
ICD-2, min^{-1}	1.0×10^{-2}	1.8×10^{-2}	8.4×10^{-2}	3.0×10^{-1}
C_{C1prec} , -	7.8×10^{-1}	6.0×10^{-1}	4.1×10^{-1}	5.0×10^{-2}
$C_{C1,0}$, -	9.8×10^{-2}	2.1×10^{-1}	4.1×10^{-1}	5.3×10^{-1}
$C_{C2,0}$, -	9.0×10^{-2}	1.6×10^{-1}	1.3×10^{-1}	3.4×10^{-1}
$C_{C3,0}$, -	3.2×10^{-2}	2.5×10^{-2}	3.1×10^{-2}	7.0×10^{-2}
$C_{C4,0}$, -			1.3×10^{-2}	1.0×10^{-2}
k_{C1prec} , min^{-1}	5.8×10^{-2}	1.6×10^{-1}	7.6×10^{-1}	5
$k_{C1,0}$, min^{-1}	1.8×10^{-3}	6.2×10^{-3}	5.0×10^{-2}	1.2×10^{-1}
$k_{C2,0}$, min^{-1}	1.6×10^{-3}	4.7×10^{-3}	1.6×10^{-2}	6.1×10^{-2}
$k_{C3,0}$, min^{-1}	5.8×10^{-4}	7.1×10^{-4}	3.7×10^{-3}	1.5×10^{-2}
$k_{C4,0}$, min^{-1}			1.5×10^{-3}	2.1×10^{-3}
k_{loss-1} , min^{-1}	1.1×10^{-2}	2.2×10^{-2}	9.8×10^{-2}	4.9×10^{-1}
k_{loss-2} , min^{-1}	1.1×10^{-3}	1.9×10^{-3}	2.1×10^{-2}	4.6×10^{-2}
k_{loss-3} , min^{-1}	1.0×10^{-6}	1.5×10^{-5}	5.5×10^{-3}	1.3×10^{-2}
k_{loss-4} , min^{-1}			3.5×10^{-4}	5.3×10^{-4}

Table 3.4. Optimized kinetic parameters. (cont.)

Sample ID	Mg-0.16-DA	Ca-0.06/ Mg-0.17-DA	Mg-0.05-DB	Ca-0.16/ Mg-0.04-DB
$k_{ncg,}$ min^{-1}	3.5×10^{-3}	3.5×10^{-3}	3.5×10^{-3}	3.5×10^{-3}
ICA-1, min^{-1}	7.1×10^{-3}	1.7×10^{-2}	3.4×10^{-3}	7.4×10^{-2}
ICA-2, min^{-1}	7.1×10^{-3}	3.2×10^{-2}	3.7×10^{-3}	1.2×10^{-1}
ICD-1, min^{-1}	7.5×10^{-3}	1.2×10^{-2}	1.6×10^{-3}	5.1×10^{-2}
ICD-2, min^{-1}	7.5×10^{-3}	2.7×10^{-2}	1.9×10^{-3}	9.6×10^{-2}
C_{C1prec} , -		4.6×10^{-1}	1.0×10^{-1}	4.0×10^{-1}
$C_{C1,0}$, -	7.3×10^{-1}	3.5×10^{-1}	6.6×10^{-1}	4.2×10^{-1}
$C_{C2,0}$, -	2.2×10^{-1}	1.6×10^{-1}	1.5×10^{-1}	1.7×10^{-1}
$C_{C3,0}$, -	5.1×10^{-2}	2.9×10^{-2}	8.8×10^{-2}	1.4×10^{-2}
$C_{C4,0}$, -				4.0×10^{-3}
k_{C1prec} , min^{-1}		2.1×10^{-1}	1.0×10^{-1}	8.4×10^{-1}
$k_{C1,0}$, min^{-1}	5.2×10^{-3}	1.1×10^{-2}	2.5×10^{-3}	5.1×10^{-2}
$k_{C2,0}$, min^{-1}	1.5×10^{-3}	5.0×10^{-3}	5.7×10^{-4}	2.0×10^{-2}
$k_{C3,0}$, min^{-1}	3.6×10^{-4}	9.2×10^{-4}	3.3×10^{-4}	1.7×10^{-3}
$k_{C4,0}$, min^{-1}				4.9×10^{-4}
k_{loss-1} , min^{-1}	1.0×10^{-2}	3.2×10^{-2}	2.5×10^{-3}	1.1×10^{-1}
k_{loss-2} , min^{-1}	8.2×10^{-4}	3.1×10^{-3}	2.0×10^{-4}	1.8×10^{-2}
k_{loss-3} , min^{-1}	6.0×10^{-6}	1.5×10^{-4}	2.0×10^{-5}	1.4×10^{-3}
k_{loss-4} , min^{-1}				5.0×10^{-6}

Sample ID	K-0.28-DA	Ca-0.15/K-0.26-DA	K-0.18-DB	Ca-0.14/K-0.13-DB
$k_{ncg,}$ min^{-1}	3.5×10^{-3}	3.5×10^{-2}	3.5×10^{-3}	3.5×10^{-2}
ICA-1, min^{-1}	9.0×10^{-3}	1.1×10^{-1}	6.9×10^{-3}	7.5×10^{-2}
ICA-2, min^{-1}	1.8×10^{-1}	2.5×10^{-1}	9.0×10^{-2}	1.9×10^{-1}
ICD-1, min^{-1}	5.0×10^{-7}	4.2×10^{-2}	7.7×10^{-7}	4.9×10^{-1}
ICD-2, min^{-1}	1.0×10^{-5}	1.2×10^{-1}	1.0×10^{-5}	1.0×10^{-1}
C_{C1prec} , -		3.2×10^{-1}		4.2×10^{-1}
C_{C2prec} , -	9.5×10^{-1}	2.6×10^{-1}	9.2×10^{-1}	1.9×10^{-1}
$C_{C1,0}$, -		1.7×10^{-1}		3.9×10^{-1}
$C_{C2,0}$, -	5.0×10^{-2}	2.5×10^{-1}	7.7×10^{-2}	1.0×10^{-3}
k_{C1prec} , min^{-1}		2		1.4
k_{C2prec} , min^{-1}	1.9×10^{-2}	3.6×10^{-1}	1.1×10^{-2}	4.6×10^{-2}
$k_{C1,0}$, min^{-1}		4.3×10^{-2}		7.5×10^{-2}
$k_{C2,0}$, min^{-1}	9.0×10^{-3}	6.3×10^{-2}	6.9×10^{-3}	1×10^{-5}
k_{loss-1} , min^{-1}		2.5×10^{-1}		1.3×10^{-1}
k_{loss-2} , min^{-1}	1.0×10^{-5}	1.0×10^{-5}	1.0×10^{-5}	1.0×10^{-6}

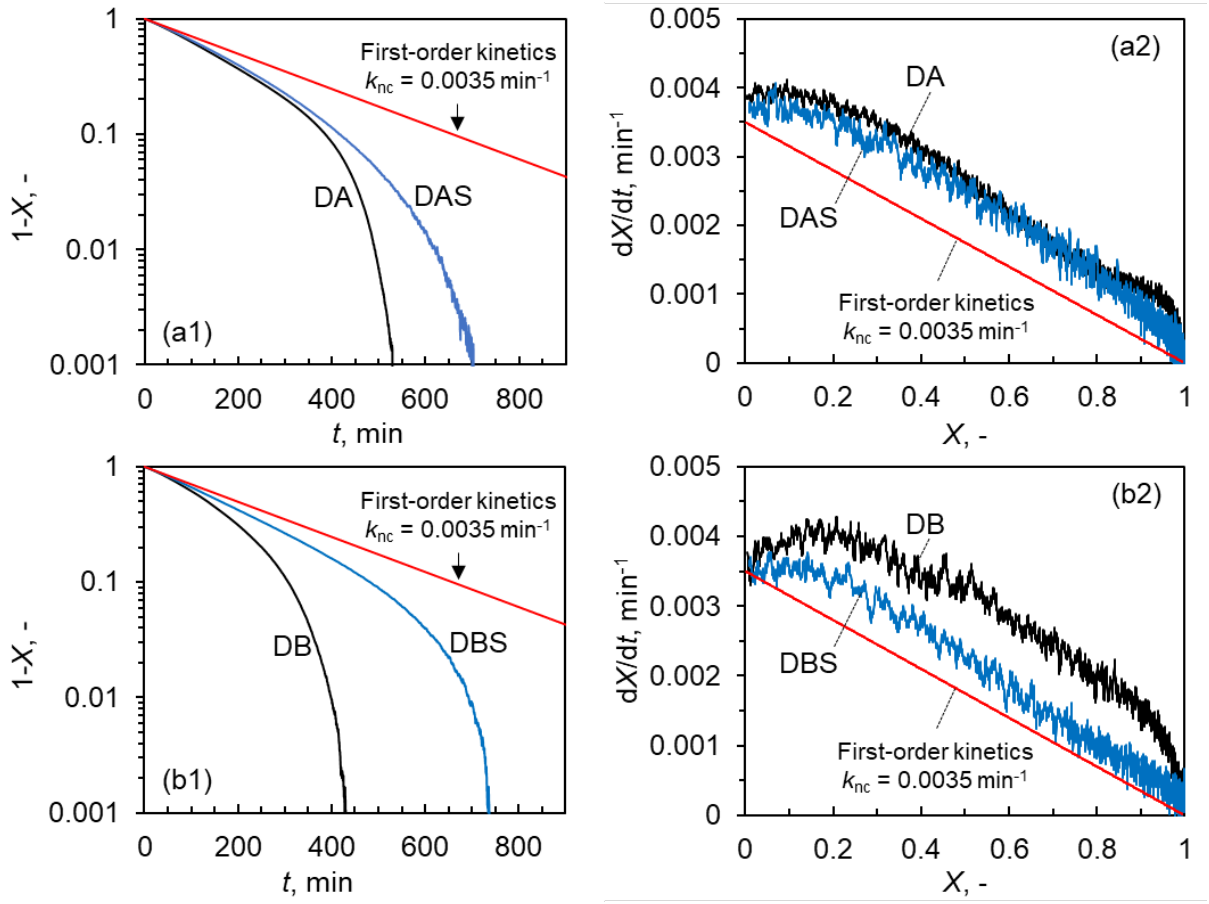

Figure 3.1. Characteristics of gasification of chars from the demineralized lignites with and without SiO_2-mixed. Effects of SiO_2 addition on change in [(a1) and (b1)] (1–*X*) with time, and [(a2) and (b2)] the rate of gasification, d*X*/d*t*, as a function of *X* for DA-DAS, and DB-DBS chars respectively. The red-colored straight lines in the graphs are drawn for indicating (1–*X*) or d*X*/d*t* of first-order kinetics with k_{nc} = 0.0035 min^{-1}.

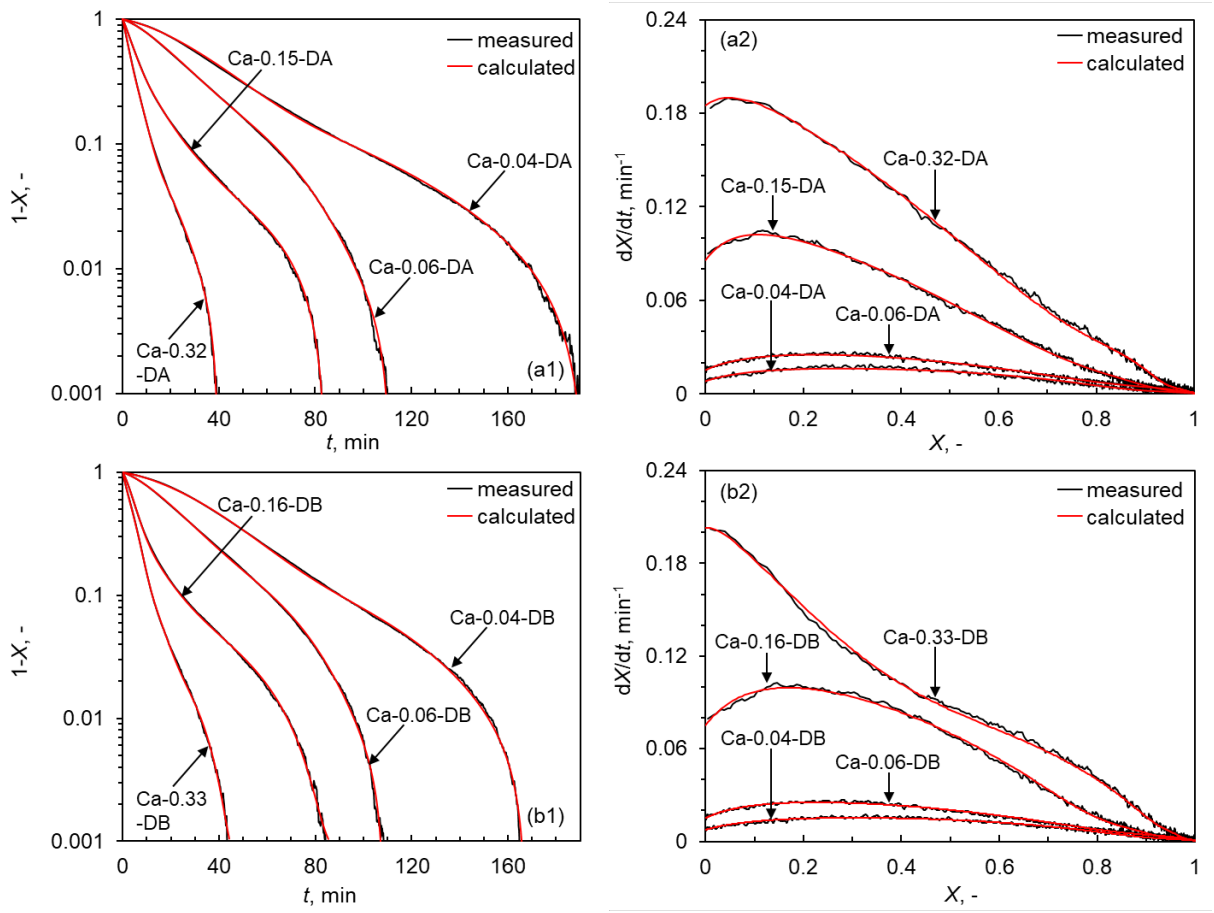

Figure 3.2. Effect of Ca concentration in char, C_{Ca}, on [(a1) and (b1)] 1–*X vs t* profiles, and [(a2) and (b2)] d*X*/d*t vs X* profiles for the gasification of chars from Ca-loaded DA and DB, respectively. Black lines, measured; red lines, calculated.

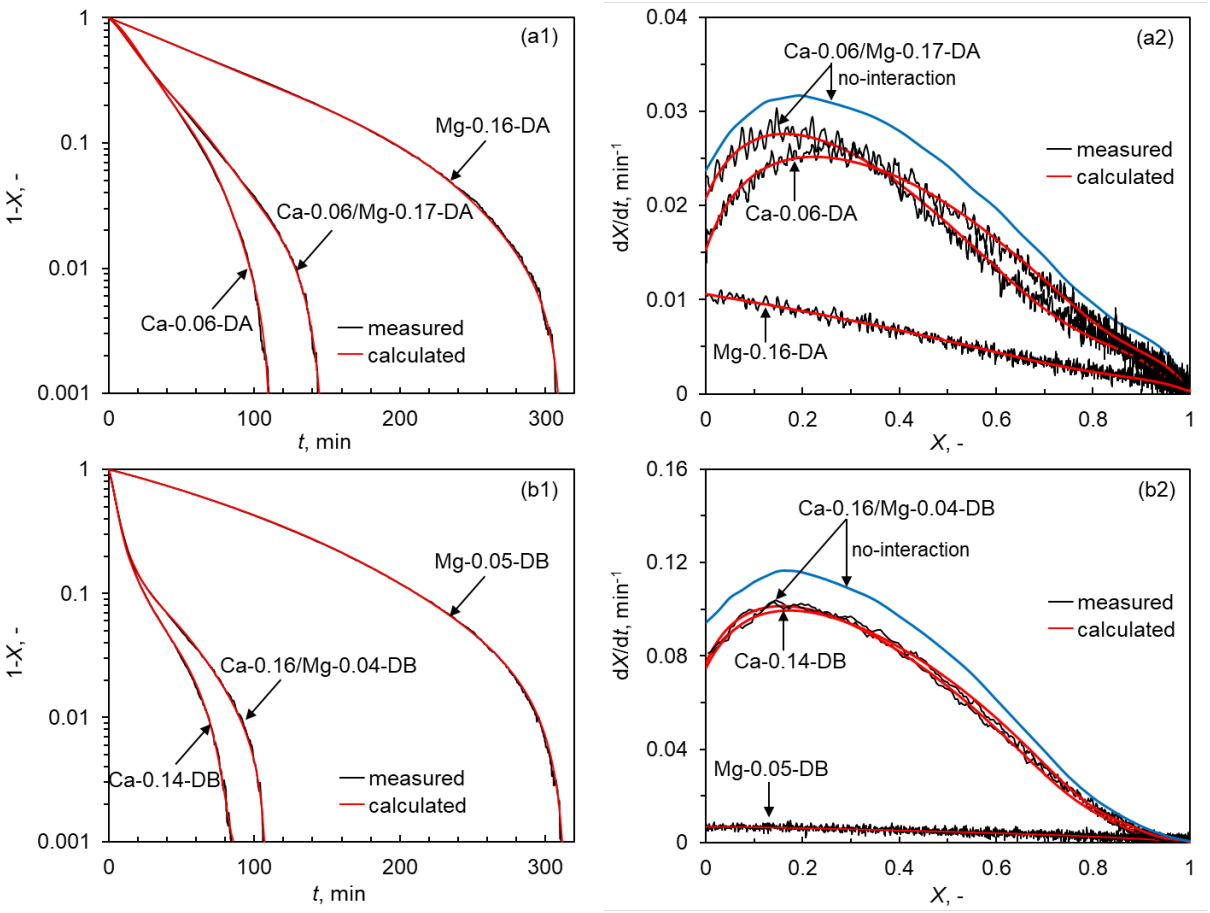

Figure 3.3. Measured and calculated [(a1) and (b1)] 1–*X vs t* profiles and [(a2) and (b2)] d*X*/d*t vs X* profiles for the gasification of chars from Ca, Mg, and Ca/Mg-loaded lignites. Blue-colored lines are drawn by assuming no interaction between Ca and Mg during the gasification.

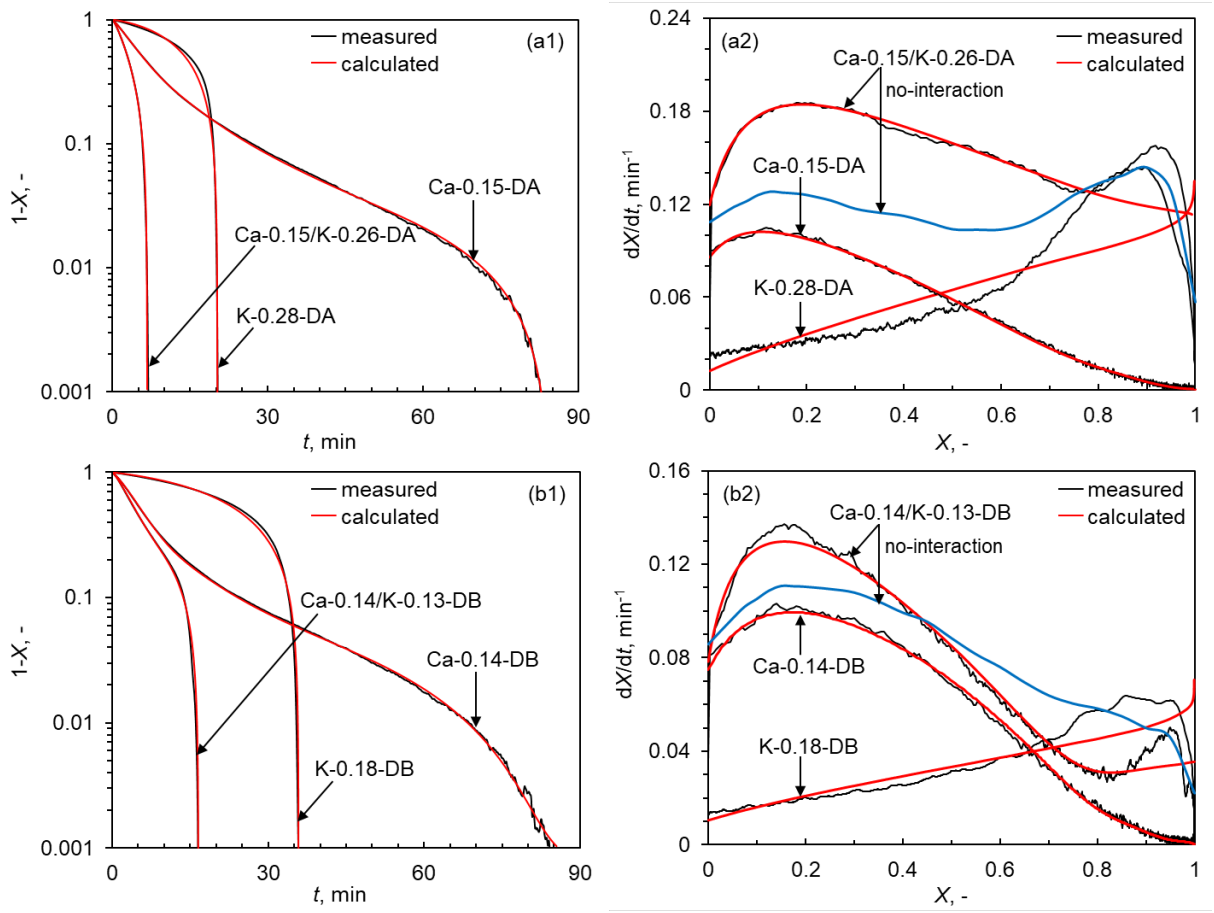

Figure 3.4. Measured and calculated [(a1) and (b1)] 1–*X vs t* profiles and [(a2) and (b2)] d*X*/d*t vs X* profiles for the gasification of chars from Ca, K, and Ca/K-loaded lignites. Blue-colored lines are drawn by assuming no interaction between Ca and K during the gasification.

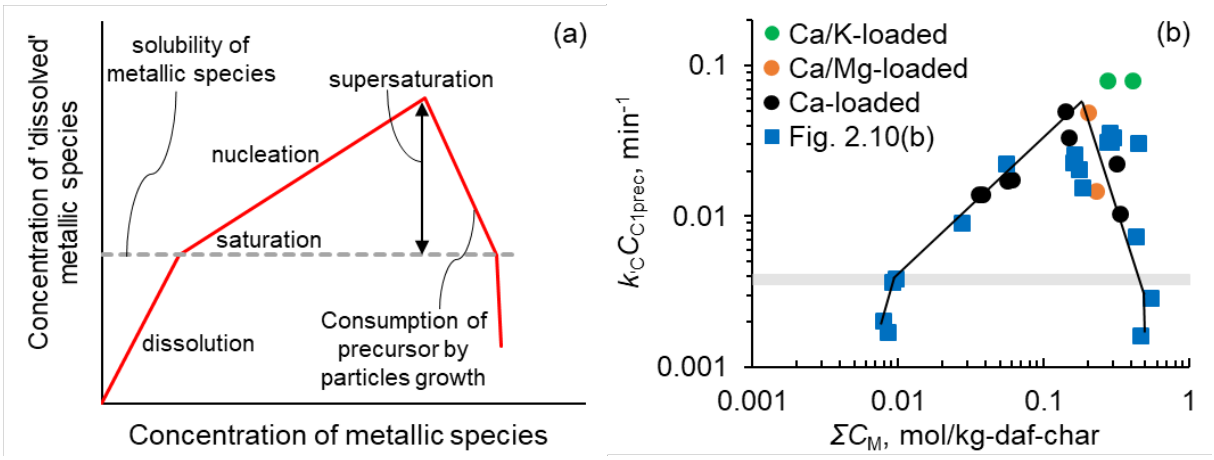

Figure 3.5. (a) Schematic expression of the relationship between the catalyst precursor concentration and the total concentration of metallic species that adopted from **Figure 2.10(a)**. (b) Plot of $k'_C C_{C1prec}$ against the total concentration of inherent/extraneous metallic species (Na, K, Mg, Ca, and Fe) at $t = 0$.

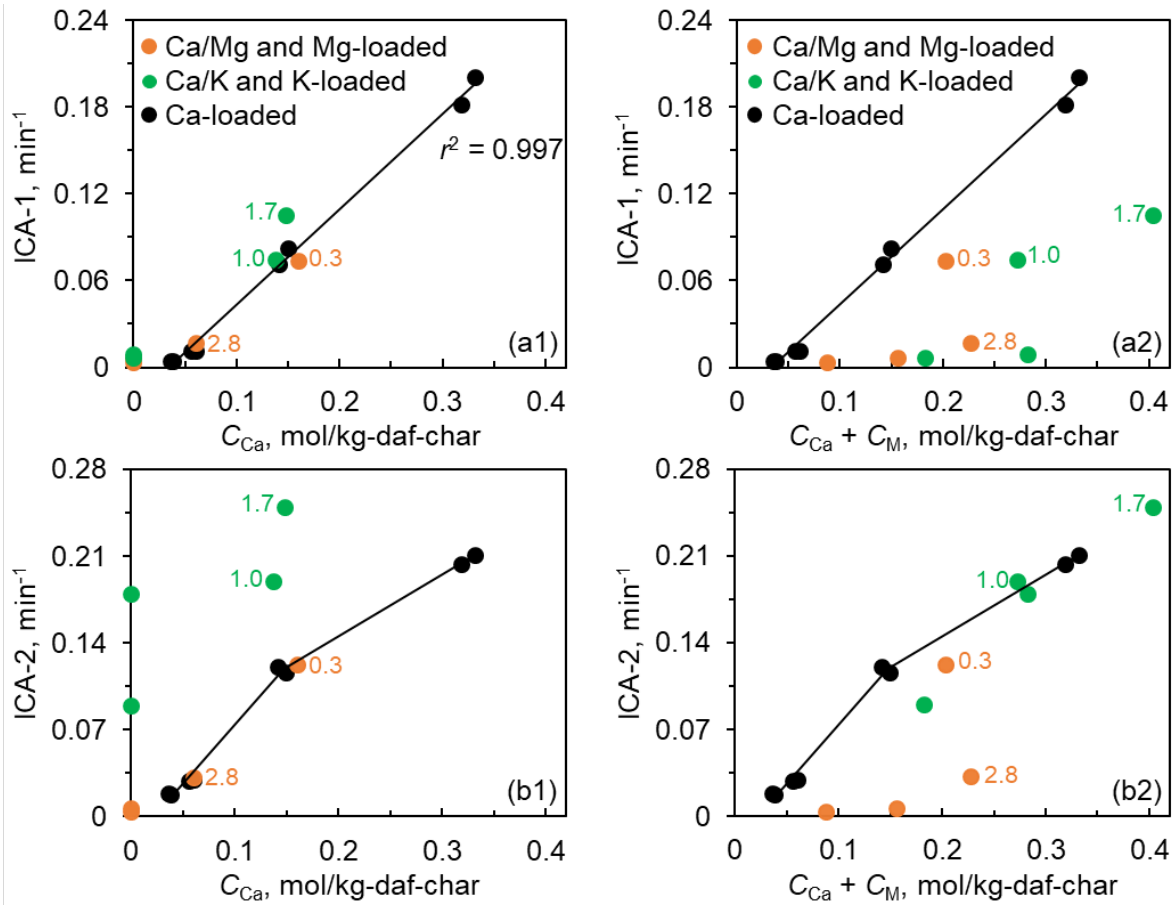

Figure 3.6. Relationship between initial (ICA-1) and potential (ICA-2) catalyst activity and the concentration of metallic species. The catalytic activities in [(a1) and (b1)] were plotted against C_{Ca}, while those in [(a2) and (b2)] were plotted against C_{Ca} + C_M (M = Mg or K). The orange and green-colored texts in the figures are displayed for showing the ratio of C_{Mg}/C_{Ca} or C_K/C_{Ca} in the Ca/Mg or Ca/K chars, respectively.

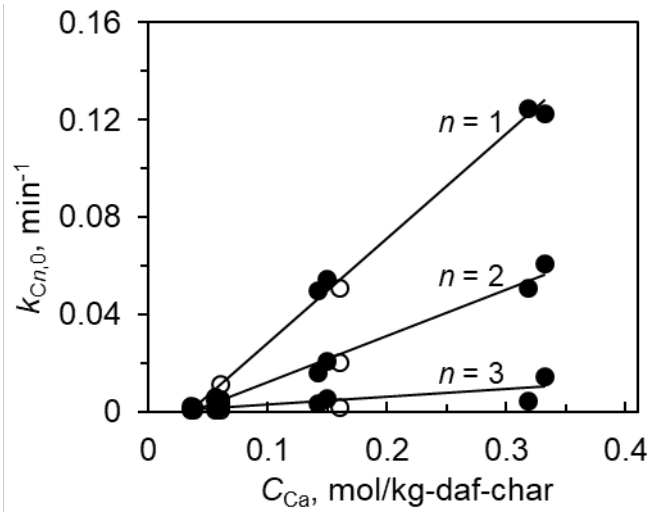

Figure 3.7. Relationship between $k_{Cn,0}$ (n = 1–3), and C_{Ca} for the chars from Ca (solid symbols) and Ca/Mg (open symbols) chars by assuming the catalysis is only contributed by Ca species.

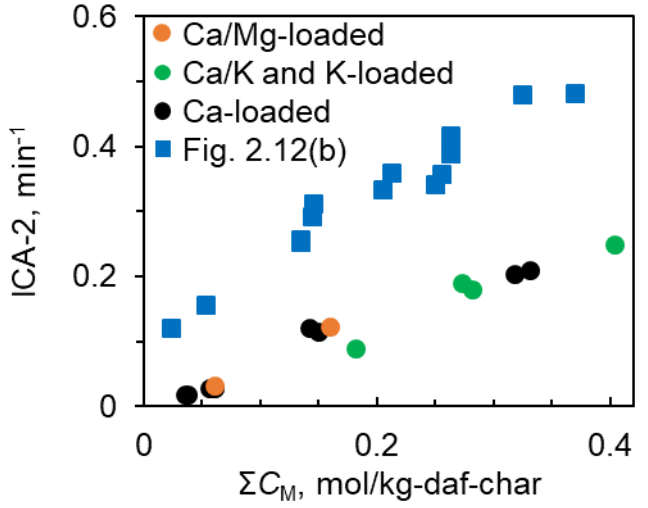

Figure 3.8. Plot of ICA-2 against the total concentration of inherent/extraneous metallic species (Na, K, Ca, and Fe) in the char at t = 0.

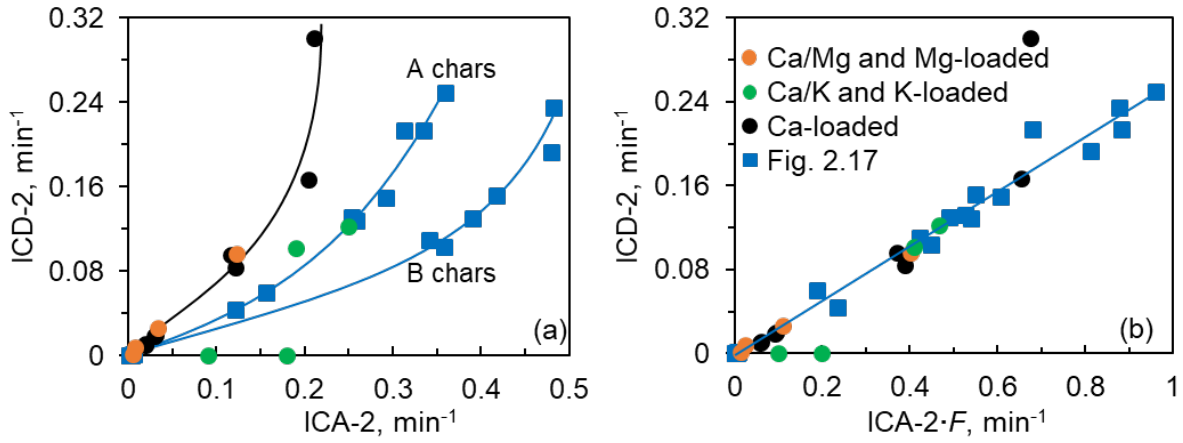

Figure 3.9. ICD-2 correlation with (a) ICA-2 or (b) ICA-2.*F* for gasification of chars from twenty lignites that contain inherent metallic species (Group A and B chars) and metal(s) loaded lignites. Parameters f_M's for the metal(s) loaded lignite chars in (b) were set as follows: f_K = 1.1, f_{Ca} = 3.2, f_{Mg} = 3.5 to fit with the linear solid line drawn in the figure that represents the function, (ICD-2) = 0.258*F* (ICA-2), from **Fig. 2.17**. The optimized parameters f_M's for inherent catalysts are as follows: f_{Na} = f_K = f_{Ca} = 1.0, f_{Mg} = 3.5, f_{Fe} = 4.9).

3.5 References

1. Q. Yang, X. Li, Q. Yang, W. Huang, P. Yu, D. Zhang, *ACS Sustainable Chemistry & Engineering*, (2019).
2. J. Hayashi, S. Kudo, H.S. Kim, K. Norinaga, K. Matsuoka, S. Hosokai, *Energy & Fuels*, **28** (2014), 4–21.
3. Y. Huang, X. Yin, C. Wu, C. Wang, J. Xie, Z. Zhou, L. Ma, H. Li, *Biotechnology Advances*, **27** (2009), 568–572.
4. P. Lahijani, Z.A. Zainal, A.R. Mohamed, M. Mohammadi, *Bioresource Technology*, **144** (2013), 288–295.
5. R.P.W.J. Struis, C. Von Scala, S. Stucki, R. Prins, *Chemical Engineering Science*, **57** (2002), 3593–3602.
6. H. Kim, S. Kudo, K. Tahara, Y. Hachiyama, H. Yang, K. Norinaga, J. Hayashi, *Energy & Fuels*, **27** (2013), 6617–6631.
7. J. Kramb, N. DeMartini, M. Perander, A. Moilanen, J. Konttinen, *Fuel Processing Technology*, **148** (2016), 50–59.
8. G. Yu, D. Yu, F. Liu, X. Yu, J. Han, J. Wu, M. Xu, *Fuel*, **254** (2019).
9. J. Wang, Y. Yao, J. Cao, M. Jiang, *Fuel*, **89** (2010), 310–317.
10. M.-Q. Jiang, R. Zhou, J. Hu, F.-C. Wang, J. Wang, *Fuel*, **99** (2012), 64–71.
11. J. Hu, L. Liu, M. Cui, J. Wang, *Fuel*, **111** (2013), 628–635.
12. J. Tang, X. Wu, J. Wang, *Fuel*, **141** (2015), 46–55.
13. R.A. Arnold, R. Habibi, J. Kopyscinski, J.M. Hill, *Energy & Fuels*, **31** (2017), 6240–6247.
14. L.R. Radovic, P.L. Walker, R.G. Jenkins, *Fuel*, **63** (1984) 1028–1030.
15. K. Formella, P. Leonhardt, A. Sulimma, K.H. van Heek, H. Jüntgen, *Fuel*, **65** (1986), 1470–1472.
16. B.C. Gorrini, L.R. Radovic, A.L. Gordon, *Fuel*, **69** (1990), 789–791.
17. H. Yang, S. Kudo, K. Norinaga, J. Hayashi, *Energy & Fuels*, **30** (2016), 1616–1627.
18. Karlström, M.J. Dirbeba, M. Costa, A. Brink, M. Hupa, *Energy & Fuels*, **32** (2018), 10695–10700.
19. H.E. Belkin, S.J. Tewalt, J.C. Hower, J.D. Stucker, J.M.K. O'Keefe, *International Journal of Coal Geology*, **77** (2009), 260–268.
20. S. Kudo, A. Mori, G. Hayashi, T. Yoshida, N. Okuyama, K. Norinaga, J. Hayashi, *Energy & Fuels*. **32** (2018) 4364–4371.
21. Y. Zhang, M. Ashizawa, S. Kajitani, K. Miura, *Fuel*, **87** (2008), 475–481.

22. Y. Zhang, S. Hara, S. Kajitani, M. Ashizawa, *Fuel*, **89** (2010), 152–157.
23. E. Byambajav, Y. Hachiyama, S. Kudo, K. Norinaga, J. Hayashi, *Energy & Fuels*, **30** (2016), 1636–1646.
24. B. Bayarsaikhan, J. Hayashi, T. Shimada, C. Sathe, C.Z. Li, A. Tsutsumi, T. Chiba, *Fuel*, **84** (2005), 1612–1621.
25. T. Kitsuka, B. Bayarsaikhan, N. Sonoyama, S. Hosokai, C.Z. Li, K. Norinaga, J. Hayashi, *Energy & Fuels*, **21** (2007), 387–394
26. M. Kajita, T. Kimura, K. Norinaga, C.Z. Li, J. Hayashi, *Energy & Fuels*, **24** (2010), 108–116.
27. L. Bai, S. Kudo, K. Norinaga, Y. Wang, J. Hayashi, *Energy & Fuels*, **28** (2014), 7133–7139.
28. Z.F. Zahara, S. Kudo, Daniyanto, U.P.M. Ashik, K. Norinaga, A. Budiman, J. Hayashi, *Energy & Fuels*, **32** (2018), 4255–4268.
29. C. Sathe, J. Hayashi, C.Z. Li, T. Chiba, *Fuel*, **82** (2003), 1491–1497.
30. S. Kudo, Y. Hachiyama, H.-S. Kim, K. Norinaga, J. Hayashi, *Energy & Fuels*, **28** (2014), 5902–5908.
31. C. Choi, U.P.M. Ashik, S. Kudo, K. Uebo, K. Norinaga, J. Hayashi, *Carbon Resources Conversion*, **2** (2018) 13–22.
32. C.S.M. de Lecea, M. Almela-Alarcón, A. Linares-Solano, *Fuel*, **69** (1990), 21–27.
33. T. late T.D. Hengel, P.L. Walker, *Fuel*, **63** (1984), 1214–1220.
34. M. Matsukata, E. Okanari, K. Kobayashi, E. Kikuchi, Y. Morita, *Sekiyu Gakkaishi*, **32** (1989), 97–109.
35. A. Linares-Solano, M. Almela-Alarcón, C. Salinas-Martínez de Lecea, *Journal of Catalysis*, **125** (1990), 401–410.
36. J.P. Joly, D. Cazorla-Amoros, H. Charcosset, A. Linares-Solano, N.R. Marcilio, A. Martinez-Alonso, C.S.M. de Lecea, *Fuel*, **69** (1990), 878–884.
37. P.N. Kuznetsov, L.I. Kuznetsova, Y.L. Mikhlin, *Fuel*, **162** (2015), 207–210.

Chapter 4

Change in Catalytic Activity of Potassium during CO_2 Gasification of Char

4.1 Introduction

Gasification is an attractive approach to convert lower-grade carbonaceous solid fuel such as lignite and biomass into syngas for power generation and chemicals production. [1.2] Combined application of CO_2 as a gasifying agent and extraneous alkali and alkaline earth metallic (AAEM) species as catalysts is an excellent option of energy-efficient gasification because these are respectively advantageous over steam in terms of latent heat to produce vapor and inherent AAEM species regarding its limited amount.

According to previous studies on catalytic CO_2 gasification of char, potassium (K) is the most active among AAEM species. [3–6] It is also known that K is mobile at temperatures over 700°C, and even can move among gasifying char particles while staying in the gasifier. [7–9] The K catalyst thus potentially works as an active and durable catalyst for the char gasification, unless deactivated by reactions with silica and alumina. [10–14]

There have so far been studies on the kinetics of the K-catalyzed char gasification, of which quantitative understanding has not been reached yet for reactor/process design and optimization. [8,15–20] A quantitative description of the rate of gasification, as a function of char conversion and K catalyst concentration as well as operating variables, is especially important.[8,18–20] Recent reports suggest that the gasification kinetics varies not only with the catalyst concentration but also the physicochemical structure of char. [21,22] Another previous report suggested an effect of change in the carbonaceous structure of char, along with low-temperature O_2 gasification, on the activity of another alkali metal catalyst, Na. [23] It is thus necessary to comprehensively understand complex interactions of the above-mentioned factors and clarify catalytic roles of the K in the CO_2 gasification.

It was also reported that chemical interactions of K species with other inorganic species in char such as CaO, Al_2O_3, SiO_2, and their composite oxides influence the rate of catalytic gasification. [6,13,24,25] In order to investigate the catalytic activity of K, it is effective to prepare K-loaded solid fuel, of which inherent inorganic species (including AAEM species) have been removed, and use it as a char precursor. It was reported that fine pulverization of

solid fuel is effective or even necessary for complete or near-complete demineralization and subsequent homogenous K loading by an ion-exchange method. [26–27]

Previous studies investigated the loss of AAEM species during pyrolysis and/or gasification of lignite and biomass, [28–30] and it was found that more or less fraction of AAEM species was released from pyrolyzing or gasifying char. Existing studies, except a few, [31,32] however, calculated the catalyst concentration just in feedstock before pyrolysis, in other words, without considering its release (or confirming no release) from the pyrolyzing or gasifying char. The amount of K retained by char should be monitored and then taken as a factor responsible for the kinetics of char conversion. In addition, it is, without saying, essential to measure the kinetics of char gasification by eliminating mass/heat transfer effects on the kinetics, particularly in case of fast gasification of char. [14]

The purpose of this study was to clarify the catalytic activity of K (k'_{cat}) per mass (m'_{cat}) or concentration in gasifying char (C_{cat}), and then examine physical and chemical properties of char that potentially influence the catalytic activity. The demineralized and K-loaded lignites with different K concentrations were pyrolyzed and *in-situ* gasified with CO_2 in a chemical reaction-controlled regime. Kinetic analysis, which also considered the rate of non-catalytic gasification and that of K volatilization, was carried out over the entire range of conversion together with analyses of intrinsic properties of gasifying char. This paper proposes a new approach to examine the catalytic activity of K that enables to reveal the dynamic change in k'_{cat} during the gasification, and then discusses factors influencing it.

4.2 Experimental

4.2.1 Sample preparation and analysis

A type of Indonesian lignite, Berau, was used as the starting material. Its properties are listed in **Table 4.1.** The lignite was dried at room temperature, pulverized by a crusher and sieved to sizes smaller than 106 μm, and then dried at 60°C under vacuum for 24 h. The lignite was further pulverized in a pot mill for 10 h. The particle sizes were reduced to < 10 μm (see **Appendix 1**). The lignite thus pulverized was demineralized by sequential washing with aqueous solutions of hydrogen chloride and hydrogen fluoride. The detailed procedure is presented in **Appendix 6**. The starting lignite and demineralized one are hereafter referred to as B and DB, respectively. DB is identical to B5 in Chapter 2. As shown in **Table 4.1**, the total content of AAEM species in B and DB were 1.02 and 0.01 wt% on the respective dry bases.

The sequential acid washing thus removed more than 99% (w/w) of the inherent AAEM species from B.

K was loaded to DB by an ion-exchange method with aqueous solutions of K_2CO_3 with different concentrations. DB was suspended in the solution at room temperature for 24 h. The volume of the solution was fixed at 50 mL/g-B0. The solid was separated from the solution by filtration, rinsed with deionized water with a volume of 1000 mL/g-DB, and then dried *in vacuo* at 60°C for 24 h. The volume of the solution, K_2CO_3 concentration, and mass of DB were set so that the K concentration in suspension was 0.1, 0.25, 0.5, 0.75, or 1.0 g-K/100 g-dry-DB (see **Table 4.2**). It was found that around 80% of K in the suspension was finally loaded to DB, regardless of the K concentration as mentioned above. The K-loaded DB with K concentration of *a* mol-K/kg-daf-DB will be denoted by K-*a* (see **Table 4.2**). Every K-loaded lignite was washed with deionized water or with 1 mol/L ammonium acetate (NH_4OAc) aq. at 65°C for 24 h for investigating the leachability of ion-exchanged K. The solid/liquid ratio was fixed at 10 g/L.

The contents of AAEM species (*i.e.*, Na, K, Mg, and Ca) in the individual lignite and char samples were determined according to previous reports. [14,31,33] In brief, a prescribed mass of B (40 mg), DB (400 mg), K-loaded DB (10–30 mg) or the char from K-loaded DB (10–30 mg) was heated in air in a muffle furnace with a heating rate, holding temperature and holding time of 1 °C/min, 620°C and 60 min, respectively. The resultant ash was dissolved in an aqueous solution of HNO_3/HF. The solid residue after evaporative removal of the water and volatile matter (*i.e.*, CaF_2, SiF_4, and AlF_3) was dissolved into 4 mM CH_3SO_3H aq. Na, K, Mg, and Ca in the solution were quantified by ion chromatography. It was preliminary confirmed that no volatilization of K occurred during the ashing, as reported in **Appendix 9**. The K concentration in every solid was successfully determined with the experimental error of within ± 2% on average.

4.2.2 Pyrolysis and CO_2 gasification

A portion (*ca.* 2 mg) of DB or K-loaded DB was subjected to the pyrolysis and subsequent gasification in a thermogravimetric analyzer (TGA, Hitachi Hi-Tech Science, model SII TGA/DTA 7200). Details of the procedure were reported elsewhere. [14,34] The lignite sample was heated in a flow of atmospheric N_2 (purity > 99.999 vol.%, flow rate; 700 mL/min) from room temperature to a prescribed temperature, *T*, of 800, 850 or 900°C at a rate of 30 °C/min, and then *T* was held for 60 min for stabilization of the sample mass. The CO_2 gasification was started by switching the flow of N_2 to that of N_2/CO_2 mixed gases (50:50 in

volume) without changing the total flow rate. As we reported previously, it took 20–30 s for complete replacement of the N_2 by N_2/CO_2 in the furnace tube. [34] During the atmosphere transition, TGA recorded apparent increase in the char mass due to change in the gas density, and then decrease due to gasification. The time for the commencement of gasification, *i.e.*, t = 0, was defined as that at which the apparent mass of char started to decrease.

The initial mass of lignite had to be sufficiently small in order to eliminate the effects of heat and mass transfer. The initial lignite mass also had to be adequate for the sensitivity of the TGA (0.2 μg). A lignite mass of *ca*. 2 mg (corresponding to initial char mass of 1 mg or even smaller) was chosen based on the preliminary validation (see **Appendix 10**). Reproducibility of mass release profile was confirmed previously, [14,34] but reconfirmed in this work, as reported in **Appendix 11**.

The char conversion by the gasification, X, was defined by the following equation.

$$X = 1 - \left(\frac{m_{\text{char}}}{m_{\text{char},0}}\right) \quad (1)$$

where $m_{\text{char},0}$ and m_{char} are the daf-based mass of char at the beginning of gasification and that at a given time, t, respectively. The daf-based mass of char was not measured directly by TGA, but calculated by considering the mass of potassium species in char as a function of X.

In addition to the above, chars from K-0.16 lignite with daf-mass-based char conversions of 0%, 60%, and 80% were prepared in a horizontal quartz tube reactor at 900°C and then washed with 3 M HCl aq. at 65°C for 24 h to remove the K species left in the char. The acid-washed chars are hereinafter referred to as K-0.16-0-A, K-0.16-0.6-A, and K-0.16-0.8-A, respectively. A portion of K-0.16-0.8-A char was mixed with SiO_2 nanoparticles by 10 wt%. [35] This mixture is herewith termed as K-0.16-0.8-A-Si. All of the above-mentioned samples were gasified at 900°C in the same manner as mentioned above.

4.2.3 Measurement of char surface area

Partially gasified K-0.02 and K-0.16 chars with different conversions were washed with water for removal of K species, dried, and then subjected to specific surface area measurements with an analyzer, a Quantachrome model (NOVA 3200e). [36] Prior to the measurement of N_2 or CO_2 adsorption isotherm at –196°C or 0°C, respectively, the sample was degassed under vacuum at 200°C for 2 h. A quenched solid density functional theory (QSDFT) method was applied to the analysis of the N_2 adsorption isotherm with relative pressure (p/p_0) lower than 0.05 to determine the pore volume, V_{N2}, and size distribution, dV/dr, of pores with width of 1–50 nm. [35] Another set of pore volume, V_{CO2}, from the CO_2 adsorption isotherm was

determined based on a non-localized density functional theory (NLDFT) for the pores with width of 0.3–1.5 nm. [37]

4.2.4 Equations for analysis of gasification kinetics and catalytic activity

The kinetics of gasification of char is generally described by the following equation:

$$\frac{dX}{dt} = \left(\frac{dX}{dt}\right)_{\mathrm{nc}} + \left(\frac{dX}{dt}\right)_{\mathrm{cat}} = k_{\mathrm{nc}}(1-X) + k_{\mathrm{cat}} \quad (2)$$

The overall rate of gasification is the sum of those by the non-catalytic gasification, $(\mathrm{d}X/\mathrm{d}t)_{\mathrm{nc}}$, and catalytic gasification, $(\mathrm{d}X/\mathrm{d}t)_{\mathrm{cat}}$, as far as these two different types of reactions occur in parallel. k_{nc} and k_{cat} are the rate constants corresponding to $(\mathrm{d}X/\mathrm{d}t)_{\mathrm{nc}}$ and $(\mathrm{d}X/\mathrm{d}t)_{\mathrm{cat}}$, respectively. It is reasonably assumed that the non-catalytic gasification and catalytic gasification follow first-order and zero-th-order kinetics with respect to the unconverted fraction of char (1–X), respectively. [31,32,38–40] The zero-th-order kinetics is based on the assumption that the catalytic species in form of molecule, cluster or nano-sized particles are dispersed in the char as the solid matrix. [32-33] Regardless of the size of catalyst, the catalytic gasification takes place exclusively in the vicinity of catalyst. k_{cat} is steady if the overall catalytic activity is maintained, but variable if either of the loss of catalysis (due to volatilization of metallic species [29] or its intra-particle deactivation [39]) or transformation of catalyst precursor [14,34].

Here, the expression of $(\mathrm{d}X/\mathrm{d}t)_{\mathrm{cat}}$ is considered assuming that k_{cat} is variable with the char conversion, X. The rate of catalytic char gasification can be expressed on the char mass basis by

$$-\left\{\frac{d\left(\frac{m_{\mathrm{char}}}{m_{\mathrm{char},0}}\right)}{dt}\right\}_{\mathrm{cat}} = k_{\mathrm{cat}} = k'_{\mathrm{cat}}\frac{m_{\mathrm{cat}}}{m_{\mathrm{char},0}} = k'_{\mathrm{cat}}m'_{\mathrm{cat}} \quad (3)$$

where k'_{cat} and m'_{cat} is the rate constant per amount of catalytic species, and the amount of catalytic species per initial mass of char on the daf basis, respectively. Both k'_{cat} and m_{cat} are variable. $m_{\mathrm{char}}/m_{\mathrm{char},0}$ is identical with 1–X, and Equation 3 is also given by

$$\left(\frac{dX}{dt}\right)_{\mathrm{cat}} = k'_{\mathrm{cat}}m'_{\mathrm{cat}} \quad (4)$$

eq. 4 is modified further to

$$\left(\frac{dX}{dt}\right)_{\mathrm{cat}} = k'_{\mathrm{cat}}m'_{\mathrm{cat},0}\,(1-\beta) \quad (5)$$

$m'_{\mathrm{cat},0}$ and α are m'_{cat} at t = 0 and degree of volatilization loss of catalytic species at a given t, respectively. β is defined to be zero at t = 0. $m'_{\mathrm{cat},0}$ is directly given from the

concentration of catalyst in the initial char in the unit of mol/kg-daf-char, as shown in **Table 4.2**.

Dividing the left and right side terms by 1–*X*, Equation 5 is transformed to

$$\left(\frac{dX}{dt}\right)_{\mathrm{cat}}/(1-X) \;=\; k'_{\mathrm{cat}}(1-\beta)m'_{\mathrm{cat,0}}/(1-X) \;=\; k'_{\mathrm{cat}}C_{\mathrm{cat}} \qquad (6)$$

The left side of this equation is so-called specific rate of gasification. The $(1-\beta)m'_{\mathrm{cat,0}}/(1-X)$ at the middle is the concentration of catalytic species in the gasifying char, which is here denoted by C_{cat}. It increases during the gasification simply with the inverse of (1–*X*) if no volatilization of catalytic species occurs. Previous studies employed C_{cat} and investigated its relationship with the specific rate of gasification. [19,23]

It is normally difficult to classify a specific metallic species by its catalytic activity. It is, therefore, reasonable to re-define the variables, m'_{cat}, $m'_{\mathrm{cat,0}}$, and C_{cat}, based on the total amount of the metallic species in the gasifying char (K species in the present study), while the loss of the species by its volatilization can be quantified with the determination of β as a function of *t* or *X*. It is also effective to define the rate constant, k'_{cat}, as the overall catalytic activity of the metallic species because it is given by the rate or specific rate of catalytic gasification per amount (Equation 3) or concentration (Equation 6) of the metallic species in the gasifying char, respectively.

4.3 Results and Discussion

4.3.1 Yield and K content of char

Figure 4.1 shows the char yields from the pyrolysis of DB and K-loaded DB at *T* = 800, 850, and 900°C as a function of K loading on the daf basis. At each temperature, the yield increases with increasing K loading, approaching 47–48 wt%-daf. The difference in the char yield between 800 and 900°C is 1 wt%-daf or smaller, regardless of the K-loading. The major part of devolatilization was thus completed upon heating the DB and K-loaded DB to 800–900°C. The increase in the char yield by the presence and abundance of K is in broad agreement with those reported previously. [9,41] It is known that organically-bound AAEM cations enhance cross-linking between macromolecules and thereby charring. [42,43] On the other hand, the porous structure of the resulting char was hardly affected by the K loading (*i.e.*, $m'_{\mathrm{cat,0}}$) over the range from 0.02 to 0.16 mol-K/kg-daf-char (see **Appendix 12**). It was hence believed that the intrinsic (*i.e.*, non-catalytic) reactivity was not influenced by $m'_{\mathrm{cat,0}}$ significantly as shown later.

The chemical form of AAEM species is one of its important properties relevant to the catalytic gasification. [14] The composition of K in the K-loaded DB is shown in **Figure 4.2** based on the leachability. The major portion, as much as 96–99%, of K was removed by ion exchanging with NH_4^+. It is also seen that a substantial fraction of K is water-soluble. This does not necessarily mean that such a fraction of K was in form of water-soluble salt, in other words, K_2CO_3. It is well known that a more or less portion of –COOK can be converted into –COOH by washing the solid even with water, but not completely unless its pH is as low as 1. [44] It is also known that the leachability of K^+ bonded to $–COO^–$ is determined by factors such as total –COO concentration in the solid, relative abundances of –COOK and –COOH and also distribution of pK_a of carboxylic groups. [44] Moreover, the washing with water of the K-loaded B0 was performed not at room temperature, but at 65°C, where pK_w = 12.9 (14.0 at 25°C). It is believed that such temperature for the washing with water, as well as sufficiently long time, 24 h, allowed K^+–H^+ exchanging and removal of K^+.

4.3.2 Gasification of chars from B0 and K-loaded lignites

Figure 4.3(a) and **(b)** show the time-dependent changes in 1–X and the rate of gasification, dX/dt, as a function of X, respectively, for the chars from DB and K-loaded DB lignites at T = 800–900°C. As expected, the gasification became faster as the K loading (*i.e.*, $m'_{cat,0}$) increased. At T = 900°C, the chars from K-loaded B0 were gasified completely within 22–145 min, while 430 min was necessary for complete gasification of the DB char, in other words, in the absence of K. The kinetic analysis of the gasification of K-0.22 char was not performed due to the heat or mass transfer limitation, as discussed in **Appendix 10**.

As shown in **Figure 4.3(b)**, for all the K-loaded B0 chars, dX/dt changes through a maximum at X in a range of 0.82–0.96. The increase in dX/dt becomes more significant as $m'_{cat,0}$ increases. In general, increase in dX/dt can be attributed to that in the intrinsic reactivity of char and/or catalytic activity of K that is represented by k'_{cat}, while its decrease can be arisen from the intraparticle deactivation of K, volatilization loss of K, and/or loss of the intrinsic reactivity. In the following sections, the dX/dt profiles are analyzed and discussed toward extracting of catalytic factors responsible for the profiles.

4.3.3 Volatilization of K during gasification

Figures 4.4(a) and **(b)** plot the K retention, 1–β, against X. The K retention is defined as the fraction of K species staying in the gasifying char, and it is given by normalizing the amount of K retained in the partially gasified char by that in the char at X = 0. These figures show some

important trends. Firstly, no volatilization loss of K occurs at $X < 0.5–0.6$. Secondly, greater $m'_{cat,0}$ results in more extensive volatilization at $X > 0.5–0.6$. Thirdly, higher temperature causes more significant release of K. It is believed from these three trends that at least a portion of K species in the gasifying char was in the form of metallic (reduced) K. This is supported by thermodynamics (see **Appendix 13**). The metal-oxide cycle consists of

$2K + CO_2 = K_2O + CO$; $\Delta G_r = –9.1$ kJ/mol-K, $K_p = 2.5$

$K_2O + C = 2K + CO$; $\Delta G_r = –7.8$ kJ/mol-K, $K_p = 2.2$

Both of these two reactions have negative Gibb's free energies at 900°C. It was believed that K species was released from the gasifying char as metallic K. Volatilization of either K_2O, K_2CO_3 or K_2O_2 is unlikely to occur at 800–900°C if the extremely low vapor pressure of K_2O_2 is considered. [45,46] It is also known that potassium oxides, which are often represented by K_xO_y ($x \geq 1$, $y \geq 1$), are important catalysts that are involved in the following cycles. [48]

$$K_xO_y + CO_2 \rightarrow K_xO_{y+1} + CO \quad (7)$$

$$K_xO_{y+1} + C_n \rightarrow K_xO_y + CO + C_{n-1} \quad (n \geq 1) \quad (8)$$

The individual changes in the K retention, $1–\beta$, were approximated by continuous functions of X using a univariate normal distribution. The results are shown in **Figures 4.4(a)** and **(b)**. The approximation of the continuous function of $1–\beta$ *vs* X was necessary to determine the changes in m'_{cat} and then k'_{cat} as a continuous function of X. Details will be mentioned later.

4.3.4 Determination of the rate of catalytic gasification

As mentioned in **4.2.4**, the overall rate of gasification consists of the non-catalytic gasification and catalytic gasification that occur in parallel. The kinetic analysis of the latter requires the removal of the rate of the former by

$$\left(\frac{dX}{dt}\right)_{cat} = \frac{dX}{dt} - \left(\frac{dX}{dt}\right)_{nc} \quad (9)$$

$(dX/dt)_{nc}$ is reasonably given by dX/dt for the gasification of DB char that was near free from the catalysis. The present authors previously reported that the non-catalytic gasification of chars from lignites and biomass obeyed first-order kinetics with respect to $1–X$. [31,32,38–40]

$$\left(\frac{dX}{dt}\right)_{nc} = k_{nc}(1 - X) \quad (10)$$

The rate constant, k_{nc}, was determined from the kinetics of the gasification of DB char (*i.e.*, k_{nc} is 0.0035 min^{-1} at $T = 900$°C). $(dX/dt)_{nc}$ is shown in **Figure 4.5** together with (dX/dt). Strictly saying, the measured (dX/dt) also involves the rate of K release from the gasifying char, and then it was corrected by

$$\left(\frac{dX}{dt}\right)_{\text{corrected}} = \left(\frac{dX}{dt}\right)_{\text{measured}} - \text{(the rate of K release)} \quad (11)$$

The measured (dX/dt) was corrected by eliminating the rate of K release from the rate of total mass release from the char. The result is shown in **Figure 4.5**.

Figure 4.5 shows (dX/dt) and $(\mathrm{d}X/\mathrm{d}t)_{\mathrm{nc}}$ together with 'corrected' (dX/dt). The difference between the measured and corrected (dX/dt) is negligibly small for the chars with lower K-loading (*i.e.*, K-0.02 and K-0.05), but a small difference is detected for those with higher K-loading (*i.e.*, K-0.09 and K-0.16). **Figure 4.6** shows $(\mathrm{d}X/\mathrm{d}t)_{\mathrm{cat}}$.

$$\left(\frac{dX}{dt}\right)_{\mathrm{cat}} = \left(\frac{dX}{dt}\right)_{\text{measured}} - \left(\frac{dX}{dt}\right)_{\mathrm{nc}} - \text{(the rate of K release)} \quad (12)$$

$(\mathrm{d}X/\mathrm{d}t)_{\mathrm{cat}}$ is further analyzed with the main focus on the catalytic activity of K in the next subsection.

4.3.5 Activity of K catalyst and its change along char conversion

Figures 4.7(a) and **(b)** show changes with X of k'_{cat} for the gasification of chars with different $m'_{\mathrm{cat},0,}$ and those for the gasification of K-0.09 char at different temperatures. k'_{cat} was calculated over the range of X up to 0.92–0.99, depending on $m'_{\mathrm{cat},0}$. The calculation was not done beyond such conversion due to no experimental data for the K retention (see **Figure 4.4**).

As mentioned in **4.2.4**, k'_{cat} is the rate of 'catalytic' gasification per amount of K retained by the gasifying char, in other words, the activity of the K. Some important trends are seen in the figure. Firstly, it is seen in **Figure 4.7(a)** that k'_{cat} increases gradually with X at $X < 0.4$, where k'_{cat} is independent of $m'_{\mathrm{cat},0}$. Secondly, at $X > 0.4$, k'_{cat} continues to increase, but the increment is more significant with greater $m'_{\mathrm{cat},0}$. The present authors initially expected that k'_{cat} was steady or near-steady over the entire range of X, following previously reported relationship between dX/dt *vs* X for the gasification of a Victorian lignite that had inherent metallic species (Na; 0.08, K; 0.01, Ca; 0.06 wt%) and SiO_2/Al_2O_3 (*ca*. 0.5 wt%). [35,48] However, under the present conditions, k'_{cat} increased significantly with X. The dependency of k'_{cat} on $m'_{\mathrm{cat},0}$ at $X > 0.4$ was also unexpected. Thus, within the ranges of the experimental conditions that more loading of K enhanced its activity at $X > 0.4$. In the case of K-0.16 char, k'_{cat} at $X = 0.99$ is about 20 times greater than that at $X = 0$. On the other hand, for K-0.02 char, k'_{cat} increased but by a factor of only 5–6. The effect of $m'_{\mathrm{cat},0}$ on the evolution of k'_{cat} along the char conversion will be discussed later together with proposal of a mechanism of k'_{cat} change during the gasification.

Figure 4.7(b) shows the effect of temperature on k'_{cat} in the same manner as in **Figure 4.7(a)**. It was confirmed that a continuous and significant increase in k'_{cat} was not an event particular to 900°C. It seems that the increase in k'_{cat} is more significant at higher temperatures.

4.3.6 Relationship between activity of K catalyst and its concentration in gasifying char

Karlström *et al*. [19] investigated CO_2 gasification of chars from biomass that were rich in inherent K species. The K contents in the chars were in the range of 0.6–1.3 mol-K/kg-daf-char. They recognized that the inherent K was the main catalyst, and therefore investigated the relationship between $(dX/dt)/(1–X)$ and K concentration in the gasifying char. According to eq. 6, *i.e*., $(dX/dt)_{cat}/(1–X) = k'_{cat}C_{cat}$, the relationship reported by Karlström *et al*. [19] can be analyzed further for examining the change in k'_{cat} along the char conversion, by ignoring the presence of other catalytic species (Na, Ca and Fe), that of Si (SiO_2 or silicate) and also the contribution of non-catalytic gasification to $(dX/dt)/(1–X)$. The present authors semiquantitatively analyzed of the data reported by Karlström *et al*. [19] and then found that k'_{cat} increased slightly or greatly until C_{cat} reached 3–4 mol-K/kg-char, and then decreased at higher C_{cat}. In the author's view, Karlström *et al*. [19] did not claim the promotion of catalytic activity, but they rather emphasized the increase in $(dX/dt)/(1–X)$ with C_{cat} (K/C atomic ratio by their definition).

The relationship between $(dX/dt)_{cat}/(1–X)$ and k'_{cat} under the present experimental conditions are presented in **Figure 4.8**. It is seen for every condition that k'_{cat} increases with C_{cat}, while the increase becomes more gradual, suggesting saturation of the catalytic activity at the final stage of gasification. [50] At lower concentrations, k'_{cat} appears to increase in a linear manner with C_{cat}. It should be noted that this linearity is not between the specific rate of gasification and C_{cat}, but between k'_{cat} and C_{cat}. In other words, the catalytic activity (k'_{cat}) as the specific rate of gasification per K concentration increases. It is also found in **Figure 4.8** that the increase in k'_{cat} slows down at lower C_{cat} for smaller $m'_{cat,0}$. Thus, even for the chars from the same parent lignite (*i.e*., DB), k'_{cat} is not determined simply by C_{cat} during the gasification.

4.3.7 Change in the intrinsic reactivity of char

The changes in the catalytic activity of K, as shown in **Figures 4.7** and 4.**8**, could be influenced by that in the intrinsic reactivity of char, which is represented by the rate constant for the non-catalytic gasification, k_{nc}. Wu e*t al*. investigated the low-temperature oxidation of

char from NaCl-loaded lignite. [23] They analyzed the relationships between the specific reactivity, (dX/dt)/(1–X), and the Na concentration in gasifying char for different initial Na concentrations, and suggested that loss of intrinsic reactivity of char caused the decrease in the specific reactivity under the catalysis. On the other hand, a recent study on the CO_2 gasification of lignite char, which was free from metallic species, showed that the first-order rate constant (*i.e.*, k_{nc}) was steady over the entire range of char conversion. [48]

The present authors examined the change in the intrinsic reactivity by quenching the gasification of K-0.16 char when X reached *ca*. 0.6 or 0.8, recovered the char, washed it with 3 M HCl aq., and then gasified the washed char again. The residual K after the acid washing was carefully quantified (see **Appendix 14**). **Figure 4.9** shows the dX/dt *vs* X profiles for different chars, *i.e.*, acid-washed K-0.16 chars at X = 0, 0.6, and 0.8, which are referred to as K-0.16-0-A, K-0.16-0.6-A, and K-0.16-0.8-A, respectively. The other char sample, K-0.16-0.8-A-Si, was prepared by physically mixing K-0.16-0.8-A with SiO_2 nanoparticles at a mass ratio of 0.1, as mentioned in **4.2.2**. This sample was prepared for intentionally causing the deactivation of residual (acid-insoluble) K prior to and during the gasification. [35,48]

Figure 4.9 shows that the dX/dt's for the different chars are very similar to each other at X up to 0.5. The linear decrease of dX/dt toward 0 at X = 1 is typical to the first-order kinetics with steady rate constant k_{nc}. [31,32,38–40] On the other hand, at X > 0.5, dX/dt's for the chars (except K-0.16-0.8-A-Si) slightly increase and then decrease. This trend arose from the catalysis of K that had been left in the chars after the acid washing. K-0.16-0-A, K-0.16-0.6-A, and K-0.16-0.8-A contained K at $m'_{cat,0}$'s of 0.026, 0.006, and 0.0003 mol-K/kg-daf-char, respectively. Details are available in **Appendix 14**. It also seems that the maximum of dX/dt shifts to higher X as $m'_{cat,0}$ decreases. The above-described trends are explained as below. The K retained in the acid-washed char had no or little catalytic activity in the early stage gasification at X < 0.5, probably because it was confined in carbon moieties to which CO_2 could not access. Then, the char was converted mainly or exclusively by the non-catalytic gasification. In the mid-to-late stage gasification, a more or less portion of K was liberated from the above-described environment and started to catalyze the gasification. At the final stage of gasification, K underwent volatilization or intra-particle deactivation by reacting with a trace amount of inherent SiO_2 while the catalytic contribution to dX/dt diminished. The above-mentioned behavior of K is supported well by dX/dt profile for K-0.16-0.8-A-Si. This char/SiO_2 blend underwent the gasification obeying the first-order kinetics over the entire range of X. The dX/dt peaks for the other three chars were absent for K-0.16-0.8-A-Si because

'mobilized' K was chemically deactivated without playing a catalytic role through reactions with SiO_2 nanoparticles. [35,38]

In view of the above discussion, it is safely concluded that the intrinsic reactivity, in other words, non-catalytic reactivity of K-0.16 char remained steady during the gasification regardless of presence/absence of the catalysis of K. The first-order rate constant (*i.e.*, k_{nc}) for the gasification of K-0.16-0.8-A-Si char was 0.0035 min^{-1}, and in good agreement with k_{nc} for the DB char. This indicates that the non-catalytic (intrinsic) reactivity of the char remained near steady over the entire range of X.

4.3.8 Discussion on mechanism of promotion of catalytic activity of K along char conversion

Partially gasified chars were prepared by gasifying K-0.02 and K-0.16 chars up to different conversions. The porous structures of those chars were characterized in the same way as mentioned in **4.2.3** and presented in **Appendix 12** and **15**. **Figure 4.10** displays the changes in the volume of pores with different sizes in K-0.02 and K-0.16 chars as a function of X. The most noticeable feature is the change in the volume of pores with sizes of 2.0–4.7 nm (hereafter referred to as $V_{2.0–4.7}$), shown in graphs (a2) and (b2). Mesopores with such size were absent before the gasification and also during the gasification at $X < 0.4$ (see **Appendix 12**). But, $V_{2.0–4.7}$ increases steeply at $X = 0.4–0.6$ for K-0.16 char, or continuously until $X = 1$ for K-0.02 char. The specific range of X for no or little increase in $V_{2.0–4.7}$, *i.e.*, $X < 0.4$ is in a good agreement with that where k'_{cat} gradually increases with no influence of $m'_{cat,0}$ (see **Figure 4.7**). It is thus speculated that, in this range, the entire or a major portion of K stayed in micropores with sizes < 1.5 nm or even smaller pores for both K-0.02 and K-0.16, where the K catalyzed the gasification but with lower activity. The gradual increase in k'_{cat} at $X < 0.4$ (see **Figure 4.7**) could be due to that in the size of micropore. This hypothesis is based on the assumption that the catalytic activity of metallic species increases with an increase in its size up to 2–5 nm. [39,50,51]

Following the above-mentioned hypothesis, at $X > 0.4$, a substantial portion of the K species in K-0.16 was released from micropores to mesopores, where it had higher or much higher activity for promoting the gasification. On the other hand, for K-0.02, the K species were not allowed to escape from micropores because the micropore volume was still sufficient in volume and/or population to hold an entire portion of K species. It was believed that the K species after released into mesopores, were much more mobile than before the release. This is consistent with not only the enhancement of catalysis but also volatility. As shown in **Figure**

4.4, no volatilization loss of K occurred at $X < 0.4$, regardless of $m'_{cat,0}$. In addition to this, such loss of K was significant from K-0.16 at $X > 0.5$–0.6, but insignificant from K-0.02. The development of mesopores was evident during the gasification of K-0.02 char (**Figure 4.10(a2)**), but it was not effective for the promotion of the catalytic activity of K species probably because it was not allowed to move to mesopores. On the other hand, for the gasification of K-0.16 char, micropores with sizes smaller than 2.0 nm were lost substantially at $X > 0.6$. Then, decreasing volume of such micropores could not hold a major portion of K species, releasing it to mesopores.

The above-described hypotheses are consistent with the data shown in **Figures 4.4–4.10**. It is, however, necessary to experimentally examine and prove the hypotheses in the future study with more detailed analyses of K-loaded chars with varieties of X and $m'_{cat,0}$. Direct measurement of the size of K catalyst particles and/or clusters would be the most effective and important subject.

4.4 Conclusion

The present authors have been studying the CO_2 gasification of chars from the K-loaded lignite with different contents of ion-exchanged K with the main purpose to quantitatively and precisely know the catalytic activity of K and its change during the gasification. The contribution of the catalytic gasification *i.e.*, $(dX/dt)_{cat}$, was successfully extracted from the overall rate of gasification, (dX/dt), by careful kinetic analysis considering the volatilization loss of K, contribution of non-catalytic gasification over the entire range of X as well as confirming the conditions for measuring the kinetics free from the heat/mass transport effects. It was revealed that the rate constant for catalytic gasification per amount of K, *i.e.*, k'_{cat}, continued to increase by 5 to even 20 times while X increased up to 0.99. Such increase in k'_{cat} was independent of the initial K content in the char ($m'_{cat,0}$) at $X < 0.4$. However, at higher X, k'_{cat} for greater $m'_{cat,0}$ increased more significantly with X. Thus, unexpectedly, the efficiency of K loading on the basis of k'_{cat} became higher with greater $m'_{cat,0}$. The increase in k'_{cat} was not due to change in the intrinsic reactivity of char, but attributed to that in the porous structure of char, in particular, the development of mesopores.

Table 4.1. Ultimate and proximate analysis, and AAEM species contents of original and demineralized lignites.

	Ultimate analysis (wt%, daf)				Proximate analysis (wt%, db)			AAEM species (wt%, db)			
Lignite	C	H	N	O[a]	ash	VM[b]	FC[c]	Na	K	Mg	Ca
B	67.5	4.5	1.1	26.9	5.0	48.7	46.3	0.005	0.012	0.241	0.766
DB	64.6	4.6	1.0	29.8	< 0.1	53.1	46.9	0.000	0.001	0.001	0.007

[a] by difference. [b] volatile matter. [c] fixed carbon.

Table 4.2. K concentration in the suspension, lignite, and char samples.

Original sample	K concentration					
	in suspension	in K-loaded lignite		in char (mol/kg-daf-char)		
	(g-K/100-g-lignite)	(g-K/100-g-lignite)	(mol/kg-daf-lignite)	800°C	850°C	900°C
DB	0.00	0.00	0.000	<0.001	<0.001	<0.001
K-0.02	0.10	0.08	0.019	0.043	0.042	0.041
K-0.05	0.25	0.19	0.048	0.100	0.098	0.095
K-0.09	0.50	0.37	0.095	0.190	0.187	0.182
K-0.16	0.75	0.63	0.160	0.298	0.287	0.280
K-0.22	1.00	0.87	0.221	0.371	0.360	0.353

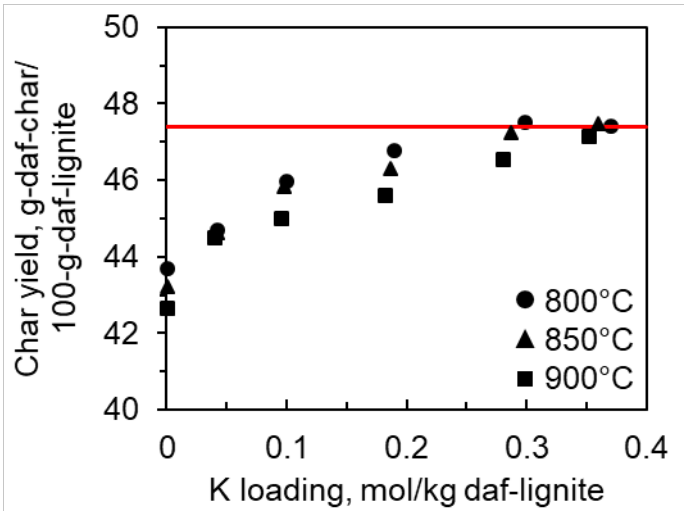

Figure 4.1. Char yields as a function of K loading level and pyrolysis temperature in TGA.

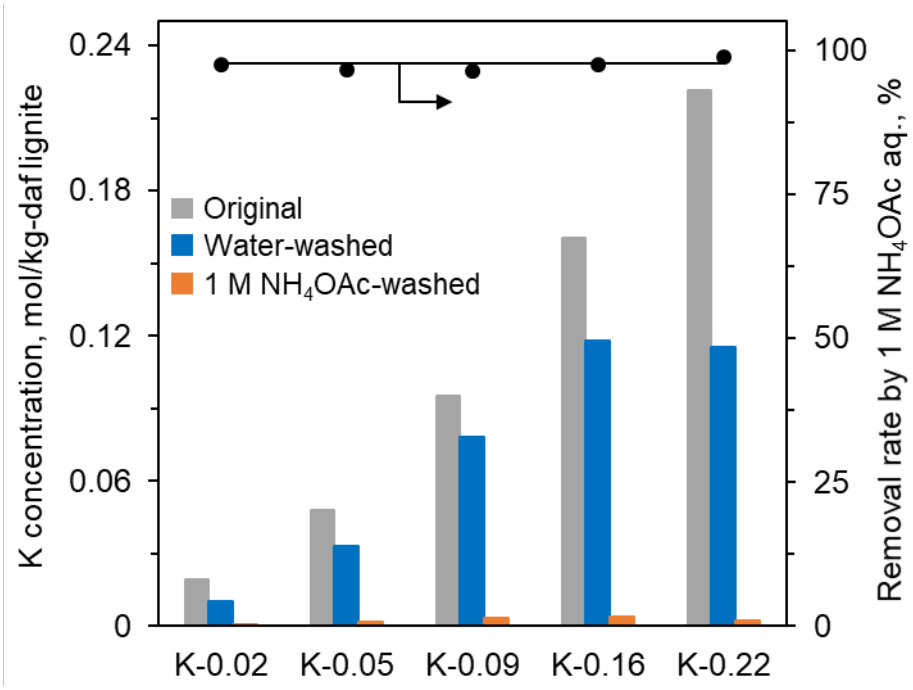

Figure 4.2. K contents in the original, water-washed and NH_4OAc aq.-washed K-loaded DB lignites and the K removal rate by the NH_4OAc aq. washing.

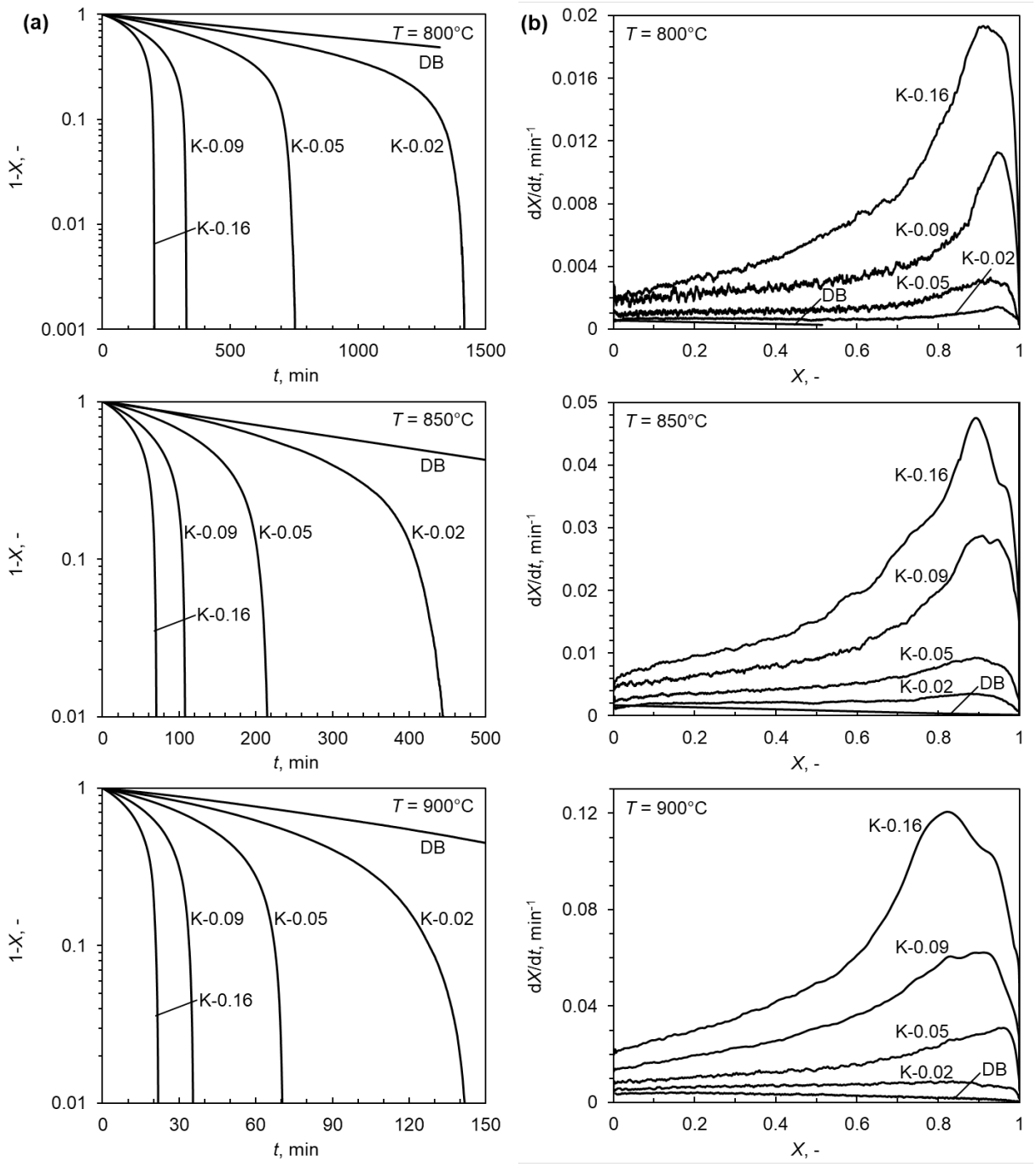

Figure 4.3. (a) Change in 1–X on a logarithmic scale with time, and (b) change in dX/dt with X. The gasification of DB char at T = 800°C was stopped at X = 0.52 due to extremely slow conversion of char.

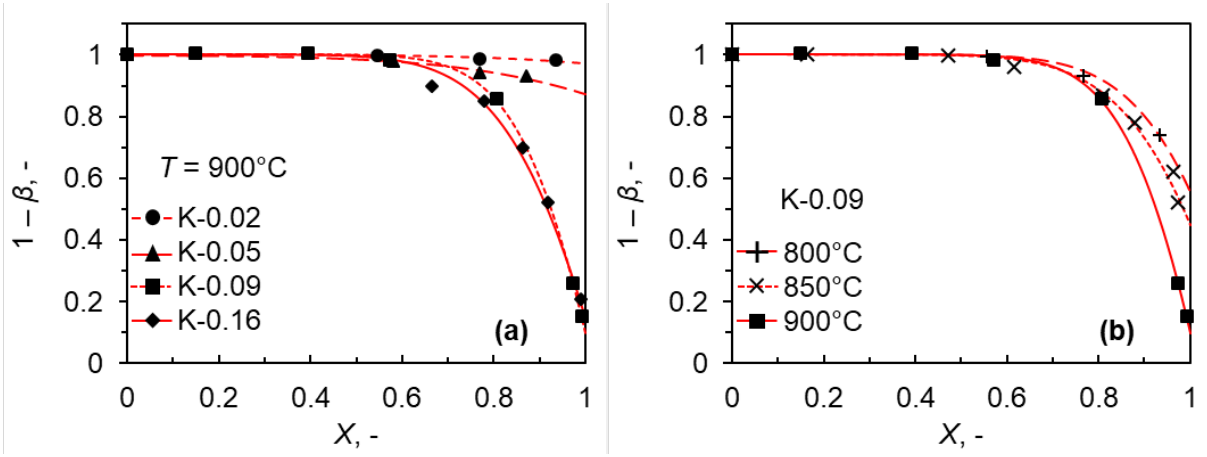

Figure 4.4. Retention of K as a function of *X* for (a) K-0.02, K-0.05, K-0.09 or K-0.16 char at *T* = 900°C, and that for (b) K-0.09 char at *T* = 800, 850 or 900°C. The K retention for every condition was approximated as a continuous function of *X*, as drawn in the figures.

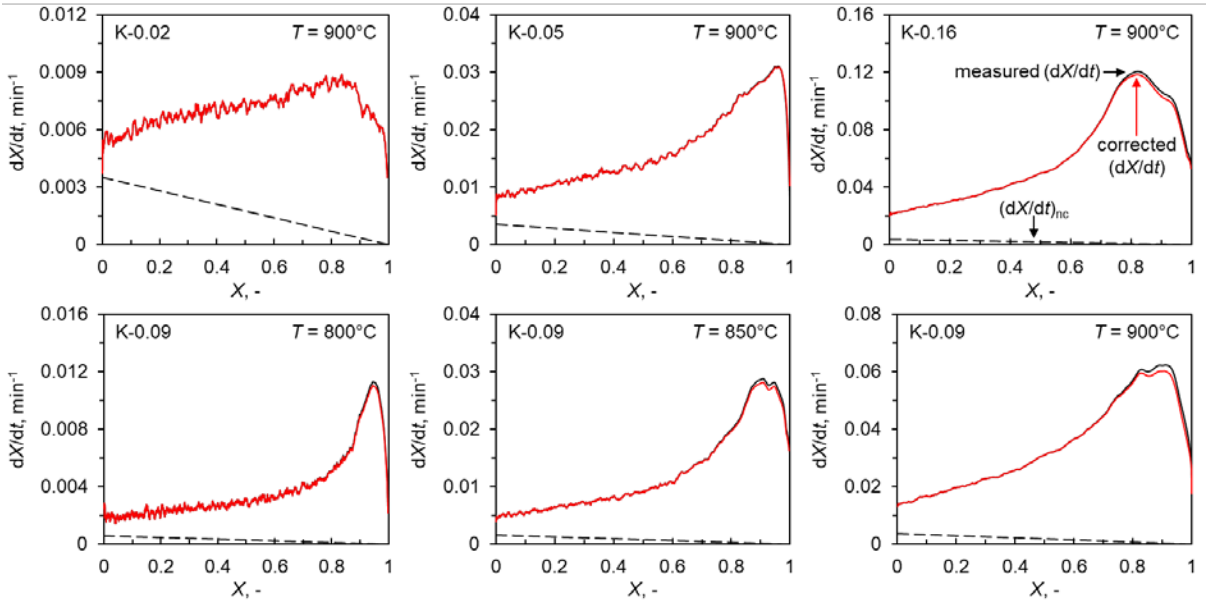

Figure 4.5. Measured (d*X*/d*t*), $(dX/dt)_{nc}$ and corrected (d*X*/d*t*) for different conditions.

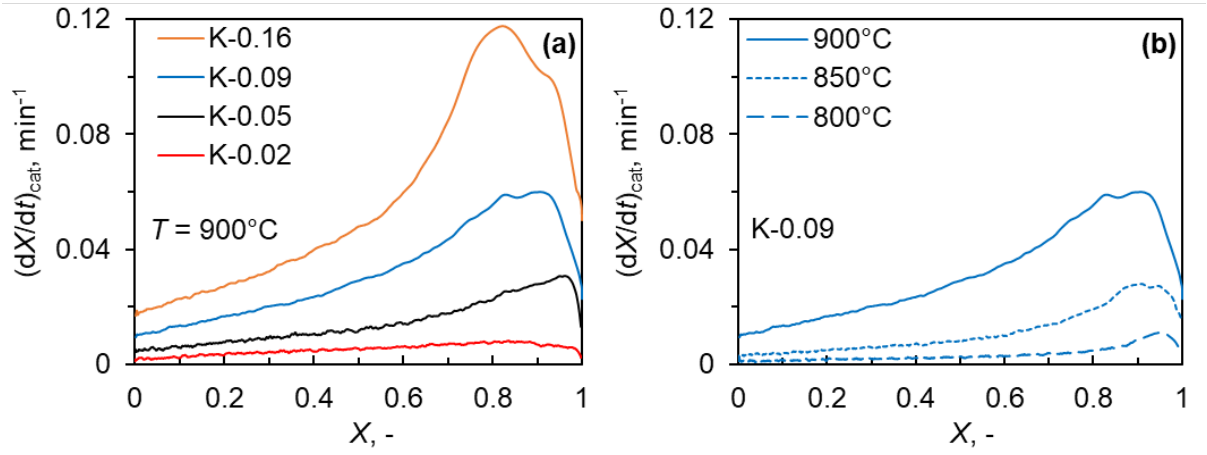

Figure 4.6. $(dX/dt)_{cat}$ as a function of X.

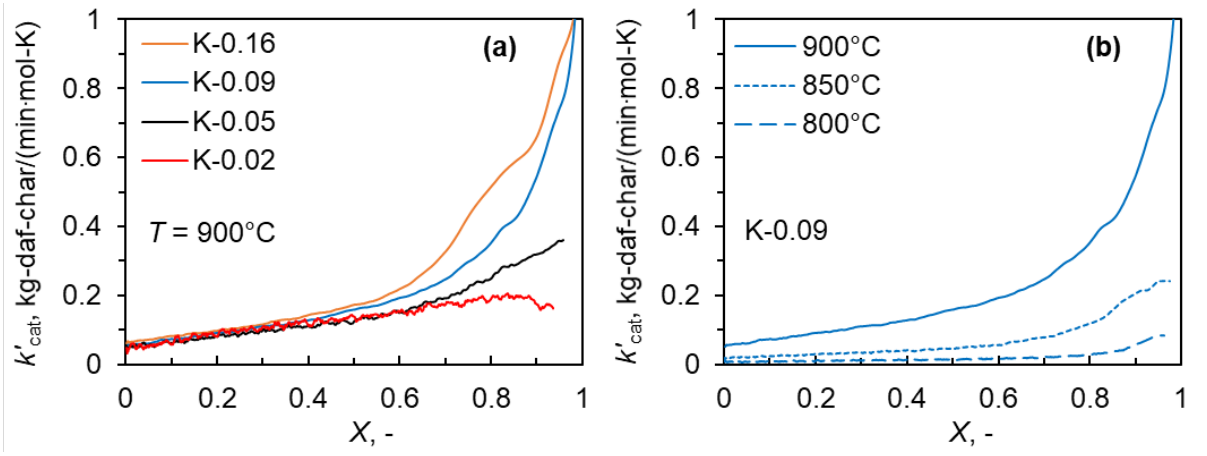

Figure 4.7. Rate constants for catalytic gasification (k'_{cat}) as a function of X for (a) K-0.02, K-0.05, K-0.09 or K-0.16 char at T = 900°C, and those for (b) K-0.09 char at T = 800, 850 or 900°C. The rate constant, k'_{cat}, is defined as the rate of catalytic gasification, $(dX/dt)_{cat}$, per molar amount of K retained by the gasifying char, m'_{cat}. In other words, k'_{cat} also represents the catalytic activity of K.

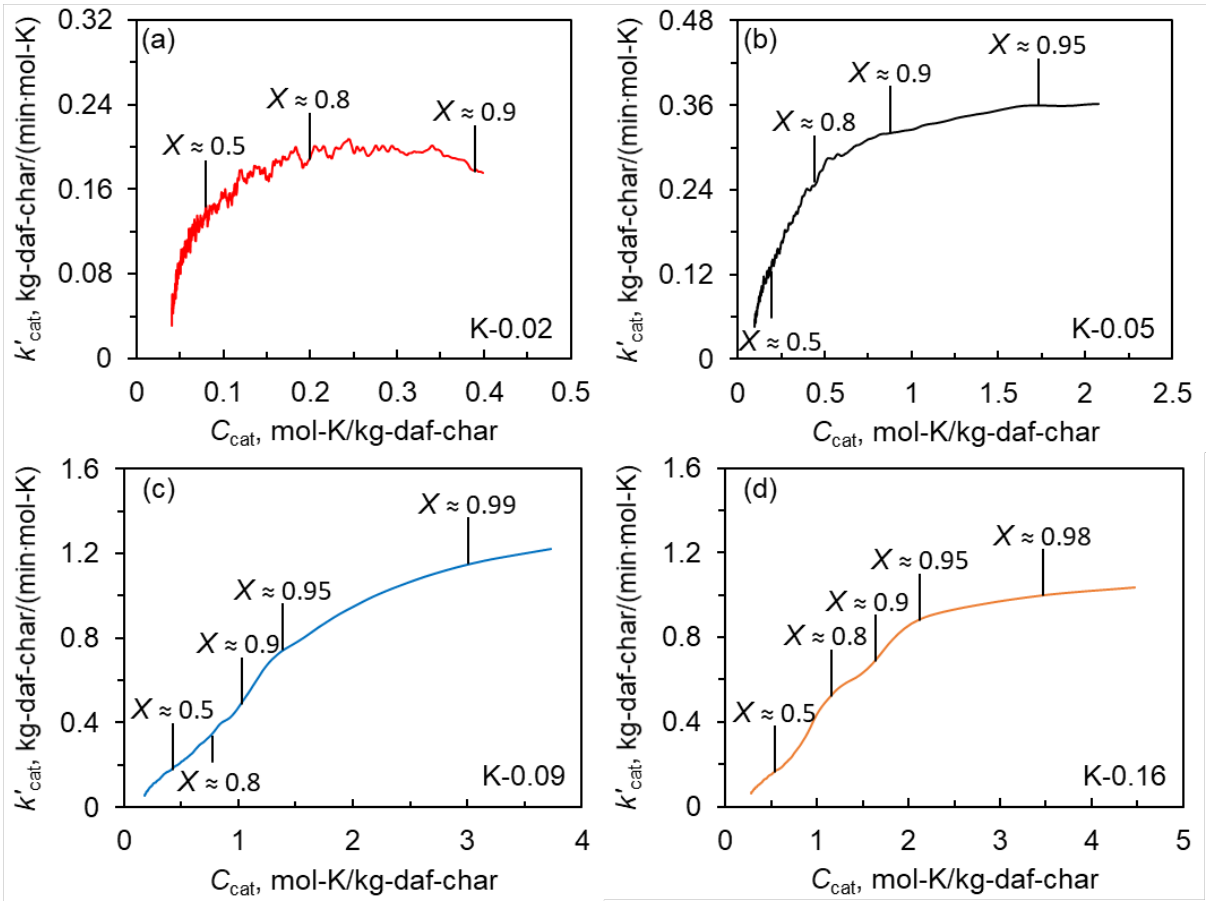

Figure 4.8. k'_{cat} as a function of C_{cat} for (a) K-0.02, (b) K-0.05, (c) K-0.09, and (d) K-0.16 chars at T = 900°C.

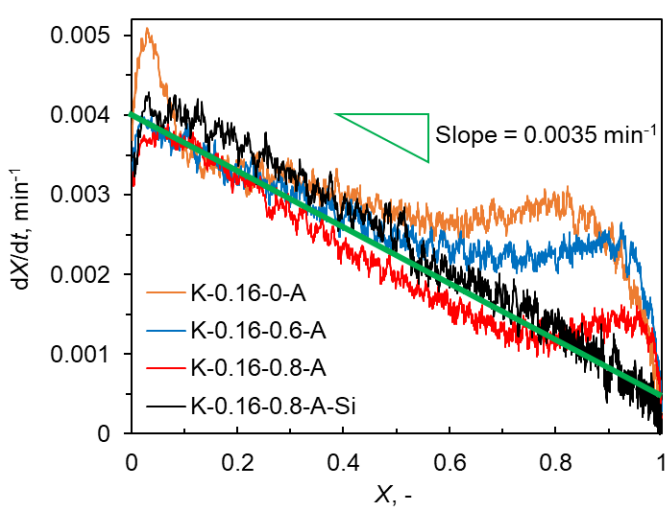

Figure 4.9. d*X*/d*t* as a function of *X* for the gasification of chars prepared by the sequence of the gasification of K-0.16 char at 900°C to *X* of 0, 0.6, or 0.8, and washing with 3 M HCl aq. A sample, K-0.16-0.6-A, indicates the K-0.16 char from the sequence of gasification of up to *X* = 0.6 and the acid washing. 'Si' means that the K-0.16-0.8-A char was mixed with SiO_2 nanoparticles before the gasification.

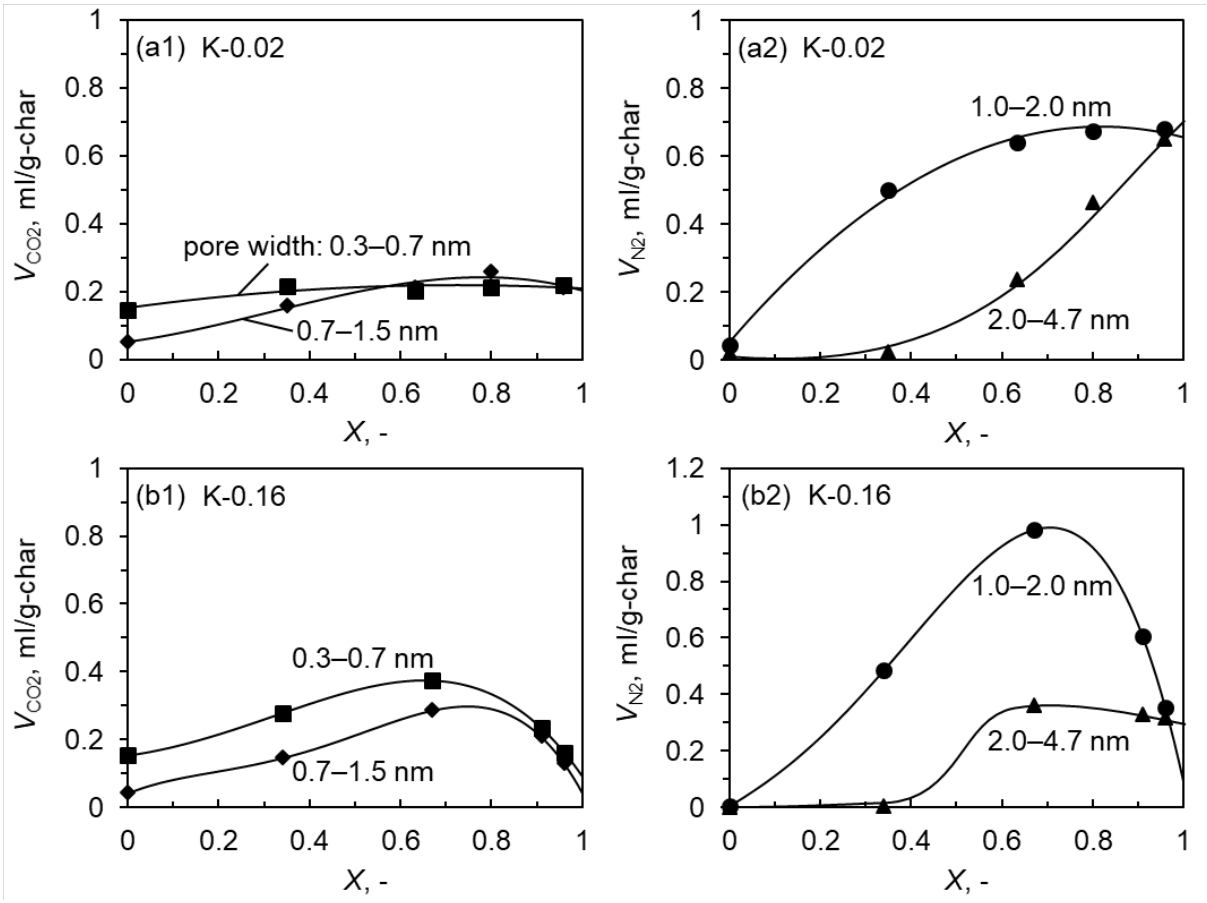

Figure 4.10. Changes in pore size distributions for K-0.02 and K-0.16 chars during the gasification. The distributions in (a1) and (b1) were derived from CO_2 adsorption isotherms, while those in (a2) and (b2) from N_2 adsorption isotherms. The NLDFT and QSDFT were adopted to analyze the CO_2 and N_2 adsorption isotherms, respectively, within the pore width range of 0.3–1.5 nm and 1.0–4.7 nm, respectively.

4.5 References

1. J. Hayashi, S. Kudo, H. S. Kim, K. Norinaga, K. Matsuoka, S. Hosokai, *Energy & Fuels*, **28** (2014), 4–21.
2. Q. Yi, W. Li, J. Feng, K. Xie, *Chemical Society Reviews*, **44** (2015), 5409–5445.
3. P. L. Walker, S. Matsumoto, T. Hanzawa, T. Muira, I. M. K. Ismail, *Fuel*, **62** (1983), 140–149.
4. S. G. Chen, R. T. Yang, *Journal of Catalysis*, **138** (1992), 12–23.
5. L. Klopper, C. A. Strydom, J. R. Bunt, *Journal of Analytical and Applied Pyrolysis*, **96** (2012), 188–195.
6. M. Perander, N. DeMartini, A. Brink, J. Kramb, O. Karlström, J. Hemming, A. Moilanen, J. Konttinen, M. Hupa, *Fuel*, **150** (2015), 464–472.
7. B. C. Gorrini, L. R. Radovic, A. L. Gordon, *Fuel*, **69** (1990), 789–791.
8. R. P. W. J. Struis, C. Von Scala, S. Stucki, R. Prins, *Chemical Engineering Science*, **57** (2002), 3593–3602.
9. H. Yang, S. Kudo, K. Norinaga, J. Hayashi, *Energy & Fuels*, **30** (2016), 1616–1627.
10. D. W. McKee, C. L. Spiro, P. G. Kosky, E. J. Lamby, *Fuel*, **62** (1983), 217–220.
11. L. R. Radovic, P. L. Walker, R. G. Jenkins, *Fuel*, **63** (1984), 1028–1030.
12. K. Formella, P. Leonhardt, A. Sulimma, K. H. van Heek, H. Jüntgen, *Fuel*, **65** (1986), 1470–1472.
13. Y. Wang, Z. Wang, J. Huang, Y. Fang, *Energy & Fuels*, **29** (2015), 6988–6998.
14. Z. F. Zahara, S. Kudo, Daniyanto, U. P. M. Ashik, K. Norinaga, A. Budiman, J. Hayashi, *Energy & Fuels*, **32** (2018), 4255–4268.
15. D. A. Sams, T. Talverdian, F. Shadman, *Fuel*, **64** (1985), 1208–1214.
16. T. Liliedahl, K. Sjöström, *Fuel*, **76** (1997), 29–37.
17. Y. Zhang, M. Ashizawa, S. Kajitani, K. Miura, *Fuel*, **87** (2008), 475–481.
18. Y. Zhang, S. Hara, S. Kajitani, M. Ashizawa, *Fuel*, **89** (2010), 152–157.
19. O. Karlström, M. J. Dirbeba, M. Costa, A. Brink, M. Hupa, *Energy & Fuels*, **32** (2018), 10695–10700.
20. Q. Hu, H. Yang, Z. Wu, C. J. Lim, X. T. Bi, Chen, H. *Energy*, **171** (2019), 678–688.
21. E. Komarova, S. Guhl, B. Meyer, *Fuel*, **152** (2015), 38–47.
22. H. Zhu, X. Wang, F. Wang, G. Yu, *Energy & Fuels*, **32** (2018), 1320–1327.
23. H. Wu, J. Hayashi, T. Chiba, T. Takarada, C. Z. Li, *Fuel*, **83** (2004), 23–30.
24. J. Hu, L. Liu, M. Cui, J. Wang, *Fuel*, **111** (2013), 628–635.

25. M. Q. Jiang, R. Zhou, J. Hu, F. C. Wang, J. Wang, J. *Fuel*, **99** (2012), 64–71.
26. A. Tomita, T. Takarada, Y. Tamai, *Fuel*, **62** (1983), 62–68.
27. K. Murakami, M. Sato, N. Tsubouchi, Y. Ohtsuka, K. Sugawara, *Fuel Processing Technology*, **129** (2015), 91–97.
28. C. Z. Li, C. Sathe, J. R. Kershaw, Y. Pang, *Fuel*, **79** (2000), 427–438.
29. D. M. Quyn, J. Hayashi, C. Z. Li, *Fuel Processing Technology*, **86** (2005), 1241–1251.
30. T. Okuno, N. Sonoyama, J. Hayashi, C. Z. Li, C. Sathe, T. Chiba, *Energy & Fuels*, **19** (2005), 2164–2171.
31. B. Bayarsaikhan, J. Hayashi, T. Shimada, C. Sathe, C. Z. Li, A. Tsutsumi, T. Chiba, *Fuel*, **84** (2005), 1612–1621.
32. T. Kitsuka, B. Bayarsaikhan, N. Sonoyama, S. Hosokai, C. Z. Li, K. Norinaga, J. Hayashi, *Energy & Fuels*, **21** (2007), 387–394.
33. C. Sathe, J. Hayashi, C. Z. Li, T. Chiba, *Fuel*, **82** (2003), 1491–1497.
34. E. Byambajav, Y. Hachiyama, S. Kudo, K. Norinaga, J. Hayashi, *Energy & Fuels*, **30** (2016), 1636–1646.
35. C. Choi, U. P. M. Ashik, S. Kudo, K. Uebo, K. Norinaga, J. Hayashi, *Carbon Resources Conversion*, **2** (2018), 13–22.
36. L. Bai, S. Kudo, K. Norinaga, Y. Wang, J. Hayashi, *Energy & Fuels*, **28** (2014), 7133–7139.
37. S. Kudo, Y. Hachiyama, H. S. Kim, K. Norinaga, J. Hayashi, *Energy & Fuels*, **28** (2014), 5902–5908.
38. M. Kajita, T. Kimura, K. Norinaga, C. Z. Li, J. Hayashi, *Energy & Fuels*, **24** (2010), 108–116.
39. H. Kim, S. Kudo, K. Tahara, Y. Hachiyama, H. Yang, K. Norinaga, J. Hayashi, *Energy & Fuels*, **27** (2013), 6617–6631.
40. S. Kudo, Y. Hachiyama, H. S. Kim, K. Norinaga, J. Hayashi, *Energy & Fuels*, **28** (2014), 5902–5908.
41. J. Kopyscinski, M. Rahman, R. Gupta, C. A. Mims, J. Hill, *Fuel*, **117** (2014), 1181–1189.
42. R. J. Tyler, H. N. S. Schafer, *Fuel*, **59** (1980), 487–494.
43. M. J. Wornat, P. F. Nelson, *Energy & Fuels*, **6** (1992), 136–142.
44. H. N. S. Schafer, *Fuel*, **49** (1970), 197–213.
45. L. Jiang, S. Hu, K. Xu, Y. Wang, S. S. A. Syed-Hassan, S. Su, C. Liu, J. Xiang, *Journal of Analytical and Applied Pyrolysis*, **124** (2017), 384–392.

46. D. Sergeev, E. Yazhenskikh, D. Kobertz, M. Müller, *CALPHAD Computer Coupling of Phase Diagrams and Thermochemistry*, **65** (2019), 42–49.
47. J. A. Moulijn, M. B. Cerfontain, F. Kapteijn, *Fue*l, **63** (1984), 1043–1047.
48. S. Asano, C. Choi, K. Ishiyama, S. Kudo, X. Gao, J. Hayashi, *Energy & Fuels*, **33** (2019), 10913-10922.
49. C. A. Mims, J. K. Pabst, *Fuel*, **62** (1983), 176–179.
50. T. W. Hansen, A. T. Delariva, S. R. Challa, A. K. Datye, *Accounts of Chemical Research*, **46** (2013), 1720–1730.
51. J. J. Willis, A. Gallo, D. Sokaras, H. Aljama, S. H. Nowak, E. D. Goodman, L. Wu, C. J. Tassone, T. F. Jaramillo, F. Abild-Pedersen, *ACS Catalysis*, **7** (2017), 7810–7821.

Chapter 5
General Conclusion

In the transitional phase to renewable energy, avoiding direct combustion of coal is indispensable. The endothermic gasification with CO_2/steam would be a key process of carbon resources conversion for chemicals and power production in the near future since it allows more efficient and more eco-friendly conversion of the coal. Lignite, which is rich with inherent catalyst species such as Na, K, Ca, and Fe, is one of the promising feeds for realizing low-temperature gasification. The quantitative understanding of the catalysis of these metallic species and also the interactions between these species during the gasification is fundamentally essential in order to enhance the performance and efficiency of a gasifier. In the present studies, we have proven the important roles of inherent and extraneous metallic species on determining the overall rate of CO_2 gasification of lignite char, which was successfully described over the entire range of conversion by employing the parallel kinetic model (PRM). The general conclusion of these present studies was summarized as follows.

It is shown that the time-dependent changes in char conversion up to 0.999 for all the twenty chars, derived from two types of original lignites by multistage removal of inherent metallic species, have been successfully described by the PRM, which considers the progress of catalytic and non-catalytic gasification, together with the presence of multicatalytic species. The overall activity of inherent catalyst species is a piecewise linear function of the total concentration of Na, K, Ca, and Fe, following a nucleation-growth mechanism that controlled catalyst activation/deactivation. The deactivation of Fe catalyst is more rapid than the others, while the presence of Mg species promoted the deactivation of other catalysts.

The amount and type of metal(s) that loaded into lignite strongly determined the rate of catalytic gasification of lignite char. For Ca-catalyzed CO_2 gasification, its initial activity was correlated well and linearly with the Ca concentration in char (C_{Ca}; 0.14– 1.33 wt%-daf-char). When Mg, which shown insignificant individual catalytic activity, was added with Ca into lignite, it deactivated a portion of the most active Ca catalyst prior to and during the gasification. In contrast, K showed synergistic performances when combined with Ca. Its overall catalytic activity was similar to Ca on an equal mol basis, but its deactivation rate was much lower. The comparison of catalytic performance between the inherent metallic species in lignite (**Chapter 2**) and the loaded metallic species into lignite (**Chapter 3**) shows that the inherent catalysts

outperformed the extraneous one during the CO_2 gasification of lignite char. Such a difference was explained by a faster deactivation of the doped Ca catalyst compare to that of the inherent Ca catalyst as the main catalyst.

The change in the catalytic activity of K (k'_{cat}) during CO_2 gasification of chars from the K-loaded lignite has successfully observed by defining precisely the contribution of the catalytic gasification *i.e.*, $(dX/dt)_{cat}$, which was conducted by considering the volatilization loss of K, contribution of non-catalytic gasification over the entire range of X as well as confirming the conditions for measuring the kinetics free from the heat/mass transfer effects. k'_{cat}, which was defined as $(dX/dt)_{cat}$ per amount of K retained by the gasifying char, increased significantly with X, depending on the initial K concentration ($m_{cat,0}$). Such a significant increase in k'_{cat} was due to not change in the intrinsic reactivity of char but its porous structure, *i.e.*, the size and volume of pores that played a role of retaining of K catalyst, in particular, the development of mesopores. It was suggested that a substantial portion of the K species in K-0.16 ($m_{cat,0}$; 1.41 wt%-daf-char) was released from micropores to newly-formed mesopores, where it had much higher activity for promoting the gasification. In contrast, for K-0.02 ($m_{cat,0}$; 0.16 wt%-daf-char), the K species were not allowed to escape from micropores because the micropore volume was still sufficient in volume to hold an entire portion of K species.

We believe that the results of these studies are a milestone for a comprehensive understanding of the kinetics and mechanism of CO_2 gasification of chars from coal/biomass. The findings can be applied for realizing fast or low-temperature gasification with optimization of inherent catalyst and/or with aid of a sufficient amount of external catalyst.

The present studies demonstrated that the doped catalyst species, which loaded via an ion-exchange method, are not competitive yet to replace the inherent catalyst, in an equal mol basis. Future studies on the gasification of chars from lignite/biomass should consider the lignite-metal species interaction to enhance the catalytic performance of extraneous metallic species. In addition, this research conducted quantitative analyses on catalytic gasification that takes place at the lab scale, specifically in a TGA. It is therefore interesting to investigate the catalyst behavior and the interaction of catalysts in larger-scale reactors.

APPENDIX

APPENDIX 1

SEM observation of particles of A and B lignites after ball milling

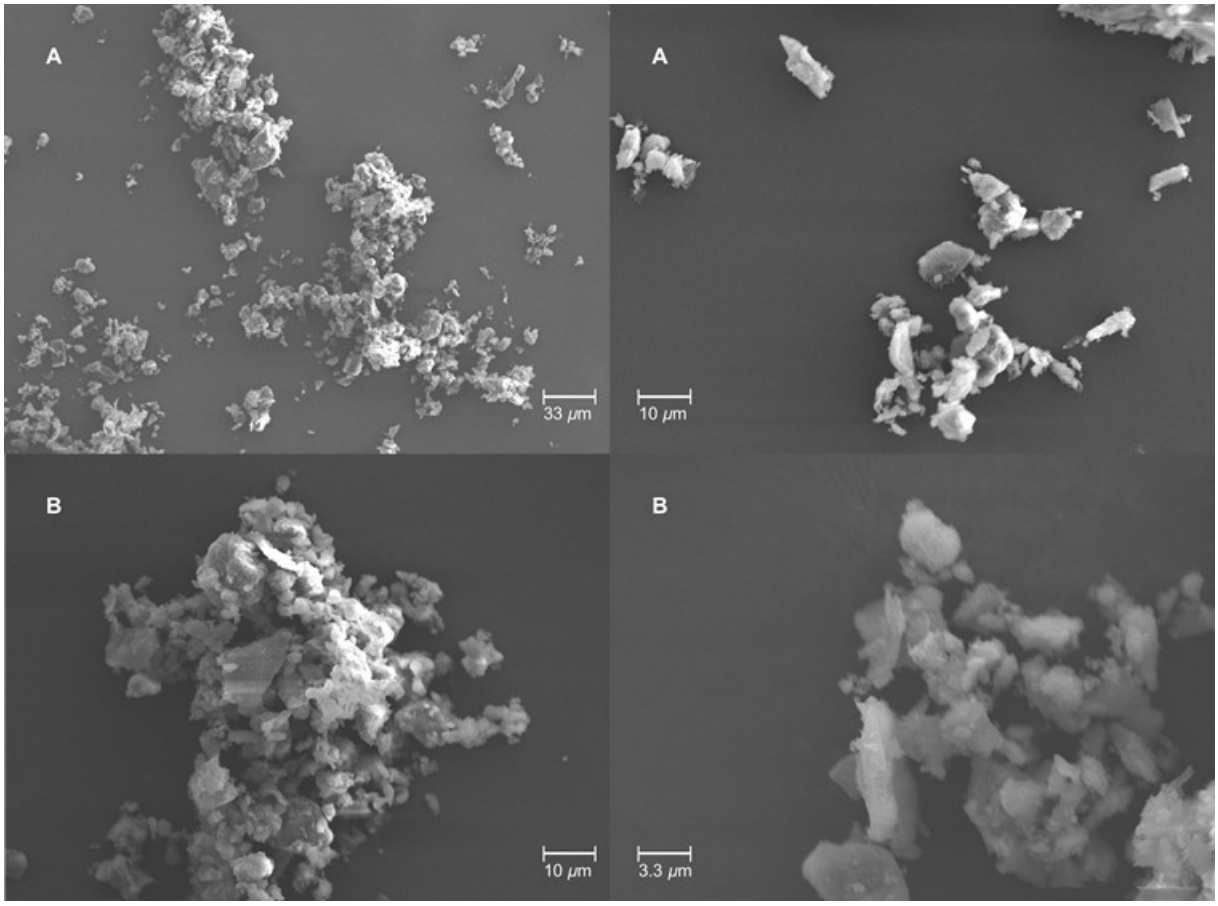

Figure A.1. SEM images of particles of A and B after pulverization by ball milling for 10 h. The particles sizes were reduced to <10 μm.

APPENDIX 2

Effect of initial char mass on the d*X*/d*t* profiles of CO_2 gasification of chars from A0 and B0

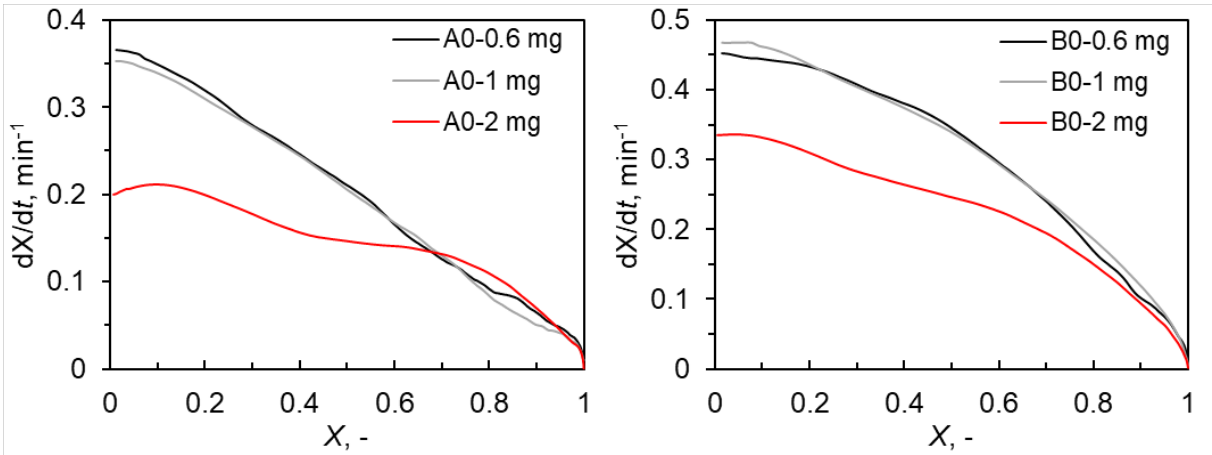

Figure A.2. Measured changes in d*X*/d*t* with *X* for gasification of A0 and B0 chars with initial char mass of 0.6, 1 or 2 mg. Each graph shows that the initial mass of 1.0 mg is sufficiently small at which the rate of gasification is chemically controlled without significant resistances to mass transport within the char bed.

APPENDIX 3

Concentration of metallic species in lignites and chars

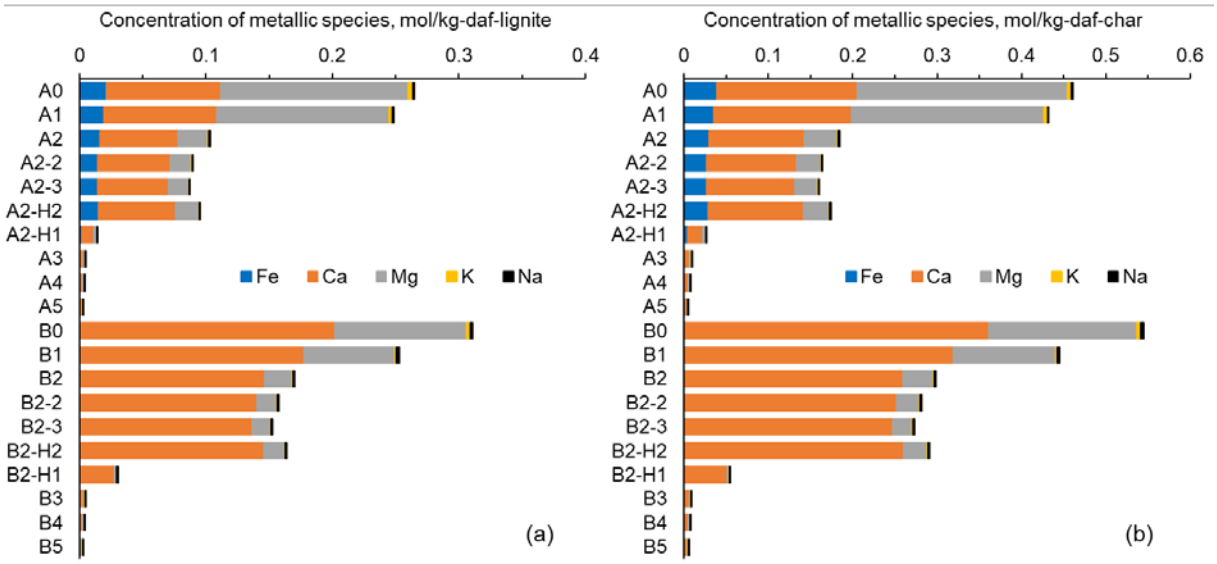

Figure A.3. Concentrations of metallic species in (a) the lignites and (b) the chars. Concentrations of metallic species in the chars were calculated by considering the initial contents of metallic species in the lignites, the char yields, and the volatilization rates. The average volatilization rates of K and Mg for both A0 and B0 after the pyrolysis were 10% and 7%, respectively. It was difficult to determine the volatilization rate of Na due to its low initial concentration, nevertheless a large amount of lignite (*ca*. 100 mg) was used for the pyrolysis and quantification of AAEM species. Thus, the volatilization rate of Na was assumed to be equivalent to K. It was safely concluded that volatilization of Ca did not occur during the pyrolysis as well gasification. For Fe, though not analyzed, it was safely assumed that there was no volatilization.

APPENDIX 4

Gibbs free energy for reactions involving catalytic species

No.	Reaction	ΔG_r at 900°C, kJ/mol-metal	K_p	Remark
1	$Na_2CO_3 + C = Na_2O + 2C$	109	1.5×10^{-5}	Na_2CO_3 is the major species. Overall ΔG for R1 and R2 is negative, and carbonate-oxide cycles are possible. Metal-oxide cycles are possible, too, but formation of Na_2O is difficult.
2	$Na_2O + CO_2 = Na_2CO_3$	-142	2.2×10^{6}	
3	$Na_2O + C = 2Na + CO$	46	8.8×10^{-3}	
4	$2Na + CO_2 = Na_2O + CO$	-80	3.7×10^{3}	
5	$K_2CO_3 + C = K_2O + 2CO$	181	8.6×10^{-9}	K_2CO_3 is the major species. Overall ΔG for R5 and R6 is negative, and carbonate-oxide cycles are possible. Metal-oxide cycles are possible, too, but formation of K_2O is difficult.
6	$K_2O + CO_2 = K_2CO_3$	-215	3.7×10^{9}	
7	$K_2O + C = 2K + CO$	-13	4.0	
8	$2K + CO_2 = K_2O + CO$	-20	8.1	
9	$MgCO_3 + C = MgO + 2CO$	-139	1.5×10^{6}	MgO is the major species. $MgCO_3$ is reactive with C, but its presence is difficult due to that of R10. Then, the catalysis of $MgCO_3$ is implausible.
10	$MgO + CO_2 = MgCO_3$	105	2.2×10^{-5}	
11	$MgO + C = Mg + CO$	259	2.9×10^{-12}	
12	$CaCO_3 + C = CaO + 2CO$	-43	7.9×10^{1}	Major species, CaO and $CaCO_3$ participate in carbonate-oxide catalytic cycles. Formation of metallic Ca is difficult.
13	$CaO + CO_2 = CaCO_3$	9	4.1×10^{-1}	
14	$CaO + C = Ca + CO$	295	7.3×10^{-14}	
15	$Fe_3O_4 + C = 3FeO + CO$	-73	1.8×10^{3}	Integration of K_p of R15–R20 leads to abundances of FeO and Fe_3O_4, and less abundance of Fe. FeO-Fe_3O_4 cycles are major catalytic cycles.
16	$3FeO + CO_2 = Fe_3O_4 + CO$	39	1.8×10^{-2}	
17	$FeO + CO = Fe + CO_2$	9	4.1×10^{-1}	
18	$FeO + C = Fe + CO$	-25	1.3×10^{1}	
19	$FeO + CO_2 = FeO + CO$	-9	2.4	
20	$FeO + CO_2 = FeCO_3$	137	7.7×10^{-7}	

*Thermodynamic data obtained from David R. Lide, ed., CRC Handbook of Chemistry and Physics, 90th Edition, CRC Press/Taylor and Francis, Boca Raton, FL

APPENDIX 5

Inorganic compounds in char and ash detected by XRD

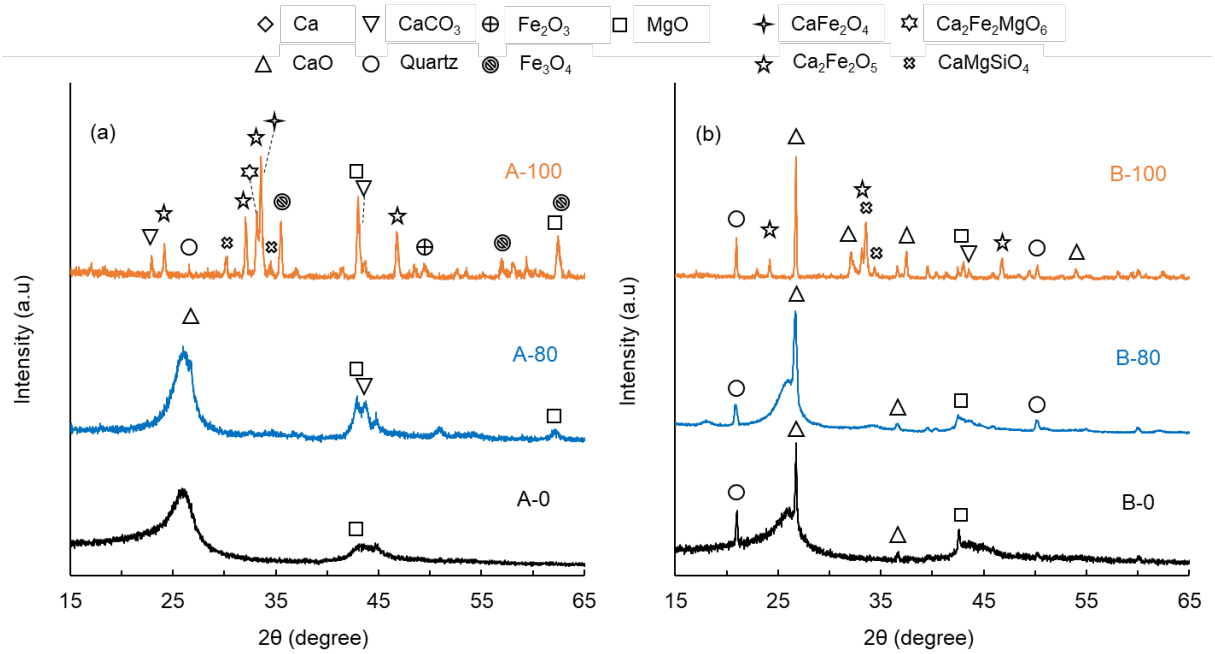

Figure A.5. XRD patterns of the chars at X = 0, 80% and 100% from (a) A0 and (b) B0 lignites.

APPENDIX 6

Flow diagram of demineralization of lignite

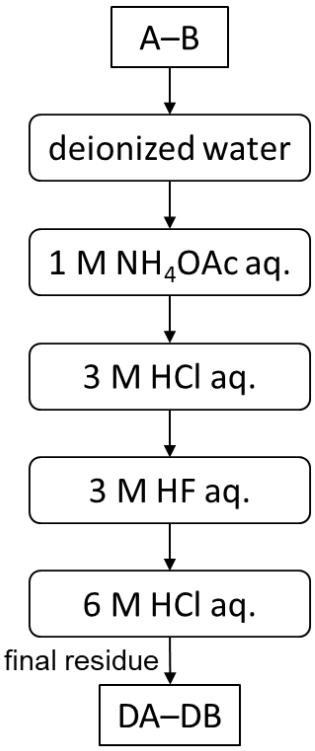

Figure A.6. Flow diagram of sequential acid washing. In brief, *ca*. 6 g of finely pulverized lignite, A or B, was washed with 0.12 L of deionized water (resistivity ≥18.2 MΩ cm) in a clean plastic beaker. The lignite/water slurry was heated at 65°C for 24 h while stirred continuously. The washed lignite was separated from the water by vacuum filtration and then washed with other 1–3 L of deionized water repeatedly until no chlorine ion was detected in the filtrate. The water-washed lignite was then washed sequentially with 1 M NH_4OAc aq., with 3M HCl aq., with 3 M HF aq., and then with 6 M HCl aq. The final residues after repeated washing with deionized water, *i.e.*, the 6 M HCl aq.-washed lignites, DA and DB, were vacuum-dried at 60°C. For each of the washing process, the ratios of solution volume to dry lignite mass were fixed at 20 mL/g.

APPENDIX 7

TEM-EDS observations of catalyst dispersion in lignite

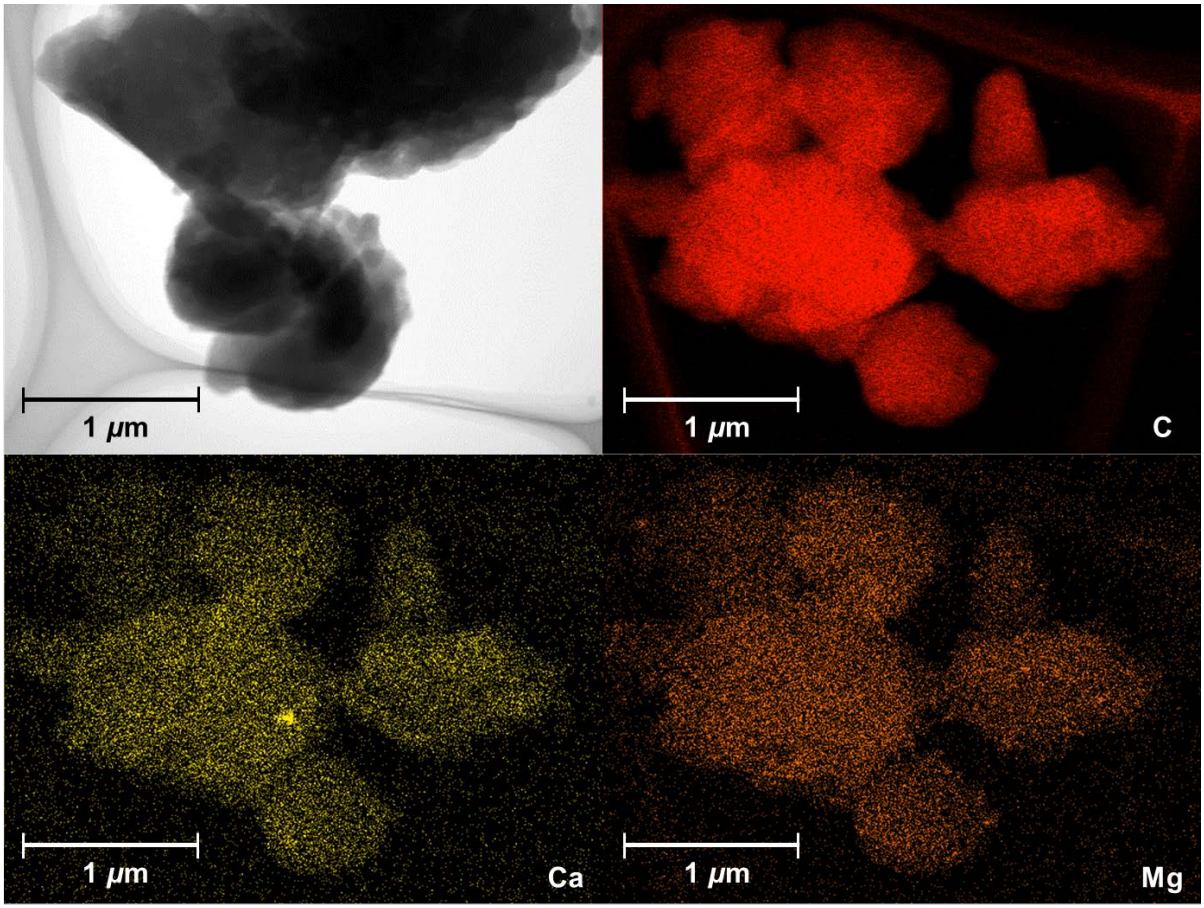

Figure A.7. The dispersion of Ca and Mg in carbon matrix of Ca-0.0.6/Mg-0.17-DA scanned by SEM-EDS (scanning electron microscope with energy dispersive X-ray spectroscopy).

APPENDIX 8

Measured 1–*X vs t* and d*X*/d*t vs X* profiles for gasification of chars from Ca, Ca/K, and K-loaded lignites for respective two runs under the same gasification conditions

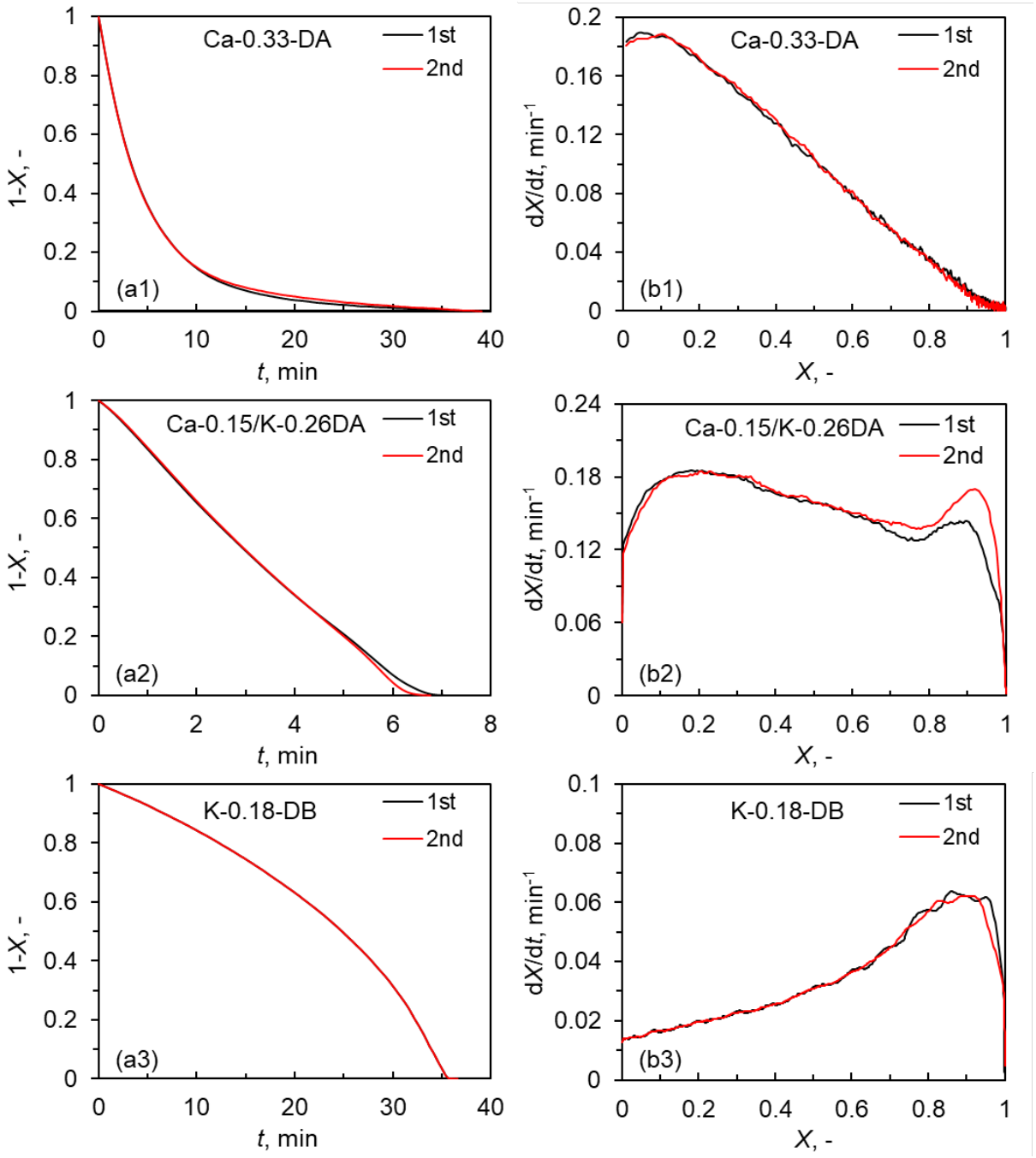

Figure A.8. Measured profiles of (a) 1–*X vs t*, and (b) d*X*/d*t vs X* for gasification of chars from (1) Ca-0.33-DA, (2) Ca-0.15/K-0.26-DA, and (3) K-0.18-DB at 900°C with two replicated runs under the same gasification conditions.

APPENDIX 9

Effect of initial mass of char from the 900°C pyrolysis of K-0.22 on its K concentration

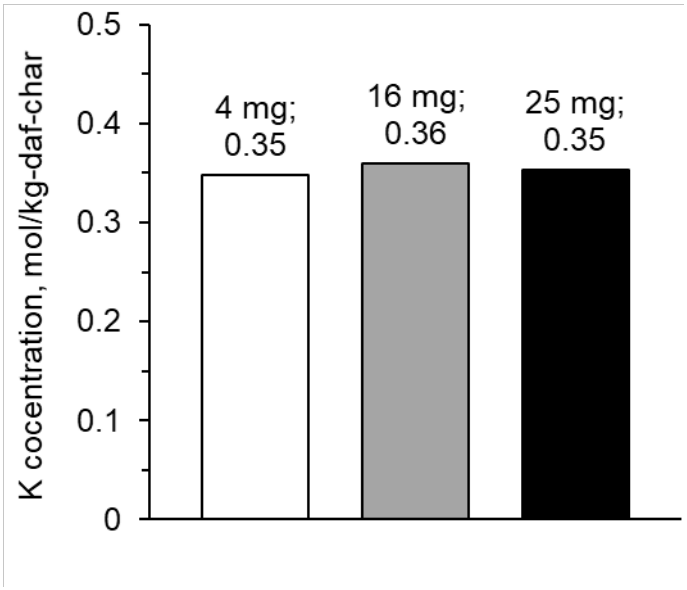

Figure A.9. Effect of mass of char from the pyrolysis of K-0.22 lignite at 900°C on K concentration. This comparison was performed for confirming the reproducibility of determination of the K concentration in char. As seen in the graph, the measured K concentration was independent of the initial mass.

APPENDIX 10

Effect of initial lignite mass on the dX/dt profile of CO_2 gasification of K-loaded chars at 800 and 900°C

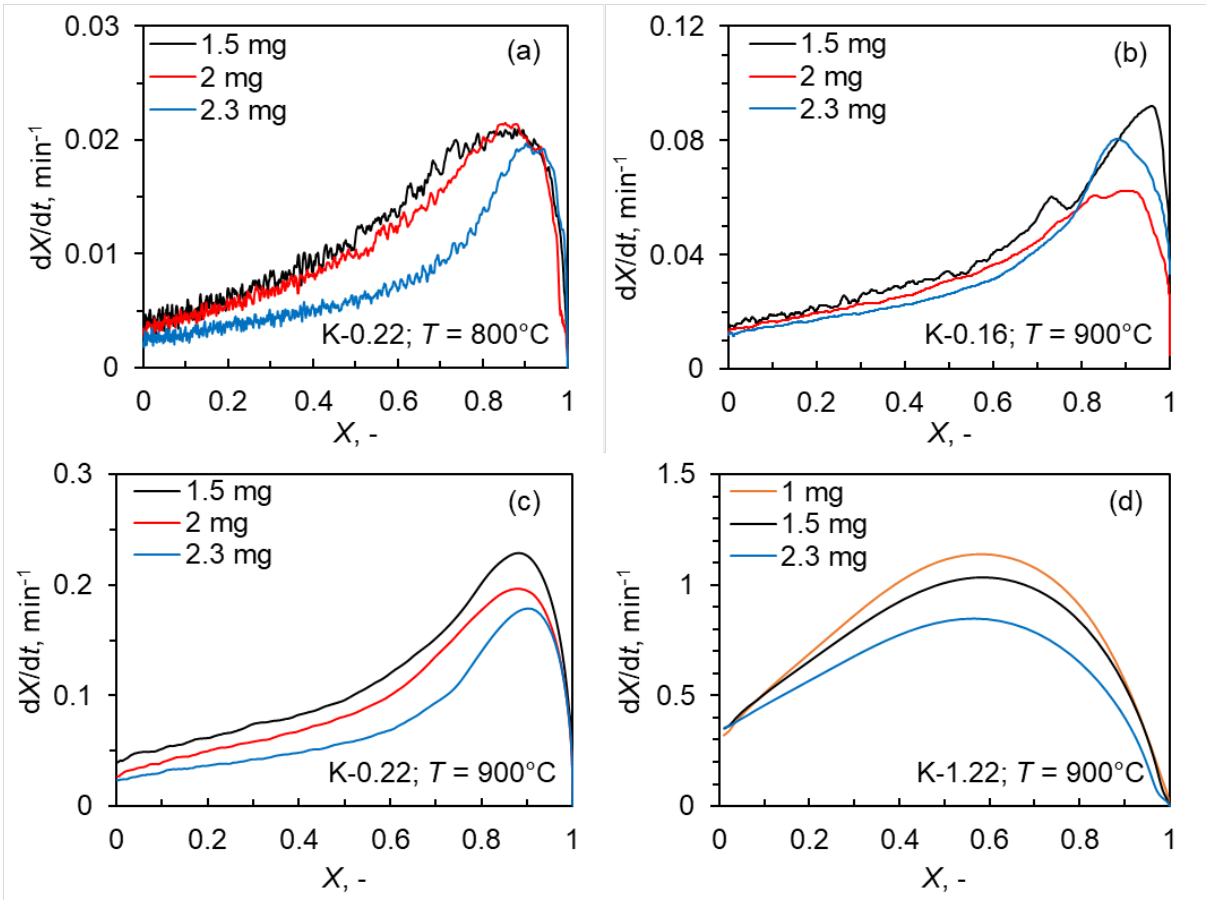

Figure A.10. Measured changes in dX/dt with X for gasification of (a) K-0.22 lignite at T = 800°C, (b) K-0.16, (c) K-0.22, and (d) K-1.22 lignites at T = 900°C with the initial lignite mass of 1.5, 2 or 2.3 mg (except 1 mg for K-1.22). The initial mass of 2.0 mg lignite is sufficiently small at which the rate of gasification is chemically controlled without significant resistance to mass transport within the char bed even for the gasification of K-0.22 lignite at 800°C. However, at 900°C, the effect of mass transport decreases with the reduction of the initial K content in the lignites and can be neglected at the K-0.09. Thus, after careful consideration, we decided to apply the kinetic analysis only on K-0.02, K-0.05, K-0.09, and K-0.16 for all T. Though not shown here, we authors also did gasification for K-0.33, K-0.55, K-0.80 lignites, in addition to K-1.22. The gasification rates of these chars were extremely high, and therefore their true kinetics were difficult to analyze.

APPENDIX 11

Measured changes in 1–X with t and dX/dt with X for gasification of K-0.05 and K-0.09 chars for respective two runs under the same conditions

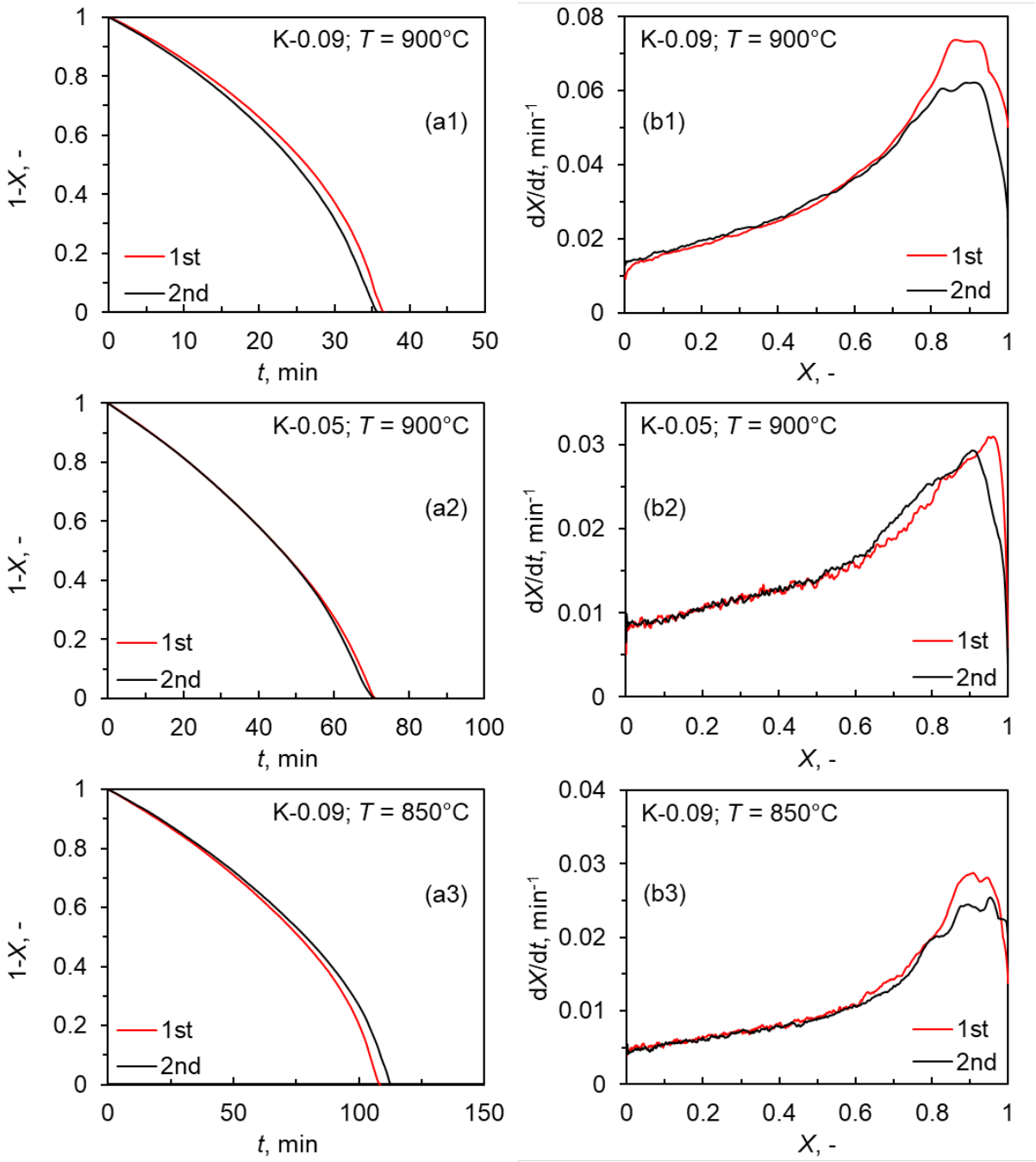

Figure A.11. Measured changes in (a) 1–X with t, and (b) dX/dt with X for gasification of chars from (1) K-0.09 and (2) K-0.05 lignites at T = 900°C, and (3) K-0.09 lignite at T = 850°C with two replicated runs under the same conditions. The rate of gasification for each replication was almost comparable in the range of X = 0–80%, but the variations at X > 80% were inevitable.

APPENDIX 12

Pore size distribution of fresh and partially gasified chars from K-0.02 and K-0.16 lignites determined from CO_2 and N_2 adsorption isotherms

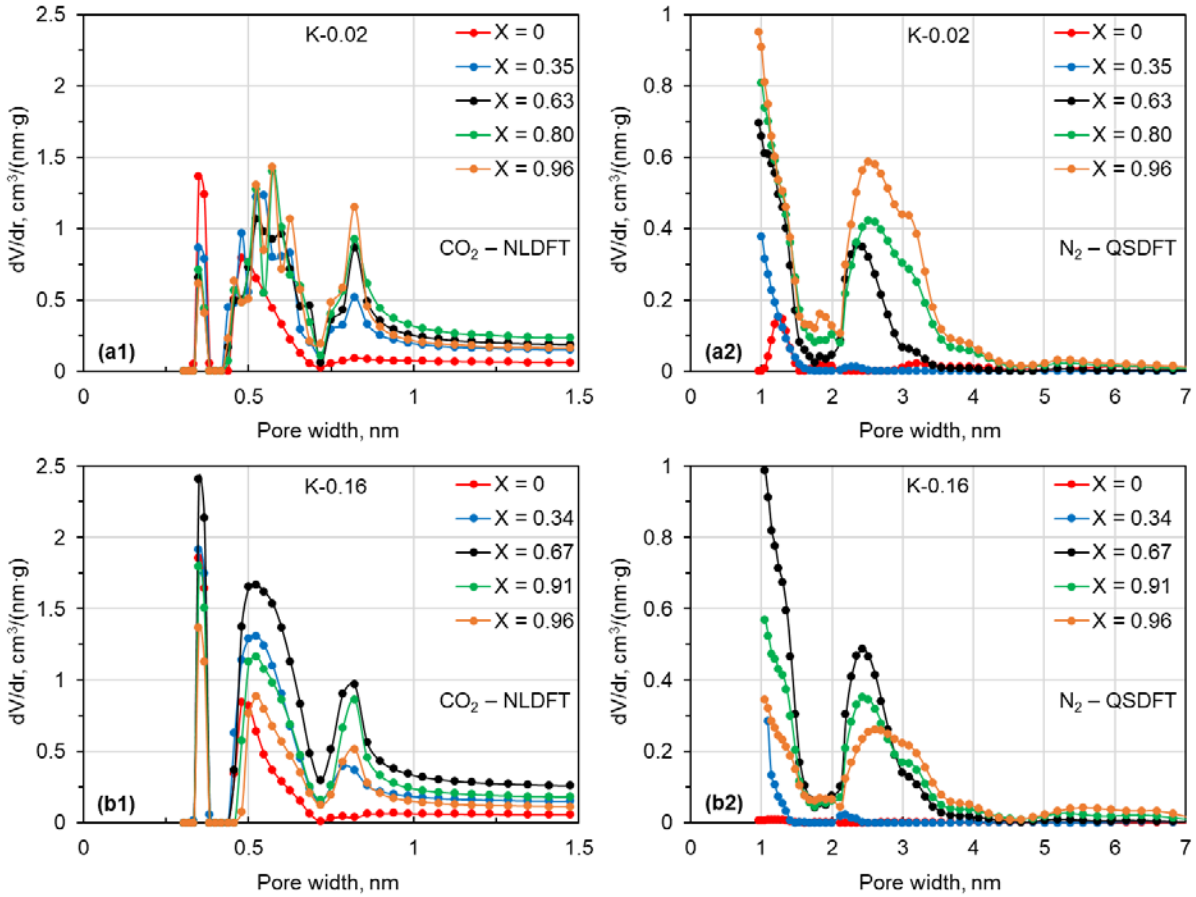

Figure A.12. Volume-based pore size distributions of fresh and partially gasified chars (K-0.02 and K-0.16). (a1) and (b1); distribution from the analysis of CO_2 adsorption isotherms by NLDFT method, (a2) and (b2); those from N_2 adsorption isotherms by QSDFT method. The micro/mesopores were classified into those with width of < 0.7 and 0.7–1.5 nm (CO_2) or 1.0–2.0 and 2.0–4.7 nm (N_2).

APPENDIX 13

Gibbs free energies for reactions involving catalytic K species at T = 800, 850 or 900°C

No.	Reaction	ΔG_r* at T, kJ/mol-K-metal			K_p at T =	Solid Ratio
		800°C	850°C	900°C	900°C	
1	$2K + CO_2 = K_2O + CO$	-11.7	-10.4	-9.1	2.5	1.3E+03 K_2O/K
2	$K_2O + C = 2K + CO$	3.5	-2.2	-7.8	2.2	2.2E+03 K/K_2O
3	$K_2O + CO_2 = K_2CO_3$	-116.2	-112.4	-108.6	6.9E+04	3.4E+04 K_2CO_3/K_2O
4	$K_2CO_3 + C = K_2O + 2CO$	108.1	99.9	91.6	8.3E-05	8.3E+01 K_2O/K_2CO_3
5	$K_2CO_3 + 2C = 2K + 3CO$	111.6	97.7	83.8	1.9E-04	4.6E+04 K/K_2CO_3
6	$2K + 2CO_2 = K_2O_2 + 2CO$	61.2	62.4	63.6	1.5E-03	3.7E+02 K_2O_2/K
7	$K_2O + CO_2 = K_2O_2 + CO$	72.8	72.8	72.7	5.8E-04	0.3 K_2O_2/K_2O
8	$K + 2CO_2 = KO_2 + 2CO$	253.9	252.6	251.3	6.5E-12	1.6E-06 KO_2/K
9	$K_2CO_3 = K_2O_2 + CO$	189.1	185.2	181.3	8.4E-09	8.4E-06 K_2O_2/K_2CO_3
10	$K_2O_2 + 2C = 2K + 2CO$	-77.5	-87.5	-97.5	2.2E+04	2.2E+10 K/K_2O_2

*Thermodynamic data obtained from David R. Lide, ed., CRC Handbook of Chemistry and Physics, 90th Edition, CRC Press/Taylor and Francis, Boca Raton, FL

APPENDIX 14

K concentration in K-0.16 lignite, and that in fresh, partially gasified and washed chars

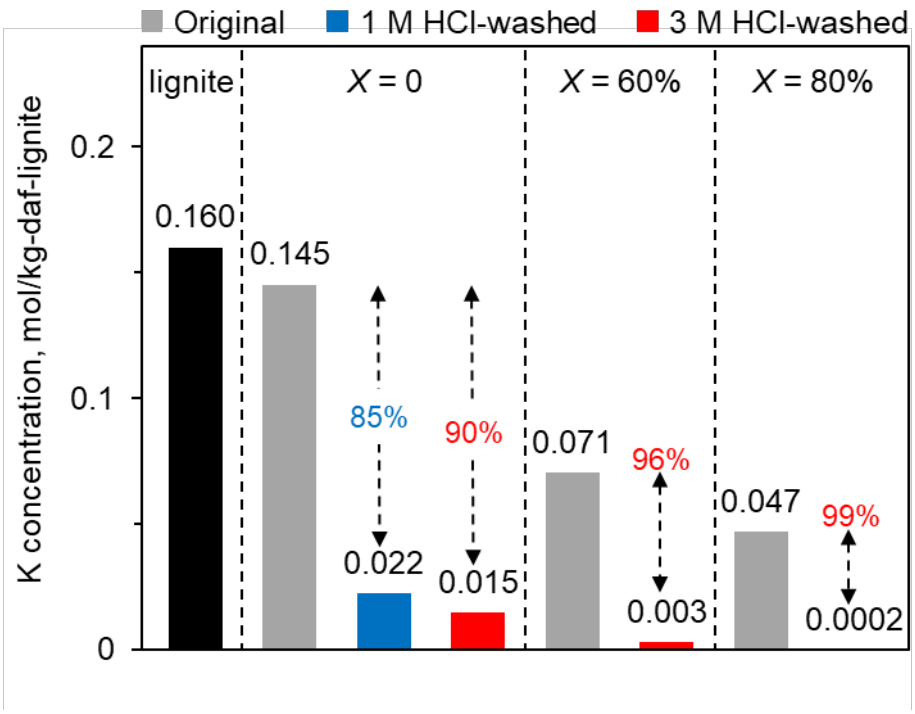

Figure A.14. K concentration in K-0.16 lignite and that in fresh, partially gasified and washed chars. K-0.16 chars with mass-based char conversions of 0%, 60%, and 80% were prepared in a horizontal quartz tube reactor (HQTR) at 900°C and washed with 3 M HCl aq. (or with 1 M HCl for X = 0% char) for 24 h to remove left K species and then referred to as K-0.16-0-A, K-0.16-0.6-A, and K-0.16-0.8-A, respectively. The K contents in these samples were quantified and then converted on a mol/kg-daf-lignite basis. The blue- and red-colored texts in the figure indicate the removal rate of K species from chars by 1 M or 3 M HCl washing, respectively.

APPENDIX 15

CO_2 and N_2 adsorption-desorption isotherms of chars from K-0.02 and K-0.16 lignites

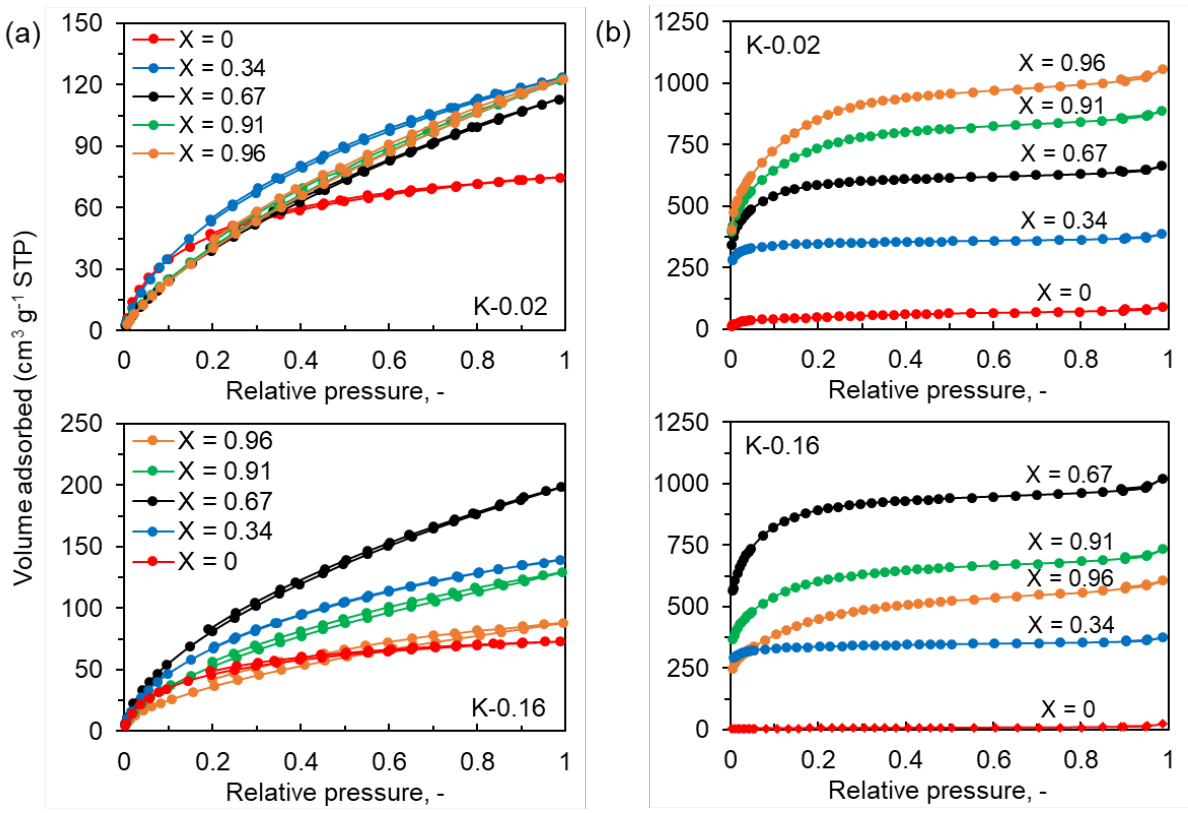

Figure A.15. (a) CO_2 and (b) N_2 adsorption-desorption isotherms of chars from K-0.02 and K-0.16 lignites.